To the Graduate Council:

I am submitting herewith a dissertation written by Vasanthakumar Narayanan entitled "Dimensional Stability of Melt Blown PET Nonwovens." I have examined the final copy of this dissertation for form and content and recommend that it be accepted in partial fulfillment of the requirements for the degree of Doctor of Philosophy with a major in Human Ecology.

Dr. Gajanan S. Bhat, Major Professor

We have read this dissertation
and recommend its acceptance:

Prof. Larry C. Wadsworth

Prof. Kermit E. Duckett

Prof. Bernhard Wunderlich

Accepted for the Council:

Associate Vice Chancellor
and Dean of The Graduate School

Dimensional Stability of Melt Blown PET Nonwovens

A Dissertation

presented for the

Doctor of Philosophy

Degree

The University of Tennessee, Knoxville

Vasanthakumar Narayanan

May 1995

DEDICATION

This dissertation is dedicated to my parents

Mr. Narayanan Kutty Nair

(ஸ்ரீ. நாராயணன் குட்டி நாயர்)

and

Mrs. Santha Narayanan

(ஸ்ரீமதி. சாந்தா நாராயணன்)

and to my

educators

ACKNOWLEDGMENTS

I would like to thank my major professor, Dr. Gajanan Bhat for his excellent support and guidance for this dissertation. I would like to thank other committee members, Dr. Larry C. Wadsworth, Dr. Kermit E. Duckett and Dr. Bernhard Wunderlich for their help and guidance over the past three years. I would like to thank Dr. William Smartt of Hoechst Celanese Corp. for his timely supply of the PET polymer for this research. I would like to thank Mr. John Scott, Mr. Brian West, Ms. Colleen Dennett, Mr. Greg Smith and other members of Techmer PM Polymer Modifiers, Clinton, TN for their help and support in processing and characterization of the PET polymer with additives. I would like to thank Dr. Ahamed Yacub Khan, Richard Meade and Larry Spires of TANDEC for their help in melt blowing PET. Finally, I would like to thank all my family members and my friends who were of great help in completing this endeavor.

Abstract

This research attempted to develop melt blown poly(ethylene terephthalate), PET nonwovens that maintained their dimensional stability at temperatures above the glass transition (i.e. 80°C and above). The high degree of shrinkage of PET fibers on exposure to heat is due to the relaxation of oriented rigid amorphous segments present within the fibers. The shrinkage can be controlled by engineering fibers that contain tie or reinforcing elements between the molecules. The overall crystallization rate and crystallinity can be increased by incorporating nucleating agents during melt blowing where the stress levels are low for any on-line crystallization to occur. Sodium benzoate, liquid crystalline polyester (LCP) and ionomer were used as nucleating/reinforcing agents to engineer melt blown PET fibers. Poly(ethylene terephthalate) without any additive was also melt blown under different process conditions to study the effect of process variables on the crystallinity of the fibers. The melt blown samples were then analyzed for their structure and properties through various techniques and it was concluded that by having tie elements or crystallites in the as-produced fibers, the shrinkage of melt blown PET fibers can be controlled to less than 10% even at 190°C. A three-phase fiber model was used to explain the shrinkage mechanism of the fibers. The fractions of different structural entities present in the fibers determine their shrinkage behavior. The fibers made from PET and sodium benzoate were smaller in diameter and better in mechanical properties compared to those from PET and liquid crystalline polyester. The addition of sodium benzoate to PET/LCP blends resulted in smaller diameter fibers with good dimensional stability. However, the resultant mechanical properties were poor. It was also observed that by ingenuously selecting the process conditions one can control the shrinkage behavior of melt blown fibers with a limited processing range of variables.

Table of Contents

Contents Page

List of Tables

List of Figures

Figure Page

1. Introduction and Purpose

Melt blowing is one of the fastest growing processes for nonwoven production. Although poly(ethylene terephthalate) [PET] can be melt blown, it has a disadvantage in that melt blown PET fabrics exhibit poor dimensional stability at temperatures above the glass transition temperature (T_g). This is due to negligible crystallinity in the final product, which is a result of the absence of stress induced crystallization. The spinline stress is very low due to the fact that there is no positive take-up mechanism unlike in melt spinning. Apart from this, the process is very rapid for any thermally induced crystallization and microstructure development to occur on the spinline.

Generally, PET has a very poor tendency to crystallize upon cooling from the melt. Although PET has polar groups, the rigidity of the benzene rings and the limited flexibility of the aliphatic groups prevent the formation of regular chain folds and close packing of molecular chains essential for crystal growth. Thus the overall crystallization rate of PET is slower than that of other common flexible polymers used in commercial fiber production. Nucleating additives have been successfully used in situations where the stress and orientation levels are low such as molding operations.

Research was undertaken to investigate the effect of nucleating additives in melt blowing PET. This investigation was carried out in three stages. In the first stage, potential nucleating agents were screened for use in PET products. In the second stage, PET compounded with selected nucleating agents were melt blown and the webs were characterized for their structure and properties. In the final stage,

process variables such as air pressure at the die, air temperature, fiber collection distance from the die and throughput were varied to study the effect of orientation on crystallinity developed during the process. A theoretical understanding was developed to explain the shrinkage mechanism in PET melt blown fibers.

2. Literature Review

2.1. Melt Blowing

Melt blowing is a one-step process to produce fabrics from thermoplastic polymers. A schematic depicting the Exxon melt blowing process is shown in figure 1. The plastic to be melt blown is fed to the extruder in the form of pellets, flakes or powder. The molten polymer is forced out of a die containing several spinneret holes. As soon as the polymer melt exits the die, a stream of high-velocity, hot air attenuates the polymer into very fine fibers. The downstream turbulence helps in entangling the fibers to produce a coherent nonwoven web that is wound on a drum [1, 2]. Almost all thermoplastic polymers can be melt blown to form a nonwoven web [3]. The most widely used polymer in melt blowing is high melt flow rate (MFR) poly(propylene) because lower viscosity melts require lower melt temperatures and are easier to draw into fine fibers. Poly(esters), nylons, poly(ethylenes) and poly(styrenes) have also been successfully processed [4, 5]. Melt blown webs have fine fibers with diameters in the range of 2-10 micrometers. This results in high surface area per unit volume of the web. The main application of melt blown webs is in the area of air filtration, absorption of oils spills, protective apparel and insulation.

The important variables in melt blowing are polymer throughput, melt temperature, die temperature, air temperature, air flow rate, screw speed and die-to-collector distance [6]. Melt blowing is a complex process that involves turbulence which is poorly understood by the scientists until today. Isolation of experimental factors is difficult because of interaction between different variables. The

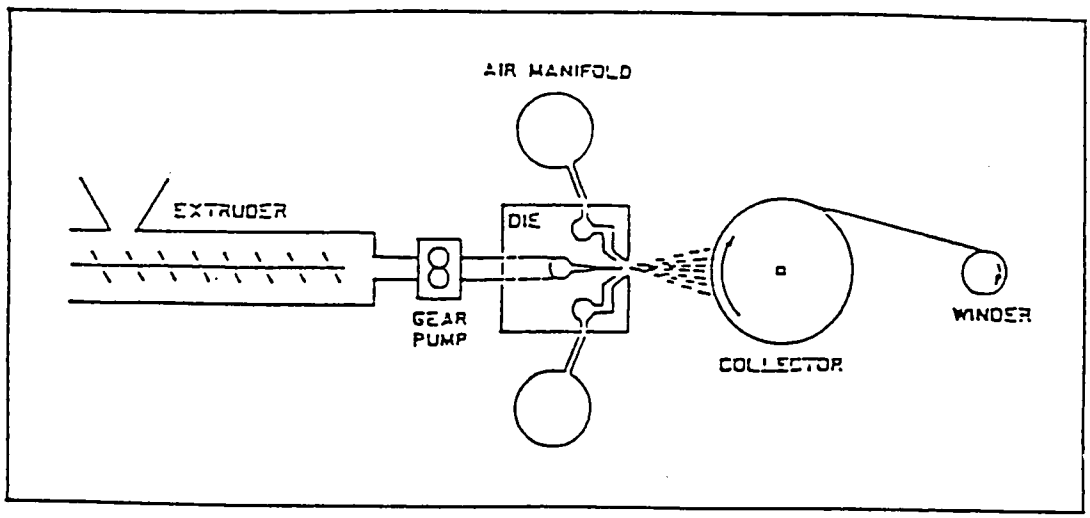

Figure 1. Schematic of the Exxon Melt Blowing Process.

Source: Malkan, S. R. and Wadsworth, L. C., INDA JNR, vol. 3, no. 2, 21-34, Spring 1991.

multifilament environment, and factors such as the humidity of the processing room, quench air temperature widely change the boundary conditions.

The process-structure-property relationships in melt blowing different molecular weight poly(propylene) resins (35 -1000 MFR) were studied by Malkan *et al.* [6,7]. Polymer throughput of poly(propylene) had a noticeable effect on the physical characteristics of the melt blown webs. The mean fiber diameter, tensile strength, initial modulus, porosity, stiffness and web density increased with an increase in throughput. However, the breaking strain and the energy required to break decreased indicating the brittle nature of the webs produced at higher throughput. The increase in fiber diameter was attributed to die swell and the change in polymer-to-air ratio for a given air flow rate. The increase in air flow rate did not result in any significant change in mean fiber diameter. The die orifice size had only minimal effects on the average fiber diameter. Birefringence values ranged from 15.2×10^{-3} for high throughput to 26.1×10^{-3} for low throughput. The molecular weight and polydispersity index were found to decrease after processing the resins into webs. However, an increase in throughput did not result in any significant change in molecular weight of the resins. The effects of throughput, air flow rate, and hole diameter on the percent crystallinity were found to be insignificant. The webs produced at high throughput showed double melting peaks which was indicative of two different melting species. X-ray studies confirmed the presence of α - form (monoclinic) and β - form (hexagonal) of crystals.

Using a single-hole die and high speed photography, the effect of polymer throughput, air velocity, polymer and air temperatures on the web properties were studied by Haynes *et al.* [8]. The filaments were found to be always continuous

without any breakage in their flight towards the collector. Also, the filaments were shown to have flapping motion depending on the air velocity and polymer throughput rate. An increase in air flow rate was found to decrease the mean fiber diameter for a fixed throughput and die geometry. However, a critical air velocity was observed, above which any increase in air flow rate had only little effect on the fiber diameter. The fiber diameter was also found to decrease with increasing processing temperatures.

The feasibility of melt blowing virgin and recycled PET has also been demonstrated [9, 10]. The shrinkage of PET webs was dependent on the air flow rate used. PET webs produced at high air flow rates shrank much more than those produced at low air flow rates because of the higher level of molecular orientation. Heat setting of melt blown PET webs or alternatively the use of PBT (poly(butylene terephthalate)) were suggested as the possible means of producing thermally stable melt blown polyester nonwovens [11, 12]. The effects of annealing on the web structure and the mode of failure of melt blown polyester webs were studied using scanning electron microscopy (SEM) [13]. The greater extension of as-blown PET webs was due to their poor crystallization and annealing resulted in brittle webs. The thermal effects on melt blown PET/PBT nonwovens were studied by Bhat *et al.* [14]. It was observed that the PET fibers tend to shrink on exposing to heat whereas that of PBT showed negligible shrinkage. The addition of up to 20 weight percent PBT to PET resulted in only a slight change in the shrinkage behavior.

The processing window for successfully melt blowing the polymers is very limited. In order to produce acceptable quality webs, one has to be in the right range of process parameters and this varies between polymers. Unlike in melt spinning,

there is almost virtually no control over the individual filaments in melt blowing. Although considerable work has been done in the past [1-14], it is very difficult to predict the structure and properties of melt blown fibers since the isolation of variables is very difficult in a multi-filament environment. Usually, a series of isothermal experiments are carried out to get an idea about the rate constants for the non-isothermal processes. Thus it is important to understand the quiescent isothermal crystallization kinetics of the polymers.

2.2. Crystallization of Polymers

Frequently, during polymer processing operations, one encounters non-isothermal situations. The temperature gradient involved could be of the order of hundreds and thousands of degrees per minute. Until now, it has not been possible to follow the crystallization behavior of polymers under these extreme conditions. The process of interest for this dissertation is melt blowing that involves complex process variables. Simulation of the non-isothermal crystallization behavior is still at its infancy. A concise review of the basic theory of polymer crystallization is provided in this section.

The properties of semicrystalline polymers are highly dependent on the crystallization conditions and crystallization mechanisms [15]. The ability of a polymer to crystallize is dependent on the chemical repeat unit, molecular weight and stereoregularity. Under suitable conditions of temperature and stress, molecular ordering takes place in all three directions in macromolecular systems. Thermodynamic and kinetic criteria should be met for polymer crystallization to take place. Thermodynamics provides information only about the initial and final states of

the material under investigation. Since the crystallization process requires varying lengths of time, the way the molecular segments participate to form an ordered crystal structure is better explained by the relatively recent kinetic theories. A concise review of the polymer crystallization theories was provided by Armstead *et al.* [16]. Under quiescent conditions, polymers generally form chain folded crystals when grown from solution or melt as shown in figure 2. The chain folded configuration is due to minimization of the activation energy. This way the crystallization is very rapid [17]. Polymer crystals tend to form thin lamellae which are large in two dimensions but are bound in the third dimension by the folds that form the basal plane. Although, Frank [18] and Hoffman [19] suggested the non-adjacent reentry model (switch-board type) to accommodate the cilia and loops, and associated density changes, neutron scattering studies [20, 21] showed that the adjacent reentry is the predominant mode of crystallization in polymers.

Thermodynamic theories involve the evaluation of Gibbs free energy between a lamella of mean thickness l and the uncrystallized polymer melt [16]. The Gibbs free energy consists of bulk and surface contributions. If the surface free energy per unit area of the fold surface of a lamellar crystal is denoted by σ_e, then the increase in Gibbs free energy is given by

$$\Delta G = \Sigma_{lat} + 2A\sigma_e - \Delta F A l \qquad \text{----------} \qquad (1)$$

where Σ_{lat} is the free energy from both the thin lateral surfaces and edges; A is the surface area of the fold surface and ΔF is the bulk free energy of crystallization per unit volume. For crystallization to occur, ΔG must be negative. The lamellar thickness l is given by

$$l > 2\sigma_e T_m(\infty)/\Delta H \Delta T \qquad \text{----------} \qquad (2)$$

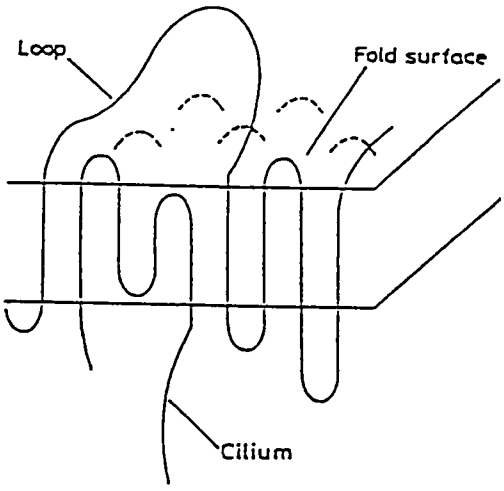

Figure 2. Crystalline Model for Polymers.

Source: Armistead, K. and Goldberg-Wood, G., Advances in polym.sci., vol. 100, 219-311 (1992)

where T_m (∞) is the equilibrium melting point and ΔT ($\{T_m (\infty) - T\}$) is the degree of supercooling. Thus lamellar thickness is very sensitive to temperature and supercooling. The equilibrium thermodynamic theories explain lamellar thickness but fail to account for chain folding. The equilibrium theory is used to calculate the Gibbs free energy as a function of segment length and it assumes that the crystal will be in a minimum free energy state. A driving force for crystallization is the degree of supercooling. The tendency for crystallization will be more for higher supercoolings.

It is now generally agreed that the morphology of polymer crystals is determined by kinetic rather than thermodynamic factors [16]. The kinetic theories state that the growth faces of a crystal have a range of possible thicknesses, each having a growth rate dependent on temperature. The kinetic theories also suggest that for crystallization to proceed, an energy barrier must be overcome via random fluctuations as a molecule attaches itself to the existing crystal, and the energy barrier increases with the crystal thickness. The 'entropic' theories provide an account for the number of conformations a molecule can take for regular crystal growth through computer simulations. An improperly placed molecule in a crystal lattice would retard the crystal growth.

In a phase transformation such as crystallization, two processes become operative [15]. Nucleation is a process by which a new phase is created within the old phase and subsequent growth takes place at the expense of the old phase. Nucleation could be homogeneous or heterogeneous. Homogeneous nucleation occurs in pure systems which is rare in a real life situation. Most of the polymer nucleation is heterogeneous, catalyzed by the impurities present in the melt or solution. Polymer nucleation can be of two types: athermal nucleation with a

constant number of nuclei and thermal nucleation with an increasing number of nuclei with time. Nucleation in polymers occurs between these two limits [22]. The 'barrier' for crystal growth is the nucleation step. The nucleation rate (I) is given by

$$\mathbf{I = I_0 \exp(-\Delta F^*/kT) \exp(-\Delta E^*/kT)} \quad \text{----------} \quad (3)$$

where ΔE^* is the energy required to build a critical nucleus; ΔF^* is the energy barrier influencing the transport of material across the crystal-melt boundary; I_0 is a constant; k is the Boltzmann constant; and T is the temperature. It can be seen that the nucleation rate is highly dependent on temperature. For secondary nucleation,

$\Delta F^*/kT = 2.07 \times 10^3/ [51.6 + (T-T_g)]$ based on the WLF equation

$\Delta E^* = 4 \sigma\sigma_e b_0 T_m^0/\Delta H_f \rho_c \Delta T$

where T_g is the glass transition temperature; σ and σ_e are the surface free energies of lateral and fold surfaces respectively; b_0 is the crystal thickness; ΔH_f is the heat of fusion; ρ_c is the crystal density; ΔT is the degree of supercooling and T_m^0 is the equilibrium melting temperature (temperature required to melt a crystal of infinite thickness). Once the nuclei are formed, the final crystal morphology is determined by the linear growth rate of crystals in different directions. The growth kinetics of polymers is explained by the equation,

$$\mathbf{G = G_0 \exp(-\Delta F^*/kT) \exp(-\Delta E^*/kT)} \quad \text{----------} \quad (4)$$

The overall kinetics determined experimentally consists of nucleation and growth kinetics [15]. A minimum amount of supercooling is necessary for nuclei to develop in a melt or in a solution. The functions ΔF^* and ΔE^* are of opposing nature; ΔF^* decreasing exponentially and ΔE^* increasing exponentially with increase in temperature. The growth rate initially increases, goes through a maximum and decreases on decreasing the temperature from T_m. The overall kinetics can be described by the Avrami equation of the form

$$\mathbf{1 - V_f^c = \exp[-Kt^n]} \quad \text{----------} \quad (5)$$

where $V_f{}^c$ is the volume fraction of growing crystals; K is a constant that contains information on geometry of crystals, nucleation and linear growth rate, t is the time and n is the Avrami exponent. For a 3-D growth of athermal nucleation type

$$K = 4/3\pi N V_c^3$$

where N represents the number of nuclei per unit volume and V_c is the total volume crystallinity. The Avrami equation is based on the assumption of constant density during phase transformation and that is not true in polymeric systems. Also, the reduction in growth rate with time, and complications due to reorganization of crystals are unaccounted for in Avrami's treatment. The Avrami equation must always be supported by additional data from morphological studies. Theoretical treatment of isothermal kinetics is much easier than that of non-isothermal kinetics. However, non-isothermal experiments could be conducted with much ease compared to isothermal experiments. The Avrami equation could be modified for non-isothermal kinetics [15] as shown by the following equation:

$$1 - V_f{}^c = K(T)/q^m \qquad \text{----------} \qquad (6)$$

where q is the cooling rate and K(T) is a temperature dependent function.

2.3. Crystallization of Poly(ethylene terephthalate)

The crystallization behavior of polymers is highly dependent on chemical structure and intermolecular forces. Polymers with simple and more linear structures such as polyethylene and polypropylene have faster crystallization kinetics compared to PET that has a more rigid backbone structure. The chain straightening and folding is much easier in the case of linear and flexible structures that form regular crystals. Chain folding is difficult in the case of PET which has rigid ring structures in the main chain. This inhibits the crystallization of PET during melt spinning. Most of

the polymer processing operations involve stretching of the filaments after the polymer has solidified to move and align the molecular chains adjacent to each other to promote crystallization. A detailed account of the stress during crystallization is given in section 3.5. Although PET has the polar carbonyl groups, the polarity is not as great as in the case of crystallites of nylon polymers. Polymer crystallization is highly cooling rate dependent. PET can be made crystalline by slow cooling or completely amorphous by quenching. Although, isothermal processing produces a crystalline material with better mechanical and thermal properties, is rarely encountered in actual polymer processing.

The overall crystallization rate of PET is usually divided into nucleation and growth rates. Both isothermal and nonisothermal kinetics could be studied using Differential Scanning Calorimetry (DSC). Other techniques to study the crystallization kinetics of PET include light scattering, optical microscopy and infrared spectroscopy. The bulk crystallization rate as determined by DSC is influenced by overall nucleation density, the rate of nucleation on the crystal surface and the rate of transport of the molecules to the growth front. The crystallization of PET was studied by Cobbs *et al.* [23] using DSC, X-ray and infrared spectroscopy. Infrared and X-ray spectra were obtained on samples annealed at 195°C for 45 minutes. The intensities corresponding to 1340, 972 and 794 cm^{-1} were used for crystallization studies. The polymer was molten at 300°C and quenched to room temperature. No presence of crystallinity was detected even after a year for these samples which is indicative of the poor crystallizibility of PET polymer. Several PET films were isothermally crystallized between 120 and 240°C for various periods of time and the crystallization rate was determined by plotting the optical density versus time. It was observed that the half-time of crystallization (time required for 50%

crystallinity to develop) showed a minimum (maximum rate of crystallization) near 190°C. But the minimum was rather broad. A possible nucleation mechanism was discussed based on Volmer-Becker-Turnbull nucleation theories [24-26]. The reciprocal of induction time was plotted against the reciprocal of absolute temperature to obtain an activation energy of 20 kcal/mole of the chain segments. Avrami's kinetic analysis showed a slight deviation from the straight line at 190°C due to heterogeneous nucleation.

The influence of molecular weight, crystallization temperature and additives on the kinetics of PET was studied by Van Antwerpen [27]. The kinetics of crystallization, both from the molten and glassy states, were studied. Samples with number average molecular weights ranging from 19,000 to 39,000 were used for the study. The spherulitic growth rate was calculated according to the equation

$$\ln G = \ln G_0 - \Delta E^*/kT - \Delta F^*/kT \quad \text{----------} \quad (7)$$

where, G is the growth rate of the spherulites; G_0 is the pre-exponential factor; ΔE^* is the free energy of activation for transporting a chain segment from the supercooled melt to the crystalline phase; ΔF^* is the free energy of formation of a critical nucleus; k is the Boltzmann constant and T is the absolute temperature. A final equation of the form

$$\ln G = \ln (-5\times10^9 + 2.93\times10^4/M_n) - 777/(T-316) - 3093\times10^5/T^2(573-T) \quad \text{----} \quad (8)$$

was used to calculate the spherulitic growth rate in nm/s. It was observed that the growth rate of PET increased as a function of crystallization temperature, reached a maximum at 180°C and decreased again. Growth rate was found to decrease with an increase in molecular weight. However, the temperature of maximum growth rate was observed to be practically independent of molecular weight. The maximum spherulite radius was found to be increasing with decreasing molecular weight for

both PET cooled from the melt, and heated from the glassy state. The growth rate was dependent on the rate of diffusion and transport of the molecules to the crystal surface and the rate of secondary nucleation. The addition of small quantities of solid additives was found to decrease the maximum spherulite radius.

Jabarin [28] investigated the nature of PET crystallization by using a combination of characterization techniques such as differential scanning calorimetry (DSC), density, small angle light scattering (SALS) and depolarized light intensity (DLI). Poly(ethylene terephthalate) films of intrinsic viscosity 0.81 were isothermally crystallized at 110, 115, 125 and 130°C for various periods of time. For the same treatment time, the higher the crystallization temperature, the more was the volume degree of material crystallized and vice versa. To achieve the same degree of crystallinity as at 130°C, the treatment time had to be almost four times at 115°C. The Avrami exponent determined using DLI was less than 3, indicative of heterogeneous nucleation, and it decreased at higher treatment temperatures. Light scattering was used to follow the spherulite radius as a function of time. The maximum spherulite radius was found to be the same at all crystallization temperatures and was used to calculate the nucleation density

$$N' = 1/[\ 4/3\pi R^3_{max.}\ ] \quad \text{----------} \quad (9)$$

$$4.1 = 4\pi R/\lambda \sin\theta_{max.} \quad \text{----------} \quad (10)$$

where λ is the wavelength of the light used; R is the radius of the spherulite; $\theta_{max.}$ is the scattering angle for maximum intensity.

There has been very little report on the crystallization kinetics of PET due to the fact that a slight change in the structure due to the different catalyst systems used alters the kinetics appreciably. Hence consistent results are not obtained while

conducting kinetic experiments. The isothermal and non-isothermal kinetics of PET were performed by Jabarin [29-31]. The chemical factors that affect kinetics include molecular structure, catalyst system, molecular weight and side reactions during polycondensation of PET. The molecular weight affects viscosity and thus the rate of transport of chain segments across the liquid-crystal interface. The physical factors that are important are the temperature, previous thermal history, nucleating additives, strain, orientation and pressure. The author used PETs of different intrinsic viscosities (I.V.) from different sources with known molecular weight, catalyst, diethylene glycol content and polymerization conditions. The samples were heated at a rate of 10°C/min. upto 294°C, and held for 15 minutes under nitrogen atmosphere, and were then rapidly cooled to the isothermal crystallization temperature. The isotherms were constructed by integrating the area under the exothermic peak using the relation,

$$X_t = [\ {}_0\int^t (dH_t/dt)\ dt\ /\ {}_0\int^\infty (dHt/dt)\ dt\ ] \qquad \text{----------} \qquad (11)$$

where dH_t is the rate of evolution of heat; t is the time and X_t is the weight of the polymer crystallized at time t. It was concluded that the crystallization rate and the mechanism of crystallization were dependent on molecular weight, temperature and catalyst system. Of these, the catalyst system exhibited greater influence on the rate of crystallization. Among the catalyst systems investigated, titanium-based catalysts exhibited the lowest crystallization rate. The half-time of crystallization is not a true measure of crystallization as the exponent changes when crystallization proceeds. Isothermal crystallization mechanisms are easier to analyze theoretically than the dynamic non-isothermal crystallization mechanisms. The dynamic crystallization experiments were performed on the same samples using a cooling rate of 5-40°C/min. A modified Avrami equation of the following form was used:

$$1 - \alpha(T) = \exp\ [-K(T)/R^n] \qquad \text{----------} \qquad (12)$$

where $\alpha(T)$ is the amount of transformed material at temperature T, K(T) is the temperature dependent exponent, R is the cooling rate and n is the Avrami exponent. It was concluded that the minimum cooling rate required to produce amorphous PET is dependent on molecular weight and catalyst system. For high IV PET, this cooling rate was 130°C/min. while for low IV PET, the cooling rate was above 400°C/min. The rate parameters were similar for both dynamic and isothermal experiments indicating that the crystallization mechanism is the same in both cases. The effect of moisture on the crystallization behavior of PET showed that the half-time and induction time decreased significantly with moisture content. Nucleation rate increased significantly with moisture content unlike growth rate.

The rate of crystallization of PET was studied using DSC in another research project [32] where it was concluded that the Avrami exponent n, is not a constant, indicative of the existence of a secondary crystallization process. The Avrami exponent, n, varied from 3 to 1.5. The rate of crystallization became slower at higher molecular weights and at higher crystallization temperatures. A new method for analyzing the dynamic crystallization of PET was proposed [33] which allows comparison with isothermal conditions assuming that no process variations take place over the entire temperature range of the experiment. The model was based on a modified Avrami equation

$$1 - U = \exp \{ -K(T)[(T_\alpha - T)/\alpha]^n \} \qquad \text{----------} \qquad (13)$$

where α is the cooling rate; T_α is the starting temperature and K(T) is the temperature dependent coefficient. Application of this equation to study the non-isothermal kinetics of PET allows one to have an extended range of temperature to determine K(T). The poor correlation between experimental data and the theoretical prediction of the Avrami equation over the entire range of crystallization is due to the fact that in

the latter one assumes constant radial growth rate which is rarely found in polymeric systems. Kim *et al.* [34] have modified the Avrami equation to take the form

$$1 - U = \exp [k f(t)^n] \quad \text{----------} \quad (14)$$

where f(t) is the integral of growth function $(1-V_c)^m$. Here, the growth rate is not constant but varied for the whole range of crystallization. Isothermal crystallization experiments were carried out in the temperature range of 180-210°C to study the validity of the above equation. The values of k and n are for the early stages of crystallization and m is the correction factor for the later stages.

It is clear from this section that any change brought about by variation in process conditions such as temperature, cooling time and pressure apart from numerous additives would considerably alter the crystallization behavior and morphological feature of PET fibers. An insight into the structural entities of the fibers is very essential in engineering fabrics of desired functional properties.

2.4. Effect of Nucleating Additives on the Crystallization of PET

As mentioned in section 3.2., the 'barrier' in polymer crystallization is the nucleation step because of the long chain nature of the macromolecules. An easy way of overcoming this 'barrier' is by incorporating artificial nucleating additives in polymer melt or solution. Nucleating agents reduce the activation energy and promote the crystallization process. In this section, a summary of literature on the effect of different types of nucleating agents on the crystallization of PET polymer is provided.

PET was extruded with several metal hydroxides [35] to study the effectiveness of nucleating additives in improving its crystallizibility. An efficient nucleating additive would increase the maximum crystallization temperature (T_{cc}) on cooling from the melt, and decrease the cold crystallization temperature (T_{ch}) on heating from the glassy state. A PET of intrinsic viscosity 0.95 dl/g was used for the study. Additives were compounded at temperatures above the T_m of the polymer. Thermal analysis was carried out using DSC. The samples were cooled at a rate of 10°C/minute from 300°C after being held at that temperature for about 5 minutes. The samples were also heated to 300°C with the same heating rate. Of all the metal hydroxides studied, aluminum hydroxide [$Al(OH)_3$] was observed to be an efficient nucleating agent at a concentration of less than one percent by weight. The TGA scans carried out on nucleating additives indicated that the metal hydroxides that released water over a narrow temperature interval spanning the processing temperature range of PET (260-280°C) were found to be the effective nucleants. When very large amounts of aluminum hydroxide were incorporated into PET, a reduction in IV was observed due to release of water. It was also observed that the metal ions did not act as efficient nucleating sites. Thus it was concluded that the nucleation of PET by aluminum hydroxide was due to the localized hydrolytic degradation of PET and also due to the localized supercooling effect initiating crystallization around the hydroxide particles.

The effect of silica nucleants on the crystallization rate of PET was studied by Turturro *et al.* [36]. A PET of 0.62 I.V. was compounded with an amorphous, thermal silica with a particle size of 12 nm. Silica particles were also surface treated with special chemicals for this study. The maximum temperature of crystallization (T_{cc}) was found to increase with low loadings of silica (2 parts silica in 100 parts of

PET). The trend was reversed and T_{cc} decreased rapidly on increasing the concentration of silica particles. Silica powder at low loadings catalyzed the primary nucleation process by reducing the net free energy of formation of unit area at the nucleus interface. At higher silica loadings, the number of polymer segments available for crystallization decreased because of the quasi-crosslinking of silica with the polymer. Thus the overall crystallization rate decreased at higher loading due to the slowing down of the secondary crystallization process. Induction period is the time during which the nuclei for further growth are developed. This induction time was found to decrease at low loadings due to primary nucleation. The trimethylsilylated silica reduced the melt-nucleant interfacial free energy, and the crystallization rate due to this treated silica was found to be much higher than that of untreated ones.

The influence of different catalyst systems and the molecular weight on the kinetics of crystallization of PET was studied by Gumther *et al.* [37]. Two different catalyst systems, one with antimony trioxide and calcium acetate, and the other with antimony trioxide with manganese acetate were used to produce PET of different molecular weights. The molar mass increased with manganese acetate thus slowing down the crystallization rate. The half-time of crystallization was smaller in the case of PET with calcium acetate catalyst systems. The spherulite size was much smaller in the case of PET with calcium acetate. The decrease in overall crystallization rate with increasing molar mass was attributed to the fact that the molecular mobility slows down due to increase in viscosity. The ability of calcium acetate to precipitate from the melt was attributed as the nucleating ability of this material.

Sodium salts of benzoic acid were tried successfully as nucleating agents for PET [38]. Nucleation of polymers could be a physical process where the oriented polymer segments deposit on the surface of the particles or it could be a chemical process where the basic chemical structure of PET is altered. PET of M_n 15,800 was used for this study. Sodium orthochlorobenzoate (SOCB) was used as a crystallization promoter. The nucleating efficiency of SOCB was found to be dependent on mixing temperature and time. Microscopic observations indicated that SOCB does not act like a classical heterogeneous nucleating additive. They rather dissolve and chemically react with PET molecules as true chemical reagents to form nucleating species. A detailed chemical reaction scheme was provided by the authors. The addition of SOCB, an organic salt resulted in the chain scission and drop in viscosity of PET unlike in the case of inorganic nucleating additives such as salt. When the reaction between the polymer and the salt of benzoic acid was completed, one end contained the sodium ion and the other an ester group. SOCB which is the most soluble in PET systems is favored over sodium benzoate as a nucleating agent. The change in the chemical structure of PET was also confirmed by infrared studies.

A review of the nucleation step in crystallization of polymers by catalyst remnants was provided by Lawton [39]. PET samples were prepared by both Dimethyl terephthalate (DMA) and Terephthalic acid (TA) routes and extruded in the form of strands. The polycondensation reaction is usually catalyzed by antimony. Phosphorous was added as a stabilizer. The Mn, P, Sb and Na content were measured by elemental analysis. Because of the higher nucleation activity, T_{ch} is insensitive to nucleating agents. DEG content and Sb concentration were the main predictors of

DSC response while other catalysts made insignificant contribution. Phosphorous exhibited a negative effect on crystallization potential.

Apart from organic and inorganic nucleating agents, polymeric additives were also tried for their ability to nucleate any other polymer. A liquid crystalline polyester (LCP - 60 mole% HBA (poly(hydroxy benzoic acid)) and 40 mole% PET) was solution blended and also melt mixed with PET at different ratios [40]. It was observed that the crystallinity was well developed in films cast from solution. The distinct exothermic peak of amorphous polymer was missing in the case of solution cast PET. In the case of melt crystallized PET, the heating experiments showed that the T_{ch} decreased on increasing the LCP content from 0 to 70%. The 'window of crystallization' (difference between T_m and T_g) was shortened and the width of the crystallization exotherm narrowed. These results indicate that in fact the LCP acted like a nucleating agent for PET. At high concentration levels of LCP (30% and above), the LCP component does not really act like a modifier but rather gets diluted by PET [41]. Much lower concentrations (less than 10 weight percent) of LCP (60/40 HBA/PET) were used by Bhattacharya *et al.* [41]. The presence of solid LCP when PET is completely molten would allow LCP to act like a nucleating agent. However, ironically, the size of the spherulites in blends was found to be much larger than that of pure PET. This observation along with DSC results indicated that LCP not only acted like a nucleating agent but also participated in the subsequent growth of superstructures. Amorphous PET fibers showed no orientation while the fibers from blends showed some orientation. The liquid crystalline polyester was found to co-crystallize with PET to produce a different crystal structure. SALS studies showed ordered domains of LCP which were responsible for the nucleation of PET. The

crystallization rate of PET with LCP was observed to be much higher than that of pure PET.

In another investigation [42] LCPs of different kinds (Vectra - HBA/HNA (poly(hydroxy naphthoic acid)) & Kodak - HBA/PET) were blended with PET at concentration levels ranging from 5 to 15% by weight. Similar results as that of the previous study [41] were obtained and LCP acted like a nucleating agent at levels of 0 to 5%. Excessive nucleation effect and imperfect crystals were observed at high levels of Vectra whereas the Kodak polymer acted like a nucleating agent only at low concentration levels. SEM photomicrographs showed fibrous structures in the case of LCPs and blends unlike that of PET which had no unusual superstructures. Linear low density poly(ethylene) (LLDPE) and poly(propylene) act as efficient nucleating agents for PET [43]. They also reduce the viscosity and improve the processibility. Low molecular weight poly(propylene) (LMWPP) was tried as a nucleating agent for PET [43]. Both isothermal and dynamic crystallization studies were done with LMWPP and PET of 0.95 I.V. The concentration of the nucleants was 3 weight percent. Primary crystallization (cooling from the melt) and secondary crystallization (heating from the glassy state) were studied using DSC. Since LMWPP solidifies at a higher temperature compared to LLDPE, the former one was thought to be establishing heterogeneous nucleating sites rapidly. Inherent transitions, the T_g and T_m were unaffected by the presence of additives but the cold crystallization exotherm appeared at a much lower temperature for nucleated resins.

The crystallization kinetics of PET blended with naturally functionalized triglyceride oil was studied by Barrett *et al.* [44, 45]. The unsaturated ester group in the castor oil and Vernonia oil was used to chemically react with PET to form

interpenetrating networks (IPNs). A PET of 0.6 I.V. was blended with triglyceride oil and sodium benzoate at 290°C in a Brabender Plasticorder Torque Rheometer (90 wt % PET with 10% oil or 1% sodium benzoate or both). The crystallization behavior of PET was affected by plasticizing effect of the oil, nucleating additives, ester interchange reactions, compositional difference, and the presence of IPN network. The crystallization rate of PET was improved when cooling from the melt and also when heating from the glassy state. The copolymer formed by the bond interchange facilitated the formation of chain folding that influenced crystallization from the melt. The mobility and plasticization effect of oil improved the crystallization while heating from the glassy state. Synergistic effects were obtained by adding sodium benzoate. Vernonia oil took more time to copolymerize with PET (slower crystallization) compared to castor oil network.

2.5. Effect of Stress and Strain on the Crystallization of PET

When a polymer melt is strained, linear primary nuclei are formed, reducing the entropy between the chains in the crystalline and amorphous phases [46]. The crystallization proceeds at a much faster rate compared to that in the unstrained melt. Thus under identical conditions of spinning, straining results in an increase in the nucleation and growth rates due to increased supercooling effects. The resulting morphology is also totally different. In fiber spinning, increasing the take-up speed above 3000 m/minute results in shish-kebab structures. The shish consists of extended linear polymer segments in the form of a bundle. The overgrowth kebab is assumed to be made of folded chain lamellae grown at right angles to the fiber axis in the form of a cylindrite thus making the structure highly anisotropic. The high strength and modulus of fibers spun at speeds above 3000 m/minute are the result of

the above mentioned morphological feature. Drawing results in the transformation of spherulites into microfibrils. In fiber spinning, one observes a purely jet flow with a significant longitudinal gradient. Within the die of reducing cross-section, the material experiences both transverse and longitudinal velocity gradients. Once the material exits the die, the longitudinal velocity gradient takes over until the material solidifies. Thus, at slow spinning speeds, the fiber has a predominantly spherulitic structure that transforms into shish-kebab structure at high take-up speeds [46]. The steady-state orientation and extension of chain molecules in a jet flow with longitudinal and transverse gradients depends on a dimensionless parameter

$$\beta = M\tau/NkTc \qquad \text{----------} \qquad (15)$$

where M is the molecular weight, τ is the stress (viscosity x shear rate), N is Avagadro's number, k is the Boltzmann constant, T is the absolute temperature and c is the concentration. In most technical cases, $\beta < 0.5$ which is very much less than that for full chain extension although the reduction in fiber diameter could be as high as 100. This fact was confirmed by Yeh [47]. The fraction of fully extended chains is about 1 percent for a draw ratio of 5 for a molecular weight of 30,000 or so. A detailed account of the differences between stress-induced crystallization (SIC) and thermally induced crystallization (TIC) was provided [47]. The characteristics of SIC include melting point elevation, high crystalline orientation (≈ 1), faster rates of crystallization ($t_{1/2} < 1$ second) and the fibrillar morphology. Natural rubber and gutta-purcha were taken for the studies on strain and thermally induced crystallization. It was concluded that SIC always results in a fibrillar structure once a critical strain is reached regardless of applied strain, unlike other studies that proposed the transformation from lamellar to fibrillar structure with increase in take-up speed. Strain induced crystallization, usually, does not occur in polymers when stretched from the glassy state because of the lack of molecular mobility. But

polymers like PET and polycarbonate show improvement in atomic packing on stretching. The molecular orientation is much higher in the glassy state because of limited relaxation. Thus, there are distinct differences between SIC in melt and in glass.

The basic morphological feature of a strain-induced polymer is fibrillar, regardless of applied strains, and regardless of whether it is stretched from the melt or from the glassy state. Fibrillar to lamellar transformation was found to occur on further heat treatment of the stretched polymer [48]. The tendency towards lamellar formation is dependent on the annealing conditions (strained vs. relaxed), molecular weight, degree of crystallinity and cross-linking. PET films were used to study the effect of different annealing conditions [48]. It was observed that the origin of lamelle (kebab) is related to temperature changes. The driving force for lamella formation is the lowering of free energy by lateral alignment of the crystallites in neighboring fibrils. Thus the theory of chain folded material [49] changing to shish-kebab type was ruled out and the resulting morphology is due to shish-kebab transformation.

Spruiell *et al.* [50] have investigated the process of strain induced crystallization and crystallization during annealing treatments of deformed bulk PET films. The effects of deformation below and above T_g on crystallization were studied. Straining the polymer below T_g resulted in a neck formation and an increase in strain rate resulted in a corresponding increase in crystallinity. Samples strained and then annealed at 80-105°C at short times exhibited lower crystallinity than before annealing, suggestive of crystallite melting and stress relaxation. The orientation of samples strained below T_g and then annealed were retained. Two deformation

regimes were identified for samples strained at temperatures above T_g. Regime I, where the strain rates and stress levels are higher, accompanied by necking. Deformation in this regime resulted in a high degree of orientation and crystallinity (stress-induced regime). Regime II, referred to as the flow regime where low stresses, orientation and little crystallization prevailed without necking. In order to get to the same levels of crystallinity at higher treatment temperatures, the strain rates had to be increased proportionately. Strain rate is very critical in the formation of nuclei and subsequent growth. The crystallite size increased with strain rate. Stress appears to be more important in the crystallization process than the amount of strain. It was concluded that stress induced crystallization occurs in PET with necking and that it occurs at a given temperature when the strain rate is sufficient to generate a critical stress level.

The importance of characterizing the crystalline and amorphous phases of PET films was stressed by Heffelfinger *et al.* [51]. X-ray studies were conducted on PET films to study the crystalline regions and infrared studies on the amorphous region of the polymer. PET has two macromolecular conformations. Trans or extended chain conformation that exists in the crystalline phase and gauche or coiled conformation that exists in the amorphous phase. It is the fraction, distribution and packing of these conformations that affect the crystallinity and associated mechanical and thermal properties of PET films. The samples were uniaxially and biaxially stretched and then annealed. The films were stretched in the machine direction to get a film with fibrillar structure. The crystallite length was found to increase with increase in stretch ratio. Infrared studies showed that the amorphous films had 13% trans structure and 87% gauche structure and that the increase in trans content was dependent on the stretch ratio. Balanced films were obtained by stretching the

machine direction stretched films in the transverse direction. This way the (100) planes of the crystallites were forced into better parallelism with the surface of the films. The structure thus produced was stabilized by heat setting. The resultant properties depended on whether the films were annealed under tension or not. The molecular chain segments were drawn taut by stretching the balanced films in the machine direction again. The crystallite lengths remained unchanged but the long spacing increased. Thus, the factors responsible for film properties were the kind and perfection of crystalline orientation, amount and direction of trans-gauche isomers in the amorphous phase, and the degree of crystallinity.

A study on the superstructure of amorphous PET films drawn above and below T_g using light scattering and optical microscopy was performed by Misra *et al.* [52]. Cold drawing of PET produced a necked region with high amount of orientation and crystallinity and an unnecked region with little or no orientation and crystallinity. Annealing of these samples caused chain folding to occur on the already present folds that act like nuclei. Low-angle light scattering and optical microscopy showed that drawing below T_g resulted in superstructures in which the oriented rods were dispersed in an oriented amorphous matrix. Annealing at fixed length did not change the superstructure although the crystals became more perfect. On the other hand, annealing without tension, resulted in a spherulitic morphology. The superstructure was observed to be volume filling in the undrawn and non-volume filling in the drawn cases. Thus, cold drawing PET resulted in the formation of rod-like superstructures surrounded by imperfect extended chain crystals. Stretching PET above T_g provided information about the structure that formed due to strain induced crystallization only since the thermal crystallization was negligible. At low elongations, a rod-like structure existed that did not contribute to crystallinity, but

was oriented in a direction perpendicular to stretching. At high elongations, the rods changed into ellipsoidal spherulites that are elongated normal to the stretching direction.

The deformation mechanisms of PET were theoretically and experimentally investigated in terms of molecular orientation and structural deformation using light scattering, X-ray diffraction and birefringence techniques [53]. It was concluded that stretching an undrawn film of high crystallinity (43%) resulted in an affine deformation of spherulitic superstructures whereas that of an undrawn film of low crystallinity (3%) resulted in crystallization leading to row-nucleated sheaf-like texture whose rows were oriented normal to the stretch direction. When the films were stretched below T_g, the strain increased considerably and did not relax with further increase of extension ratio, resulting in a high amount of orientation of chain segments [53]. On the other hand, on stretching polymers above T_g, the strain relaxed and the orientation was gradual. Below T_g, the crystallites acted like crosslinks between chain segments and above T_g, the number of connecting segments decreased in amount. The degree of molecular orientation, and hence the physical properties of PET is dependent on the strain rate, extension ratio, molecular weight and elongation temperature [54]. The degree of orientation is related to molecular weight of PET. For higher molecular weight materials, higher orientation temperatures should be used achieve high levels of orientation. Mechanical properties are related to molecular orientation. Biaxial stretching would result in strain induced crystallization that is dependent on strain rate and temperature. Shrinkage properties are related to the morphology and degree of crystallinity due to strain induced crystallization.

The structural changes that take place during stretching of oriented crystalline PET films were studied using rheo-optical FTIR [55]. The main mechanism of deformation in the case of freely annealed samples was observed to be that of chain folding followed by the molecular slip of chains whereas in the case of taut annealed samples, longitudinal slip was observed to be the main mode of deformation. FTIR was also used to observe the molecular changes that take place during stretching of PET yarns [56]. The main mode of deformation is the unfolding of chains. The gauche content (898 cm^{-1}) was observed to diminish on stretching. The deformation mechanism was correlated well with the mechanical properties of PET yarns. The effect of winding speed on the physical structure of PET films was studied by Heuvel *et al.* [57]. There was a sharp increase in the overall density at take-up speeds above 3500 m/min. DSC results showed that the crystallization exotherm was beginning to vanish at speeds above 4500 m/minute and that the distinction between T_g and T_{ch} was unclear. The melting peak was observed to be sharper with an increase in take-up speed. X-ray photographs showed an amorphous halo for speeds below 3000 m/min. At higher speeds, there was an increase in orientation and crystallization reflected by sharper points in the X-ray pattern. The crystal size also increased with take-up speed along with the crystalline orientation factor (f_c). Structural models of yarns spun at different speeds were also proposed. The absence of any kind of diffraction pattern from SAXS measurements indicated that the crystals were not of the folded chain type. This confirmed the view point that the strain induced crystallization is more of intermolecular character than thermally induced crystallization. An increase of 0.1 in specific viscosity corresponds to an increase of 500 m/minute in winding speed. The important parameters that affect strain induced crystallization during spinning are temperature, shape of the orifice, method of cooling, drawing and denier.

The physical structure of fibers is drastically altered by changing the process conditions during melt spinning [58]. It was observed that little or no crystallization takes place at the highest spinning speed (10% at about 1500 m/minute) and this was little affected by throughput rate or spinning temperature. The fibers spun at maximum speed cooled most rapidly. Considerable crystallinity levels were obtained during isothermal spinning especially when the take up speed was increased. The temperature at which the maximum rate of crystallization occurs was observed to be higher in the presence of stress in the spinline. The critical stress required for any crystallization to occur was found to be 0.08 - 0.09 g/denier [59]. Structure development during low speed isothermal spinning was observed to be similar to that of high speed spinning [60]. The windup speed and residence time of fiber in the oven influenced the final percent crystallinity value and orientation. The increase in rate of crystallization due to mechanical deformation above Tg was examined. An explicit equation for spherulite growth rate was developed in terms of experimentally measurable quantities.

The rate of crystallization of PET was observed to be highly dependent on orientation [61]. Nucleation and growth of crystallites occurred in milliseconds in oriented PET compared to minutes for unoriented PET. The main effect of orientation was to bring the molecular chain segments close together to reduce the configurational entropy thereby reducing the induction time for nucleation and crystal growth. The Avrami equation could not be used to describe the crystallization behavior of oriented PET. The orientation of crystals in semicrystalline samples depends on the orientation of amorphous segments prior to crystallization. The effect of molecular orientation on the crystallization rate or half time was clearly seen at

higher crystallization temperature. Orientation factors were observed to be different during the course of crystallization because of the change of orientation in the amorphous phase. The shrinkage and chain folding in drawn PET fibers were studied by Wilson [62]. The overall shrinkage process involved a rapid shrinkage due to the disorientation of frozen amorphous segments that results in fiber shrinkage. If the time and temperature are appropriate this is followed by crystallization. It was concluded that there is no cause and effect relation between shrinkage of fibers and chain folding. These results were confirmed with infrared studies. The shrinkage was also correlated with tensile modulus and birefringence.

The role of stress induced crystallization on the dimensional stability of uniaxially drawn PET films was studied by Mascia *et al.* [63]. It was concluded that the level of shrinkage is independent of temperature upto 150°C. The thermal shrinkage was the highest for 2:1 draw ratio for a drawing temperature of 100°C and below the glass transition temperature of PET. The drawn samples became dimensionally stable as indicated by the total percent crystallinity value of 43% that could be obtained only by annealing. A very high correlation between the birefringence value and exothermic enthalpy was obtained for all drawing conditions. If the drawing temperature is relatively high and the strain rate is low then PET fibers/films will stretch with no resulting orientation due to molecular relaxation. This is called flow drawing. The fibers spun at 1000 m/minute, and the films, exhibited flow drawing because of the low degree of preorientation at 20 to 30°C above their T_g. The drawing tension became zero and the samples were isotropic. The partially oriented yarn spun at 3000 m/min. with preorientation did not exhibit any flow drawing.

2.6. PET/LCP Blends

The thermotropic liquid crystalline polymers (TLCP) are widely used in blends with other compatible engineering polymers in the range of 5 to 30 weight percent [64]. The addition of LCP results in enhanced processing and reinforcement of the base polymer. The disadvantages are prohibitively high resin cost, special processing equipment and brittleness of the polymer blends. However, these LCPs find usage in high value added products where performance overrides the price. LCPs are commercially used in the form of films and fibers. A review on this subject was provided by Dutta *et al.* [65]. The literature on polymer/LCP blends is found to consist of the phase behavior and thermal studies, the miscibility of blends, and the morphology of blends. The addition of small amounts of LCP significantly affects the processibility and a reinforcing microfibrillar morphology is obtained. However, the interfacial adhesion between the components was observed to be very poor resulting in highly anisotropic and brittle materials. The crystallization behavior of HBA/ HNA LCP was studied by Kamal *et al.* [66]. It was observed that two crystallization mechanisms become operative; a rapid crystallization that indicated a rod-like growth of crystals with an Avrami exponent of 2, and a slow crystallization process where the degree of crystallinity varied linearly with the logarithm of time. The values of the thermodynamic properties like heat of fusion (ΔH_m), entropy of fusion (ΔS_m) and specific surface energy (σ_e) were found to be much lower than those of flexible polymers.

The high strength and modulus of fibers/films of PET/LCP blends is due to the molecular orientation of the mesophase during processing [67]. The unique properties of LCPs are their reinforcing nature and the ability to reduce the melt

viscosity of the concerned polymer systems. The phase behavior of blends of a liquid crystalline and a non-liquid crystalline polyester was studied using DSC, dynamic mechanical analysis (DMA) and optical microscopy [67]. Blending did not result in any change in transition temperatures (T_m & T_i) of the components in the solid and the melt region. The enthalpy (ΔH_i) and entropy (ΔS_i) of isotropization were found to decrease with the addition of the second component. However, when these results were normalized with the basis weight of repeat units of the first component, no decrease was observed. Thus, it was concluded that the two components remained separate, thermodynamically stable, immiscible phases throughout the temperature changes for the different compositions studied. On the contrary, phase inversion was observed at only 60 weight percent of the second component. It was also concluded that although phase separation existed at all compositions studied, the extent of microphase separation was beyond the resolution limit of the optical microscope used. Annealing of the blend (50/50 wt/wt) at 125°C did not affect the texture of the specimen. LC polymers formed the dispersed phase with the non-LC component forming the continuous phase.

The effect of blending temperature, composition and shear rate on PET/Vectra A900 LCP blend viscosity and morphology was studied by Perkins *et al.* [68]. At any given shear rate, the maximum in melt viscosity occurred for the lowest LCP content and an intermediate blending temperature. This effect is highly pronounced at low shear rates. At a given temperature, increasing LCP content up to 50% resulted in a drop in melt viscosity because of the predominant LCP-rich morphology. SEM studies confirmed that for a 58% PET and 42% LCP composition that LCP was dispersed as droplets in the PET matrix. This trend was reversed at low shear rates between 42% and 60% of LCP and the viscosity was found to increase. A co-

continuous morphology was observed that was not ideal for melt viscosity reduction. However, at high shear rates, an increase in LCP content was found to decrease the viscosity monotonically. As the LCP content was increased to 77%, the viscosity dropped again, due to a two-phase morphology where PET was dispersed as elongated and oriented globules.

Blends of PET with several LCPs were studied for their thermal and phase behavior [69]. It was concluded from the DSC results that there was no transesterification between PET and LCP either during extrusion or during DSC scans. The crystallization temperature on heating (T_{ch}) decreased and the degree of crystallinity increased on adding LCP to PET indicative of LCPs nucleating effect. The strength and modulus was low at a 2% level of LCP due to the lack of fibril formation. The strength and modulus showed a maximum at 10% LCP due to the elongation of LCP phase in the PET matrix. At 20% LCP level, the strength and modulus dropped again as the bonding between LCP and PET matrix was lost. The factors that affect the fibril formation include the residence time, concentration of dispersed phase, miscibility of the blends and die shape. For fibril formation, the viscosity ratio should be close to unity or less. At higher viscosity ratios, the deformation of the LCP phase becomes difficult. The composition is another factor that determines which material forms the dispersed and which forms the continuous phase. The effect of blend ratio and stretch ratio on the morphology of the LCP phase in extruded films and strands were studied [70]. The LCP was crystalline and oriented whereas PET was amorphous and unoriented. The LCP in the skin portion had higher orientation and fibrillar structure compared to the LCP in the core portion of the strands which had spherical structures. The LCP phase in all LCP/PET blends became thinner and had higher orientation with increasing extension ratio. The

strands at low stretch ratios contained many uneven fibrils and sometimes branches or elliptical structures. The strands with very low LCP content often formed disc-like structures at the end of the fibrils.

In situ composite fibers made of LCP and PET were spun and studied for their mechanical properties [71]. In the case of low IV PET/LCP blends, the tensile strength decreased initially and then increased as the LCP content was increased. Low IV PET requires low processing temperatures that results in unmelted regions of LCP additive, explaining the low strength. However, use of higher IV PET increased the strength of the fibers monotonically. The modulus increased in both cases. Elongation, as expected, decreased abruptly with an increase in LCP content. Heat treatment of these fibers affected only the tensile strength. The thermal behavior and mechanical properties of a PET/PHB and PET blend as-spun and highly drawn fibers were studied by Mehta *et al.* [72]. The percent crystallinity was calculated according to the equation

$$X_c\,(\%) = [\Delta H_b / \Delta H^*_{PET}]\,[1/(1-b)]\,100 \qquad \text{----------} \qquad (16)$$

where ΔH_b is the heat of fusion of the blend, b is the weight percent of LCP in the blend and ΔH^*_{PET} is the heat of fusion of 100% crystalline PET. Contrary to earlier observations, both the T_g and T_{ch} were shifted to higher temperatures. The half time for crystallization of PET was observed to increase on adding LCP. LCP was thought to restrict the mobility of PET chains. Optical studies showed that LCP was well distributed in the PET matrix. Mechanical properties showed a significant increase in modulus and strength in the case of 90/10 PET/LCP drawn fibers compared to as-spun PET fibers. The effect of draw ratio, extrusion rate and spinning temperature on the mechanical properties of a PET/PHB 60 fiber was studied by Lee [73]. The draw ratio was found to have a significant influence on the tensile modulus whereas the

change in extrusion rate did not affect the fiber properties. Neither the extrusion nor the cooling temperature had any net effect on the fiber modulus.

2.7. Structure and Properties of PET Fibers

The mechanical and thermal properties of PET fibers depend largely on the crystal structure, size and orientation of the crystallites and the amorphous regions within the fiber. The crystal structure of drawn PET fibers was studied by Daubney *et al.* [74]. The unit cell that contains the repeat unit - CO. C_6H_4.CO. O. $(CH_2)_2$. O - was identified as triclinic with dimensions a = 4.56 Å, b = 5.94 Å, c= 10.75 Å and angles α = 98.5°, β = 118°and γ = 112° for a crystal density of 1.455 g/cm^3, assuming a constant amorphous density of 1.335 g/cm^3. The molecules are nearly planar in configuration. It was concluded that the high melting point of PET is due to the rigidity of the aromatic group and not due to intermolecular forces. In most drawn PET fibers, the c-axis of crystals is tilted at an angle of 5° to the fiber axis. The properties of PET fibers are highly structure-sensitive and the structure depends on the processing conditions. The way the molecular structure influences the mechanical properties was studied by Ward *et al.* [75]. PET shows two dynamic mechanical transitions: one at -40°C called γ - transition that is associated with the motion of end groups and the other at +80°C (T_g) called the β - transition that is associated with the motion of carbonyl groups. PET shows a drop in modulus at this glass temperature range. Infrared and nuclear magnetic resonance (NMR) studies indicated that the β - transition is a combination of processes that occur at the molecular level. At low temperatures, methylene groups rotate and at high enough temperatures, benzene rings participate in rotation and eventually, the whole material in the non-crystalline region participates in the molecular rotation. The influence of

crystallinity and orientation on the mechanical properties below and above T_g were studied using DMA and NMR. The β - transition peak and position were greatly affected for oriented crystalline and unoriented amorphous fibers. The longitudinal compliance was reduced by increased crystallinity and orientation irrespective of the temperature of measurement. These results were attributed to the reduction in the molecular mobility for oriented crystalline samples. The IR measurement of crystallinity was found to be much higher than that of X-ray and correlated well with birefringence measurements. It was concluded that the constant density assumption for non-crystalline regions could be incorrect. At low draw ratios, a fiber of high orientation and little or no crystallinity was produced as determined by IR dichroic measurements. Drawing results in entanglements between molecules as determined by stress-strain curve as no crystallization or chemical crosslinks occurred. Evidence for this result was also obtained from NMR studies that showed close approach of neighboring atoms. At high draw ratios, reinforcement of structure could take place through stress-induced crystallization.

The effect of annealing on the structure of drawn PET fibers was studied by Fischer *et al.* [76]. It was observed that the main effect was the perfection of crystals arranged normal to the fiber axis. The crystal size was also found to increase with increasing annealing temperatures. The cause of density difference between crystalline and amorphous regions is due to chain folding of the molecular chains at the crystal boundaries. The degree of crystallinity should be calculated using 'effective' amorphous and crystal densities that depend strongly on the crystallization temperature. The 'effective' density was found to increase on annealing. The crystal structure and morphology of crystallites in as-produced and annealed fiber samples of PET was studied using two-dimensional profile fitting of X-ray diffraction peaks

[77]. It was observed that the lengths of the a and b axes decreased and that of c axis increased on annealing. Since the crystals in as-produced PET were not in equilibrium, annealing resulted in relieving internal stress and thus a change in macromolecular conformation. The crystal sizes increased with annealing and applying tension caused the crystals to grow preferentially along the fiber axis. However, the volume of the crystallites did not increase significantly with the applied tension. The crystal modulus was found to increase with a decrease in tilting angle between c-axis and the fiber axis. A three-phase model for PET was proposed by Fu [78]. This included a crystalline phase, an amorphous phase and an oriented amorphous phase known as 'rigid amorphous' phase. Subtraction of the crystalline portion from the total X-ray diffraction pattern provided information about the structure of the non-crystalline phase. The azimuthal scattering pattern of the amorphous phase was observed to be isotropic whereas that of oriented non-crystalline phase was observed to be anisotropic. The rigid amorphous phase not only had the molecules aligned in the fiber direction, but also correlated with crystal orientation. This intermediate phase is thought to be influential in the crystal growth, and the amount and structure is dependent on the mechanical and thermal history of the fiber. Thermal analysis was done to confirm the presence of intermediate phase. It was concluded from further analysis [79] that the structure-property correlation is better explained by the three-phase model compared to the conventional two-phase model. About one-third of the X-ray diffraction intensity was observed to be due to the rigid amorphous phase. Based on SAXS experiments, the crystallites were assumed to be separated by the regions of amorphous material and both crystalline and amorphous regions were surrounded by an intermediate phase. The predicted values of tenacity and modulus of PET fibers were higher than those obtained using a conventional two-phase model.

3. Materials and methods

3.1 Materials

A solid state polymerized PET of intrinsic viscosity 0.9 was used for this study. The additives compounded with the polymer include an organic salt, an inorganic compound, a thermotropic liquid crystalline polyester and an ionomer. The chemical structure, trade name and source are given in Table 1.

3.2 Experimental Procedure

3.2.1. Injection Molding

The additives were tested for their nucleating ability by injection molding with PET and characterizing the molded samples. The process conditions shown in Table 2 were kept constant for all samples to make an absolute comparison. A total of 12 samples were produced as shown in Table 7. Prior to the runs, PET and LCP were dried at 120°C and the ionomer at 60°C for 12 hours. At first, PET was injection molded without any additives. In the successive runs, PET was dry blended with different additives in appropriate weight percentages. In between the runs, neat PET was used to purge the materials in the screw to avoid any contamination. The injection molded samples were sealed air-tight for further characterization.

Table 1. Material, Structure, Trade Name and Source.

Material	Chemical Repeat Unit	Trade Name	Source
PET	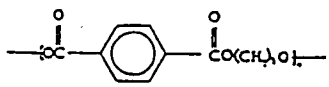	SSP	Hoechst Celanese
LCP	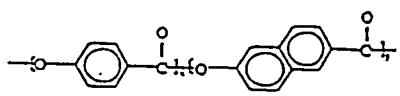	VECTRA	Hoechst Celanese
Ionomer	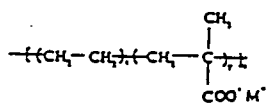	SURLYN	DuPont
Sodium Benzoate	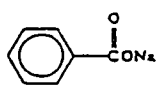	——	Aldrich Chemicals
Copper Sulfate Pentahydrate	$CuSO_4 . 5H_2O$	——	Aldrich Chemicals

Table 2. Injection Molding Conditions.

Machine Type	-	ARBURG Model No: 221-55250
Die Temperature	-	300°C
Mold Temperature	-	25°C
Screw Speed	-	200 rpm

3.2.2. Compounding of PET with Additives

The successful nucleation additives, sodium benzoate and LCP were compounded with PET pellets in a twin screw extruder. The conditions of extrusion were kept the same for all samples as shown in Table 3. A known quantity of sodium benzoate is dissolved in water and the aqueous solution is uniformly sprayed on to the pellets to ensure uniform coating. The pellets were then dried at 120°C for about 12 hours in an oven. A co-rotating twin screw type extruder was used to thoroughly melt mix PET with the nucleating additives. Initial runs of PET dry blended with additives in the hopper of a six-inch melt blowing line at TANDEC yielded poor quality webs. This is the reason for thoroughly mixing the solid additives with PET in a twin screw extruder. The compounded materials were quenched in a water bath prior to pelletizing. The pelletized samples were tightly sealed to prevent moisture uptake.

3.2.3. Melt blowing of PET Compounded with Additives

The compounded PET samples were melt blown producing fine quality webs using a six-inch wide die. The process conditions as shown in Table 4 were kept constant for the different samples produced in order to make the comparison between samples as accurate as possible. Prior to processing, the compounded PET pellets were dried at 120°C for 12 hours. Unlike our previous experience on the injection molding machine and the twin screw extruder, processing problems such as fly (short melt blown fiber floating in the air) and changes in web density were encountered on switching from PET to PET with additives. Utmost care was taken to produce uniform and soft webs with similar hand. It was very difficult to control the web thickness and basis weight of the webs produced. This could be attributed to the poor

Table 3. Compounding Conditions.

Machine Type	-	LEISTRITZ Twin Screw Extruder with co-rotating screws (34 mm diameter)
Pelletizer	-	KILLION
Die Temperature	-	215°C
Screw Speed	-	200 rpm
Head Pressure	-	4.1 to 4.8 MPa
Cooling Distance	-	10 to 13 cm in water

Table 4. Melt Blowing Conditions for PET with Nucleating Additives.

Samples Produced:		
(1) PET		
(2) PET + 10% LCP		
(3) PET + 1% Sodium Benzoate		
(4) PET + 10% LCP + 1% Sodium Benzoate		
(5) PET + 10% LCP + 1% Ionomer		
Conditions:		
Throughput Rate	-	0.4 grams/hole/min.
Die-to-Collector Distance	-	23 cm
Air Pressure	-	21 KPa
Die Temperature	-	274°C
Air Temperature	-	264°C

draw down of the LCP component in the blends. When LCP was processed alone without other materials, a poor quality web with very large but strong fibers was obtained.

3.2.4. Melt blowing of PET without Additives

In order to investigate the effect of process variables such as throughput, air pressure at the die, die temperature, air temperature and the die-to-collector distance (DCD) on the properties of the melt blown webs, PET without any additives was melt blown varying the above mentioned factors at two levels. The details of the melt blowing run are shown in Table 5. Due to the complexity of the process such as the interaction between the air temperature, air velocity and throughput, the production of control samples with similar appearance and properties was difficult. However, efforts were made to produce control webs of almost same thickness and density.

3.3. Characterization Techniques

3.3.1. Thermal Analysis

Injection Molded Samples:

A DSC 25 with a Mettler TA 4000 controller was used to characterize the injection molded specimens of almost the same thickness and a sample mass of approximately 15 mg. An inert environment was maintained throughout the scan to avoid thermal degradation. Both non-isothermal and isothermal kinetics were performed using the DSC. For non-isothermal studies, the samples were scanned at a rate of 20°C/min. PET samples were held at 300°C in the DSC cell for 3 minutes for complete melting of crystals. Cooling rates of 20, 40 and 60°C/minute were used.

Table 5. Melt Blowing Conditions for PET Webs Produced under Different Process Parameters without any Additives.

Sample ID	Throughput Rate (ghm)	Die-to-Collector Distance (cm)	Air Pressure at the die (KPa)	Air Temperature (°C)	Die Temperature (°C)
PET #1	0.3	10	10	282	282
PET #2	0.3	10	21	282	282
PET #3	0.3	10	28	282	282
PET #4	0.3	20	28	282	282
PET #5	0.3	20	28	304	282
PET #6	0.15	20	28	304	282
PET #7	0.15	20	28	288	276
PET #8	0.15	20	28	271	271

Isothermal studies were done by measuring the time taken for 50% crystallinity to develop at 232°C. A cooling rate of 20°C/minute was used to reach the desired isothermal temperature from the melt kept at 300°C for 3 minutes.

Melt Blown Samples:

A DSC 25 with a Mettler 4000 control system was used for the thermal characterization of as-produced melt blown webs without any additives. A nitrogen atmosphere was used throughout the study. A sample mass of 10 mg was used. Samples were heated at a rate of 20°C/minute from 50 to 300°C. A DSC 20 was used for analyzing the melt blown samples with additives. The same conditions of testing were followed. The percent crystallinity from the heating and cooling DSC curves was calculated according to the formula

$$\mathbf{X_c\ (\%) = [(\Delta H_{ex}/\ \Delta H_{th})\ X\ (1/(1\text{-}b))\ X\ 100]} \qquad \text{----------} \qquad \mathbf{(17)}$$

where X_c is the percent crystallinity; ΔH_{ex} is the experimental heat of fusion determined from the DSC curves; ΔH_{th} is the theoretical heat of fusion (the difference between the enthalpy of 100% amorphous and crystalline materials) determined from ATHAS tables [78] and b is the weight percent of the additive.

$$\Delta H_{ex} = \Delta H_m - \Delta H_c$$

where ΔH_m is the heat of fusion of the melting endotherm in J/g and ΔH_c is the heat of fusion of the crystallization exotherm in J/g.

$$\Delta H_{th} = H_c - H_a$$

where H_c is the enthalpy in J/g for a 100% crystalline solid and H_a is the enthalpy in J/g for a 100% mobile amorphous liquid.

It has been shown that a two-phase conventional model is inadequate to explain the fiber structure and its relation with properties. Assuming a three-phase model, crystallinity was determined by using the above mentioned equations. The experimental heat capacity (ΔC_p) at the glass transition temperature was determined using the DSC scan. The percent amorphous material present in the fibers is given by the relation,

$$\% \text{ Amorphous} = \Delta C_{pex}/\Delta C_{pth} \quad \text{----------} \quad (18)$$

where ΔC_{pth} is the heat capacity change of 100% amorphous material and ΔC_{pex} is the experimental heat capacity determined at the glass transition temperature using the DSC scan. Depending on the value of T_g (in this case, mid point), correct values of theoretical heat capacity were obtained from the ATHAS tables [80]. Finally, the rigid amorphous fraction was calculated from the relation,

% Rigid Amorphous = 1 - Crystalline fraction - Amorphous fraction -----(19)

3.3.2. Shrinkage Studies

The thermal shrinkage of melt blown PET webs was determined in the machine direction according to the formula,

% Shrinkage = [(Original length - Final length)/ Original length] X 100 ---- (20)

Samples were annealed without tension at 110, 150 and 190°C for 3 minutes in a vacuum oven. In the case of melt blown PET with additives, because of the difference in thickness of the webs, the samples were kept in the oven for the duration corresponding to the thickness of the samples as shown in Table 6. The mean thickness of 5 samples was determined. The samples annealed at different temperatures were tightly sealed for further analysis. The shrunk samples were characterized using DSC to study the amount of different entities present in the fibers.

Table 6. Shrinkage Studies.

Oven Type	-	Scientific Products DK 63
Temperatures	-	110, 150 and 190°C
Original length	-	12.7 cm

Material	Average Thickness (μ)	Treatment time (min.)
PET	211	3
PET+1% Sod. Benzoate	248	3
PET+10% LCP	863	12
PET+10% LCP+1% Sod. Benzoate	1195	17
PET+10% LCP+1%Ionomer	1479	21

3.3.3. FTIR Studies

A Nicolet 5DXC Spectrometer with a 1mw HeNe Laser source was used to study the orientation and crystallization of different melt blown fibers. Most of the web samples were thin enough for obtaining a clear spectrum. The annealed samples were also analyzed for their crystallinity and orientation. The relative changes in the trans (crystalline + amorphous) and gauche isomers present in the PET melt blown fibers, and their changes due to process variations were also studied.

3.3.4. Birefringence Studies

A Carl Zeiss Optical Microscope with a tilting compensator was used for measuring the retardation of light by the fibers. A thin section of the webs was chosen for the study. It was not possible to study the single fibers because of the high degree of bonding between fibers. Isolating the fibers was thought to induce some orientation that was not originally present in the fibers. About 15 readings were taken for each samples and the average values are reported. In all the cases, the + and - values were taken till the entire fiber became dark and the average values of retardation was noted from the tables. Using the scales in the optical microscope fiber diameter was also measured. The birefringence was calculated according to the formula

$$\Delta n = \text{value of retardation / fiber diameter} \quad \text{--------} \quad (21)$$

3.3.5. Mechanical Properties

The tensile properties of the fabrics were determined by testing 2.54 cm wide and 25.4 cm long samples in a United tensile tester (Model SSTM-1-E-PC). A gage length of 12.7 cm with an elongation rate of 12.7 cm per minute was used for the study according to ASTM D1117-80. An average of five readings is reported for each sample tested.

3.3.6. Fiber Diameter and Fracture Studies

A Hitachi S-4500 scanning electron microscope was used to determine the fiber diameter. Magnification levels were changed to obtain 20 to 30 fibers per frame. The fiber diameter was accurately measured by using a scale that had 50 divisions per 2.54 cm. Two lines were drawn at 45° and the fibers that crossed these lines were taken for measurement. An average of 100 fiber readings is reported for each sample. A PC compatible program was used for the statistical analysis of the fiber diameters. Mean, standard deviation, the coefficient of variation, the fiber diameter distribution , box and whisker plot and skewness parameters were determined. The melt blown webs were fractured in the United tensile tester and the fracture surfaces were analyzed using the SEM to determine the ductile or brittle nature and also the unusual features if there were any.

3.3.7. Physical Properties of Nonwovens

Basis weight was measured according to the ASTM method D3776-85 by cutting samples of dimensions 10.16 cm X 10.16 cm and weighing them on a Mettler

microbalance. An average of five readings was expressed in g/m^2. Thickness was measured using a TMI thickness gage according to ASTM method D1777-64. An average of five readings was reported in micrometers. Air permeability was determined using the Frasier air permeability tester according to ASTM method D737-75. A water head of 1.27 cm was used for the measurements. An average of five readings was reported in $m^3/m^2/s$. Bursting strength was tested using a Mullen tester according to ASTM method D3787-80A. An average of five readings is expressed in kPa.

3.3.8. Rheology:

A Tinius Olsen extrusion plastometer model MP 987 was used to measure the melt flow index of neat and compounded PET at 280°C. A single point newtonian viscosity was calculated for comparative evaluation between the samples. The die had a diameter of 2.1 mm and a length of 8 mm. A constant load of 2.16 kg was applied to extrude the strands. The following equations were used to arrive at the viscosity in Pa.s :

Melt flow rate (g/minute) = melt density (g/cc) X area of cross section of the die (sq. cm) X velocity of the polymer (cm/s) --------- (22)

Newtonian Shear rate (s^{-1}) = 8 [velocity of the polymer (cm/s) /diameter of the die] --------- (23)

Newtonian shear stress = 4.09 X 10^3 Pascals (Constant)

Newtonian Viscosity = Newtonian shear stress/Newtonian shear rate (Pa.s) ------- (24)

4. Results and Discussion

4.1. Injection Molded PET Samples

The non-isothermal cooling behavior of PET from the melt is shown in Figure 3. The polymer was cooled from 300°C to 50°C at a rate of 20°C/minute. As we know, ordering of polymer molecules results in a release of heat and thus the polymer crystallization is an exothermic process. As shown in the figure, two mechanisms become operative: the left hand portion of the exotherm is dominated by the nucleation mechanisms and the right hand portion by the growth and diffusion mechanisms (viscosity dependent). The effect of a nucleating additive is to shift the T_{cc}, the temperature of maximum crystallization on cooling, to higher temperatures. The T_{cc} values for injection molded PET samples with different additives are shown in Table 7. The samples were cooled at 20, 40 and 60°C/minute from 300°C to 50°C after being held at 300°C for 3 minutes. There was a shift of about 16.5°C for PET mixed with 2% sodium benzoate. The trend is the same for increased cooling rates. Thus, it is evident that sodium benzoate acts as an efficient nucleating agent in commercial PET processing where the cooling rate is of the order of several hundred degrees per minute. LCP, ionomer and copper sulfate pentahydrate alone did not show any significant nucleating ability. But, when LCP was combined with sodium benzoate, a synergism in nucleation was seen with a temperature shift of 15.5°C at a cooling rate of 20°C/minute. LCP alone crystallized at a temperature much higher than that of pure PET. However, the heat of fusion value was negligible when compared to that of PET.

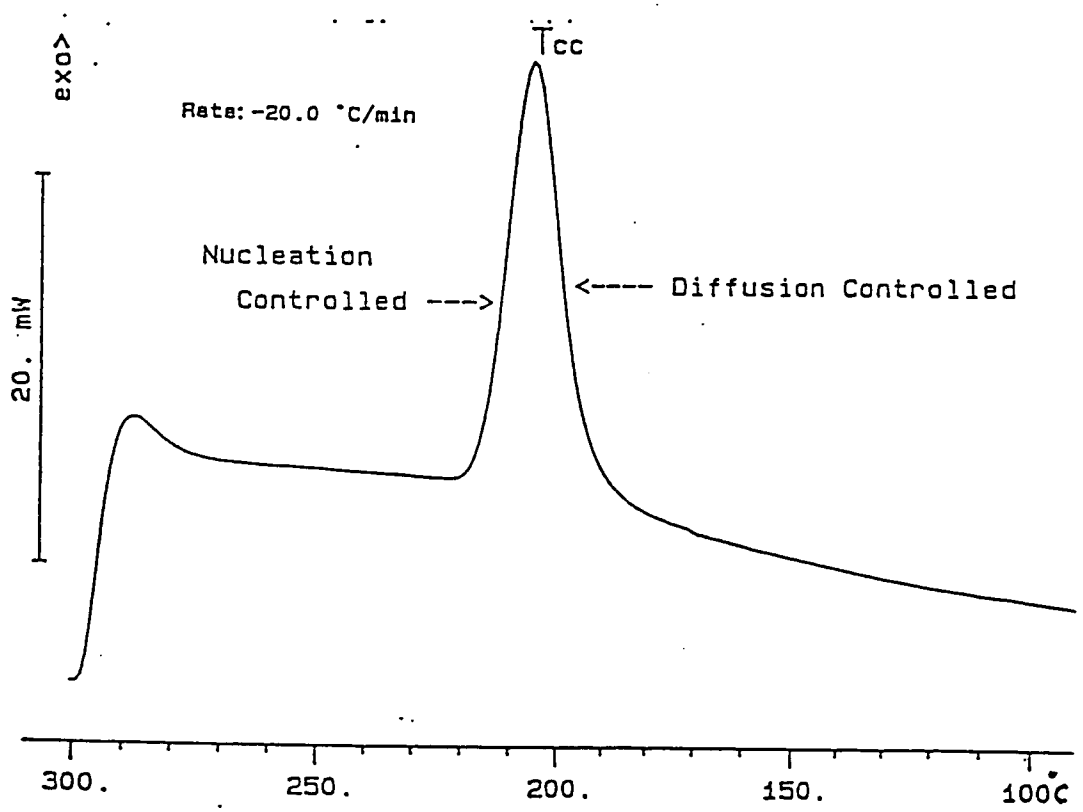

Figure 3. Crystallization Behavior of PET on Cooling from the Melt.

Table 7. Crystallization Temperatures of Injection Molded PET with and without Additives at Different Cooling Rates (from the DSC scans).

Material	Cooling Rates		
	20°C/min.	40°C/min.	60°C/min.
PET	208.2	144.6	69.9
PET + 1% Liquid Crystalline Polyester (LCP)	207.5	139.1	57.8
PET + 10% LCP (Trade name - VECTRA)	203.9	145.7	57.4
PET + 1% Ionomer (Trade name - SURLYN)	208.3	139.2	57.6
PET + 10% Ionomer	207.2	137.8	59.9
PET + 2% Sodium Benzoate	224.7	171.8	99.2
PET + 2% Copper Sulfate Pentahydrate (Cu S)	206.3	147.7	58.2
PET + 1% LCP + 2% Sodium Benzoate	223.7	171.9	109.4
PET + 10% LCP + 1% Ionomer	210.3	144.6	53.8
PET + 10% LCP + 3% Ionomer	204.1	140.6	55.7
PET + 10% LCP + 2% Cu S	203.4	132.4	37.6
LCP	234.0	190.5	139.3

NOTE : The samples were held at 300°C for 3 minutes and then cooled at rates of 20, 40 and 60 deg. C/min. The samples were also heated to 300°C from 50°C at a rate of 20°C/min.

Figure 4 illustrates the typical heating scan (20°C/minute) for an injection molded amorphous PET sample. It shows a T_g at 80°C, a crystallization exotherm at 129°C and a broad melting endotherm with a melting point at 257°C. The effect of nucleating additive is to decrease T_{ch} and increase T_m. As can be seen from Table 8, a decrease of about 11.8°C was observed for PET sample injection molded with 2% sodium benzoate. The melting point increased by about 4.2°C. The synergistic effect of adding sodium benzoate with PET/LCP blends is also seen by the reduction of about 9.6°C in T_{ch} and an increase of 3.4°C in T_m. LCP, ionomer and copper sulfate pentahydrate alone did not have any visible influence on T_{ch} or T_m. LCP had an isotropization temperature (T_i) of 276°C where the crystal to nematic transition took place. Table 8 also contains the percent crystallinity values from heating and cooling curves.

A frequent error made in calculating the percent crystallinity is the assumption that ΔH_{th} is constant over a wide range of temperatures. But, according to the ATHAS table of thermal properties [80], ΔH_{th} is in fact a function of temperature. Figure 5 illustrates the change in enthalpy of a solid (100% crystalline material) and that of a liquid (100% amorphous material) with temperature. The liquid heat capacity is always higher than that of the solid because of the unrestricted motion of the molecular segments. The theoretical heat of fusion has a cubic function with temperature as shown in Figure 6. Since the difference between the transition points (T_m, T_{ch} and T_{cc}) is only of the order of a few degrees, a linear function was assumed between consecutive points in calculating the percent crystallinity. A lower value of ΔH_{th} was obtained at T_{ch}. Assuming a constant value for ΔH_{th} would result in an error of over 20%. This correction procedure was used for every temperature while calculating the percent crystallinity values. The contribution of additives in the

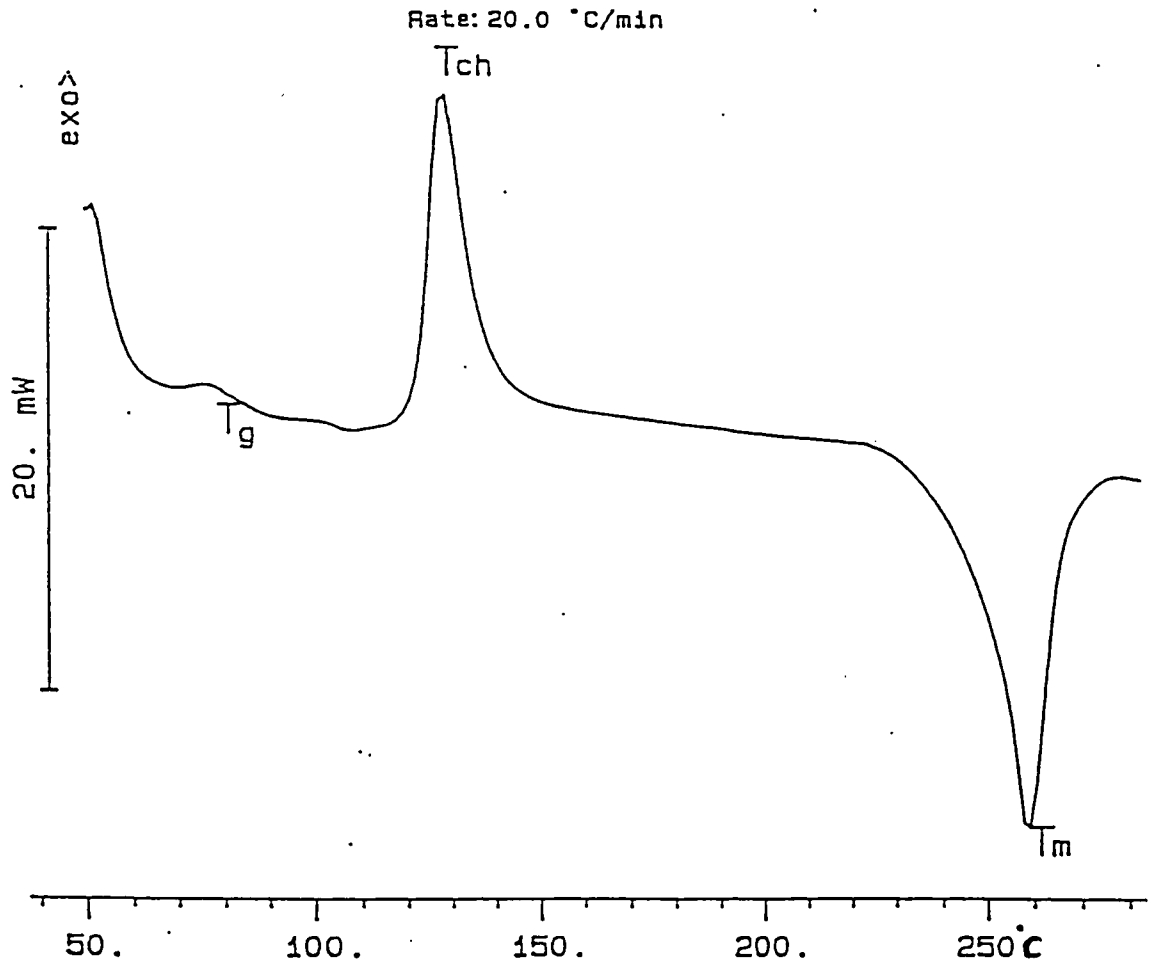

Figure 4. Crystallization Behavior of PET on Heating from the Glassy State.

Table 8. Transition Temperatures and Percent Crystallinity of Injection Molded PET with Additives.

Material	DSC Parameters			
	T_{ch}	T_m	Crystallinity on heating (%) ($\Delta H_m - \Delta H_{ch}$)	Crystallinity on cooling (%) (ΔH_{cc})
PET	129.2	257.0	N. D.	44.60
PET + 1% LCP	129.0	254.3	N. D.	46.66
PET + 10% LCP	127.7	255.9	5.86	43.37
PET + 1% Ionomer	127.8	255.8	2.43	45.95
PET + 10% Ionomer	134.1	258.3	N. D.	46.76
PET + 2% Sodium Benzoate	117.4	261.2	23.74	46.82
PET + 2% Copper Sulfate Pentahydrate	134.8	258.1	8.21	47.16
PET + 1% LCP + 2% Sodium Benzoate	119.6	260.4	10.8	48.66
PET + 10% LCP + 1% Ionomer	129.0	261.2	2.83	49.49
PET + 10% LCP + 3% Ionomer	129.0	255.9	2.03	44.11
PET + 10% LCP + 2% Cu S	124.3	261.2	9.02	50.47
LCP	-	(T_i) 276-280	negligible	negligible

NOTE : The samples were heated to 300°C from 50°C at a rate of 20°C/min.

N. D. - Not Detected
T_i - Temperature of isotropization

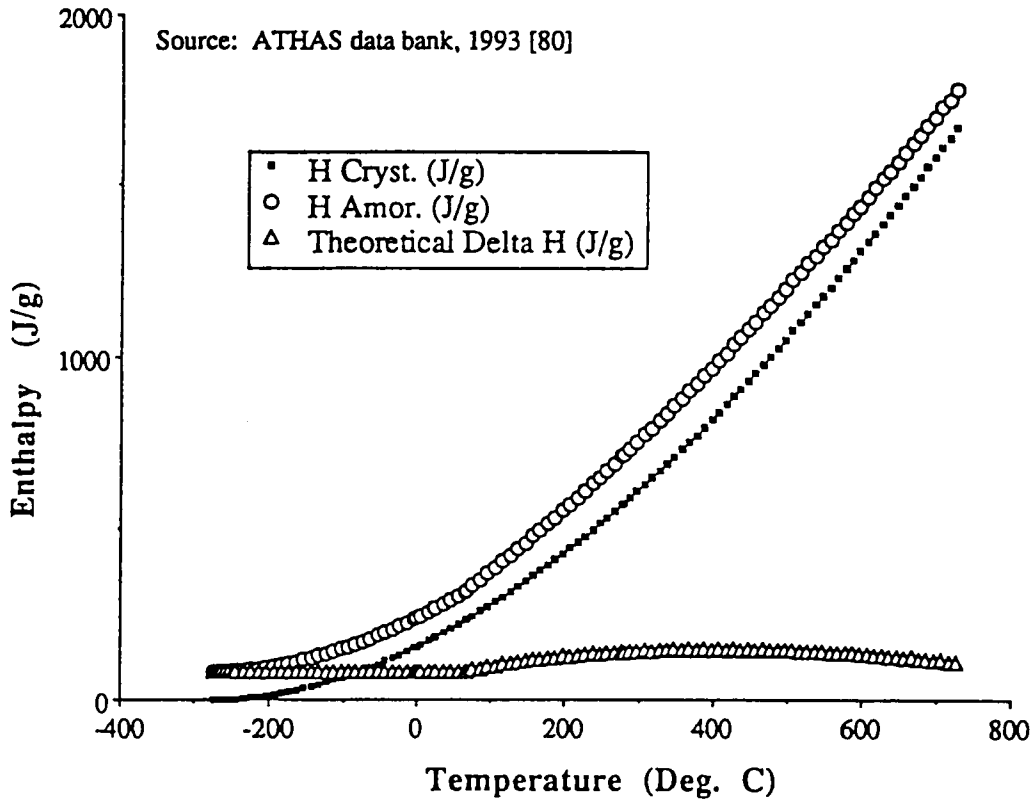

Figure 5. Enthalpy Vs. Temperature for PET (Theoretical).

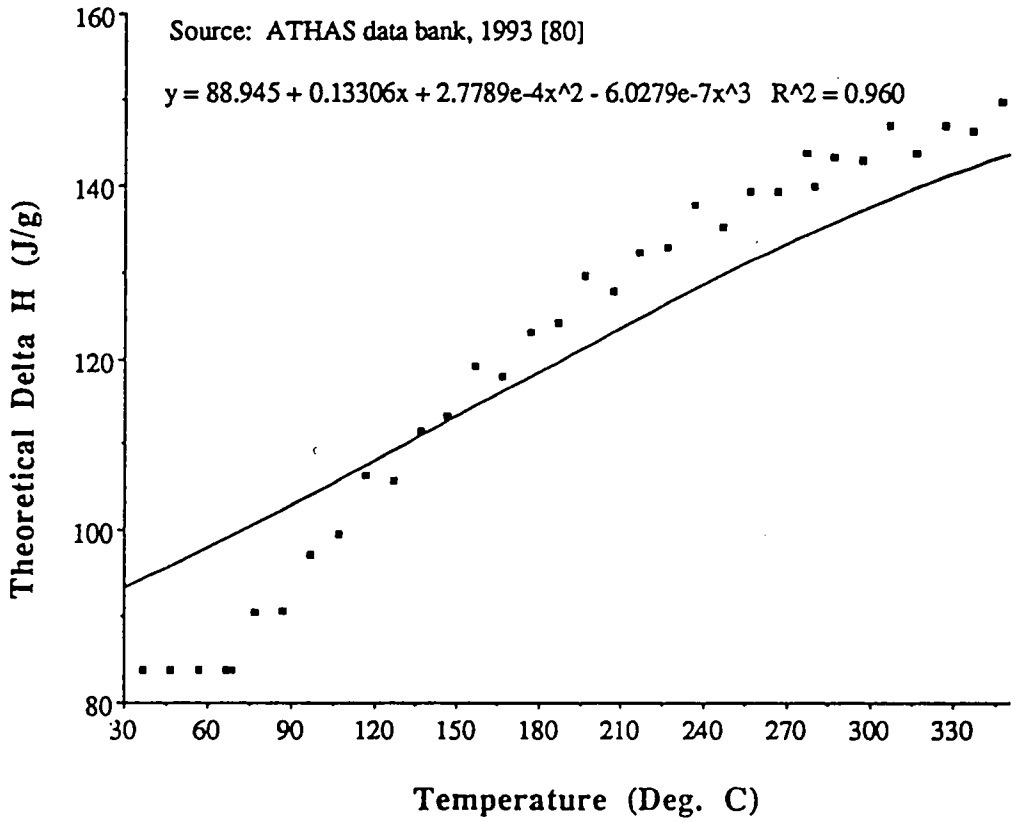

Figure 6. Theoretical Delta H Vs. Temperature for PET.

calculation was eliminated by subtracting the weight percent of additives from the theoretical heat of fusion. This way, the crystallinity values obtained were that of the PET component only.

As shown in Table 8, no crystallinity was detected for pure PET injection molded specimens, suggesting that the samples were essentially amorphous. The PET sample with 2% sodium benzoate had the higher percent crystallinity values. No crystallinity was detected for samples with low weight percent LCP. Samples with the copper sulfate additives were brittle, indicative of crystalline fraction, although it was much smaller than that containing sodium benzoate. All the samples with more than two components showed synergistic effect. The additives were chosen for compounding with PET based on their nucleation efficiency. Thus it could be seen that sodium benzoate is the most successful additive, followed by LCP, copper sulfate and the ionomer. The percent crystallinity values for different samples on cooling from the melt at 20°C/minute are almost the same indicative of the fact that although the nucleation rate increases in the case of additives, the growth rate remains the same.

The non-isothermal and isothermal kinetics determined from DSC are shown in Figures 7 and 8 respectively. The sigmoidal shape of the curves is typical of polymer crystallization. The relative crystallinity values were calculated by partitioning the area under the crystallization peak on cooling from the melt, in this case, cooled at a rate of 20°C/minute, into small areas and dividing each area by the total area of the peak. It can be seen from the figure that PET with sodium benzoate had considerably higher percent crystallinity by the time the other samples started to crystallize. This indicates the increase in overall crystallization rate of PET with

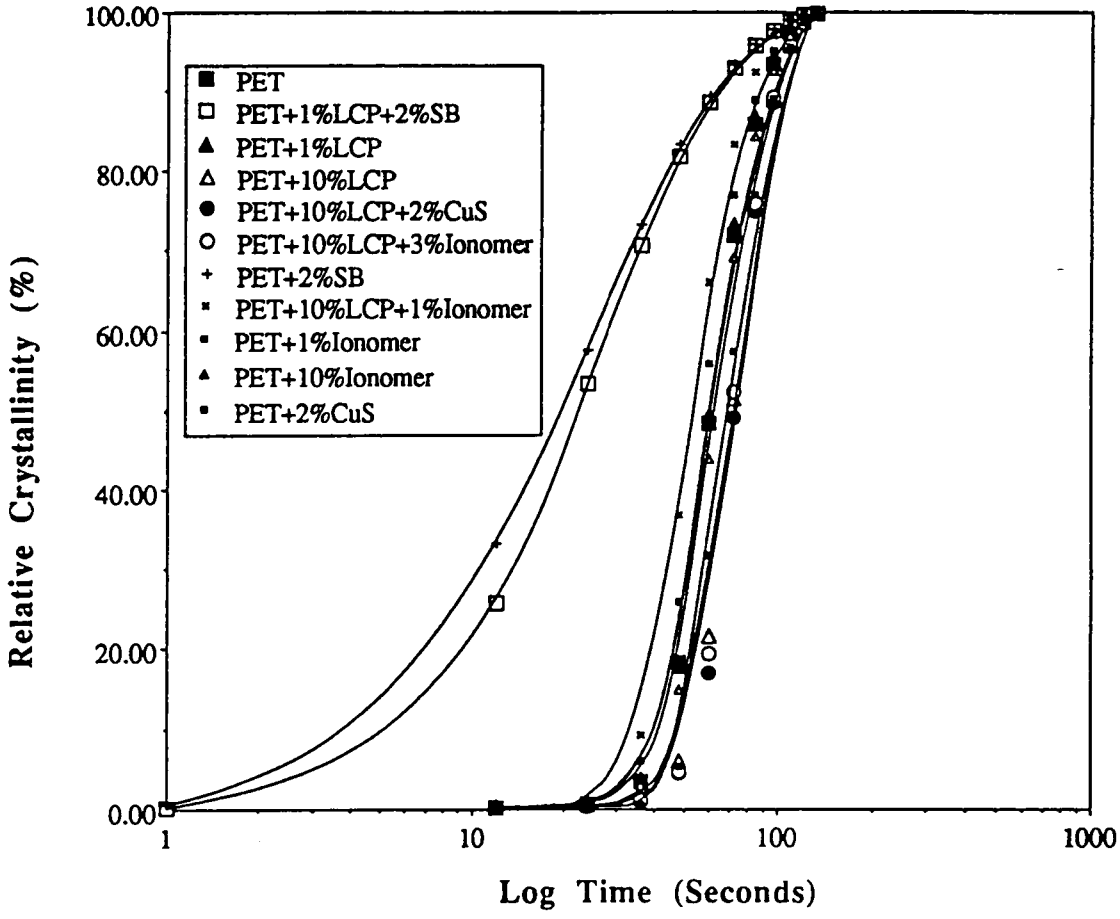

Figure 7. Non-isothermal Kinetics of Injection Molded PET Samples with Additives.

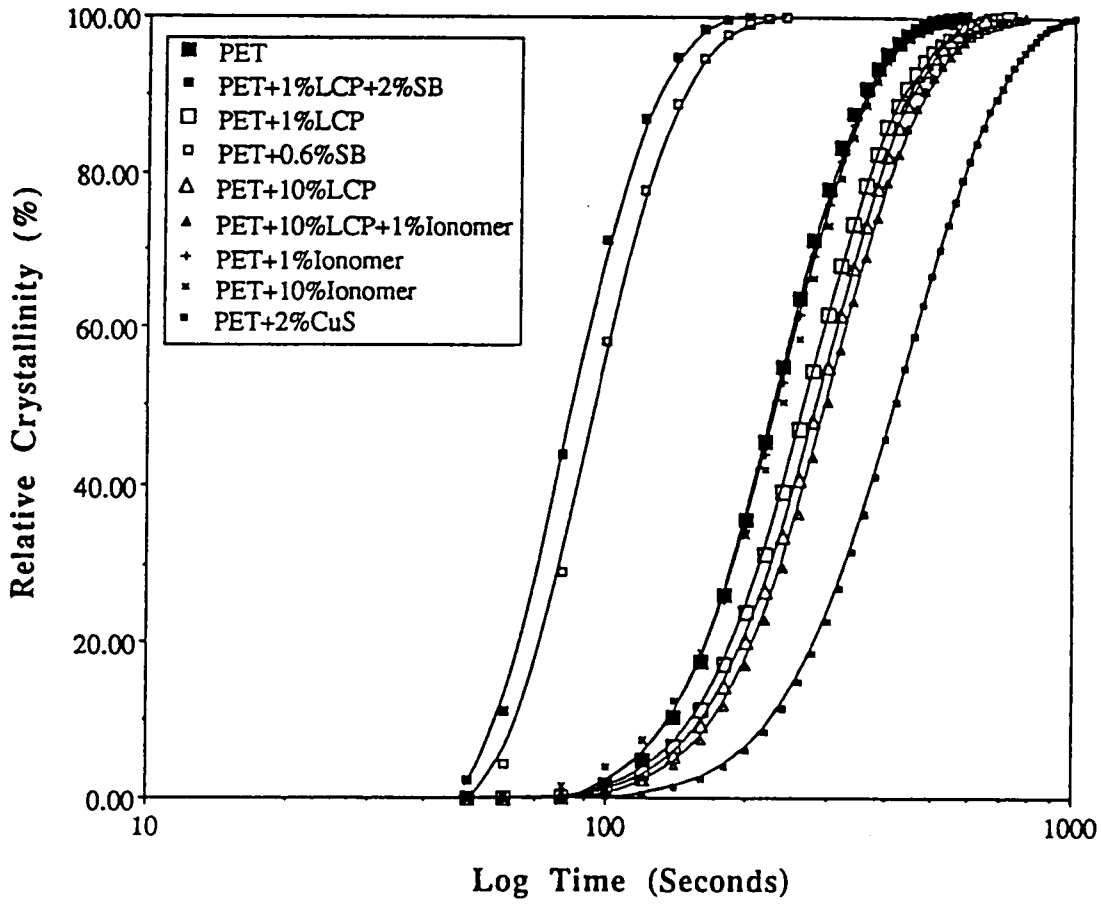

Figure 8. Isothermal Kinetics of Injection Molded PET with Additives.

sodium benzoate, and PET with LCP and sodium benzoate. samples with other additives fall in the same area as that of pure PET. Isothermal kinetics were performed at 232°C. The exotherm was allowed to reach the base line before useful calculations were made. As can be seen from Figure 8, the crystallization rate of PET with successful additives was much higher than that of the unsuccessful additives. The potential nucleating additives and their combinations were thus obtained from these experimental investigations using the kinetic studies. It was tactfully assumed that the higher crystallization rate of PET samples with additives would prevent the shrinkage of PET during further thermal treatment.

4.2. PET Melt Blown Webs with Nucleating Additives

Table 9 shows the DSC results of different melt blown webs produced under identical processing conditions with nucleating additives. Almost all the additives showed nucleating ability, as can be seen from the shift in T_{ch}. PET with 1% sodium benzoate produced a moderately crystalline web with 9.82 percent crystallinity. Other webs had essentially no detectable crystalline fraction. The additives, in fact, acted like diluents as can be seen from the reduction in T_g (Table 10). The crystals have a regular three-dimensional ordering with a definite melting point. The amorphous fractions have no order and become mobile at T_g. The rigid amorphous fractions resemble the crystallite in properties and become mobile between T_g and T_m. The as-produced PET melt blown webs have a large fraction of rigid amorphous content that may be responsible for their high shrinkage values on further heat treatment. The least shrinkage was obtained in the case of melt blown webs with PET and sodium benzoate although they had higher rigid amorphous content. Thus the shrinkage behavior of melt blown PET webs was found to be very different.

Table 9. Transition Temperatures and Percent Crystallinity of PET Melt Blown Webs with Additives.

Material	DSC Parameters		
	T_{ch}	T_m	% Crystallinity on heating (ΔH_m - ΔHch)
PET	130.4	258.6	N. D.
PET + 10% LCP (Trade name - VECTRA)	124.1	256.3	N. D.
PET + 1% Sodium Benzoate	116.2	259.2	9.82
PET + 10% LCP + 1% Sodium Benzoate	120.3	258.2	N. D.
PET + 10% LCP + 1% Ionomer	127.0	257.1	N. D.

NOTE : The samples were heated to 300°C from 50°C at a rate of 20°C/min.

N. D. means Not Detected

Table 10. T_g, Percent Crystalline, Amorphous and Rigid Amorphous Fractions and Shrinkage for Melt Blown PET with Nucleating Additives.

Material	T_g (°C)	Percent Crystalline Fraction	Percent Amorphous Fraction	Percent Rigid Amorphous Fraction	Shrinkage at 110°C (%)
PET	80.9	N. D.	18.30	81.7	30.70
PET + 10% LCP	74.3	N. D.	64.74	35.25	3.31
PET + 1% Sodium Benzoate	72.2	9.82	21.31	68.87	2.68
PET + 10% LCP+ 1% Sodium Benzoate	75.8	N. D.	54.75	45.24	7.09
PET + 10% LCP + 1% Ionomer	78.3	N. D.	31.07	68.93	2.83

Note : Shrinkage studies were done at 110 deg. C for 3 minutes in a vacuum oven

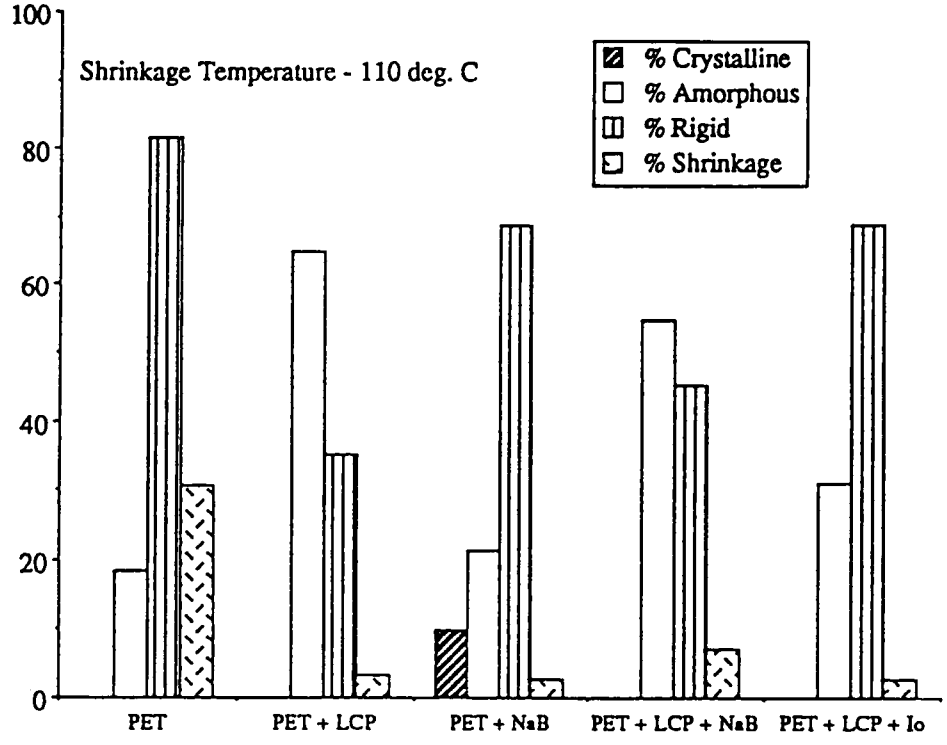

Figure 9. Relative Amounts of Different Structural Entities and the Shrinkage Values for As-produced PET Melt Blown Webs with Additives.

depending on the type of additive used and the amount of crystalline, amorphous and rigid amorphous present in the sample.

In the case of PET melt blown webs with no detectible crystallinity, the shrinkage could be attributed to the presence of large amount of oriented rigid amorphous fraction. There is no restriction on the motion of these rigid segments on exposure to heat because of the absence of crystallites as tie links. The crystallites already present in the web restrict the motion of the amorphous or the rigid amorphous molecules in the case of melt blown webs that contain PET in combination with sodium benzoate. In the case of PET melt blown fibers that contain LCP, the LCP component being of lower viscosity at the processing temperature range compared to PET, might encapsulate the PET phase forming a sheath-core composite structure. Two model structures were proposed for melt blown fibers with PET and LCP as shown in Figure 10. In both cases, the PET component is prevented from shrinking by the rigid LCP phase. Thus the shrinkage values of the melt blown webs produced from blends were lower in all the cases with LCP as reinforcing phase. In fact, fracture studies performed on the melt blown fibers made of PET and PET/LCP blends revealed the evidence of a matrix-fibril type of composite fiber as shown in the SEM pictures (Figures 11-13). The droplets of the LCP component gets elongated into discontinuous fibrils within the matrix of PET as shown in the SEM pictures.

The shrinkage studies were also performed at 150 and 190°C. There was a considerable increase in the percentage shrinkage values in the case of PET fibers that contained no additives as shown in Figure 14. Even at 190°C the fibers made of PET and additives had exceptional dimensional stability with shrinkage values less than

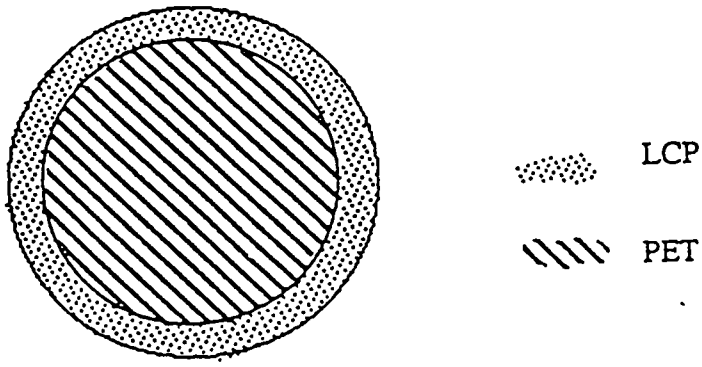

Core - Sheath Type Fiber

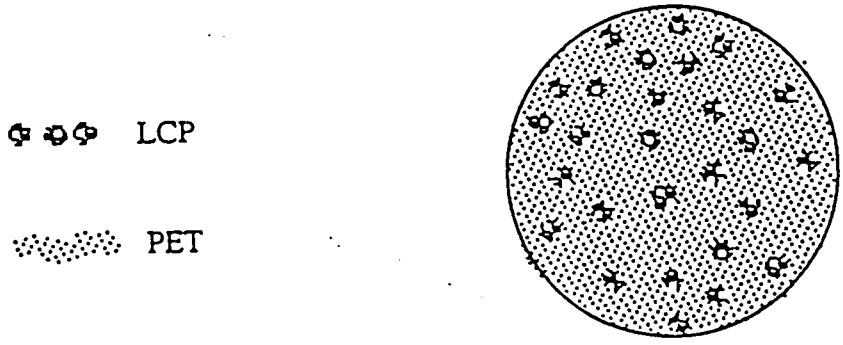

Figure 10. Proposed Models for Fibers of PET/LCP Blends.

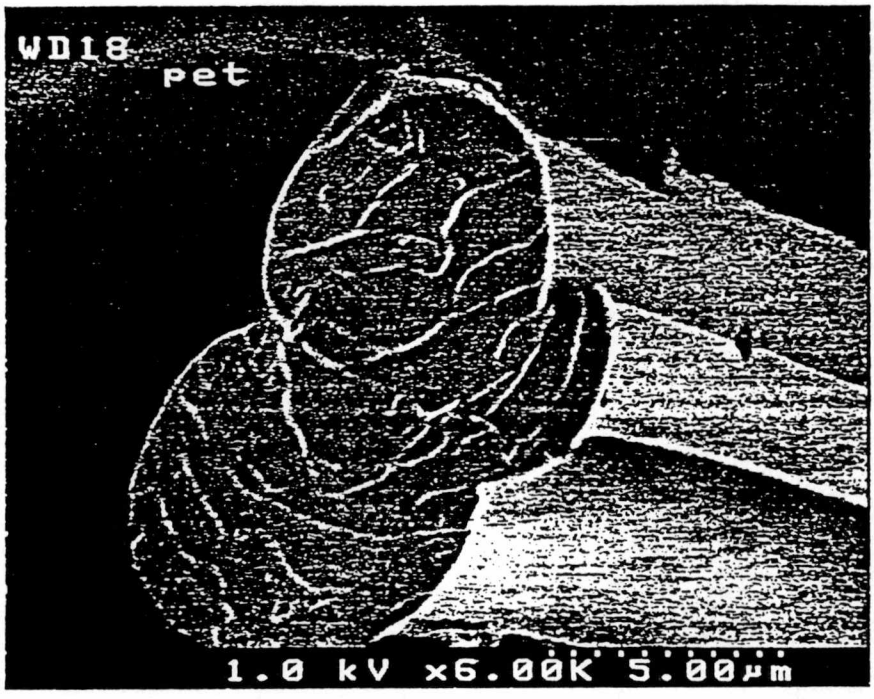

Figure 11. Fracture Surface of PET Melt Blown Fibers without Additives (X 6000).

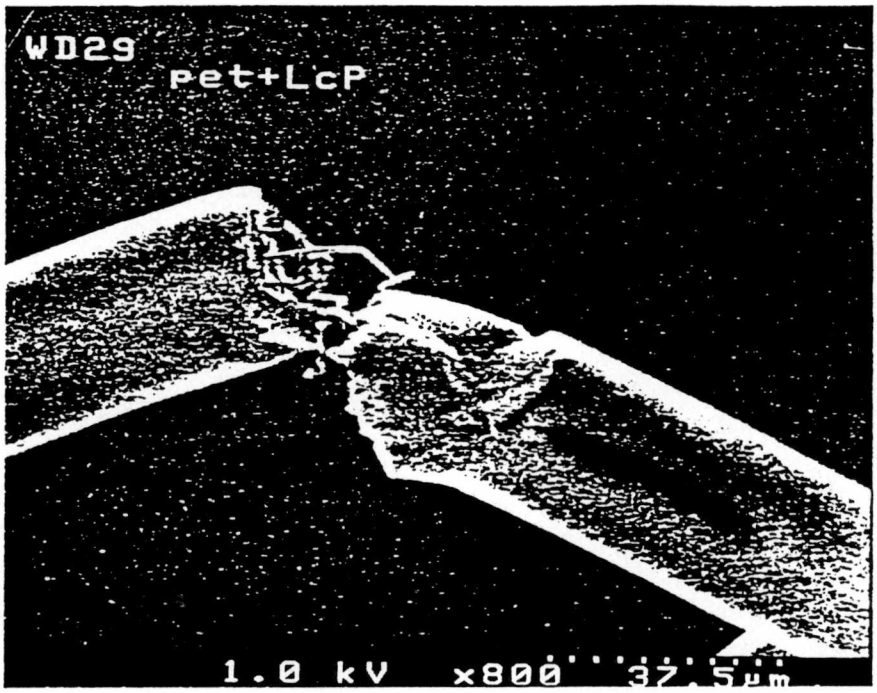

Figure 12. Fracture Surface of PET Melt Blown Fibers with LCP Fibrils (X 800).

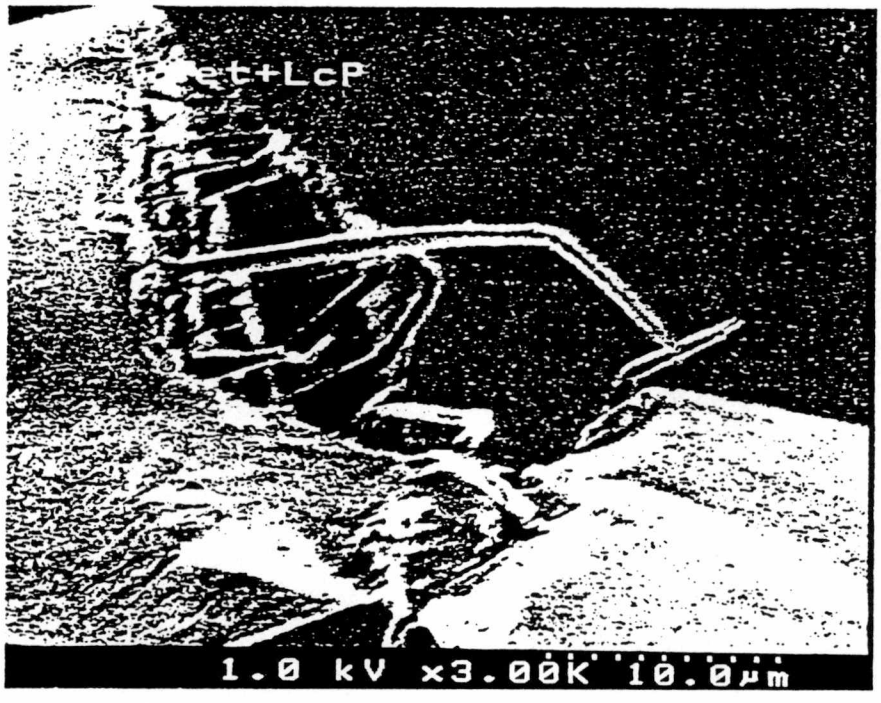

Figure 13. Fracture Surface of PET Melt Blown Fibers with LCP Fibrils (X 3000).

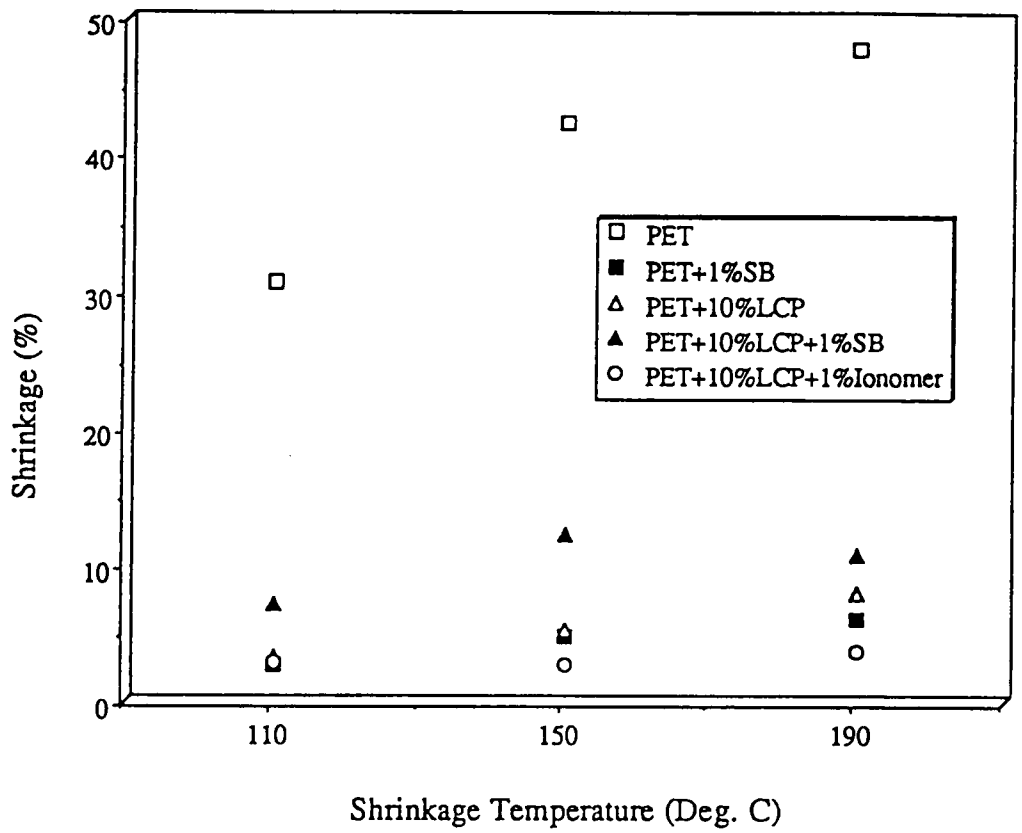

Figure 14. The Effect of Temperature on the Shrinkage of PET Melt Blown Webs.

10%. DSC was used to determine the relative amounts of crystalline, amorphous and rigid amorphous contents of the shrunk melt blown fibers. Figure 15 illustrates the change in the percent rigid amorphous content with increase in shrinkage temperature. In all the cases, the samples were annealed without constraint for the same period of time. PET fibers had considerably higher amount of oriented amorphous fraction compared to PET fibers that contained additives. Among the fibers that contained additives, PET /LCP had the lowest value suggestive of very low shrinkage values. Although, the rigid amorphous content was higher in the case of fiber that had PET/sodium benzoate, shrinkage was prevented by the crystallites present in the as-produced fibers.

The competing mechanisms of shrinkage and crystallization are evident from the above figures. The reduction in the rigid amorphous content of all samples at 110°C (shrinkage temperature) is due to the disorientation of the oriented amorphous chains. At 110°C, this is presumed to be the dominant mechanism. At 150°C, the material is already crystalline (T_{ch} being 130°C), and there is a further reduction in the rigid amorphous content. Figure 16 illustrates the increase in crystallinity of different samples on annealing. Crystallinity was detected only in the case of as-produced PET fibers that had sodium benzoate. The increase in crystallinity at 110°C of all the samples other than PET is due to the presence of more number of nucleating sites on heating from the glassy state. This is also responsible for higher percent crystallinity values in the case of fibers that contained additives at higher shrinkage temperatures. Thus in the case of PET fibers that had no additives, the shrinkage is mainly due to disorientation at 110°C and above, and the level of shrinkage is determined by the shrinkage and crystallization temperatures and times during annealing. Presence of nuclei/additives has a great influence on the shrinkage and

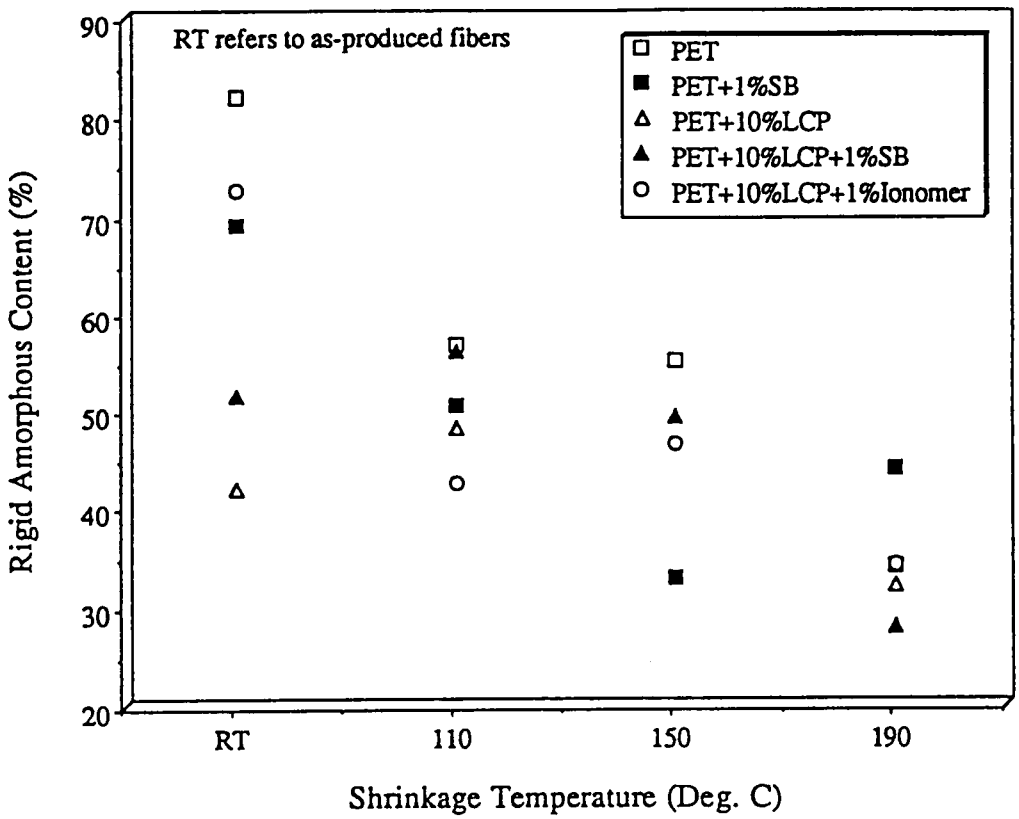

Figure 15. The Effect of Temperature on the Rigid Amorphous Content of PET Melt Blown Webs with Additives.

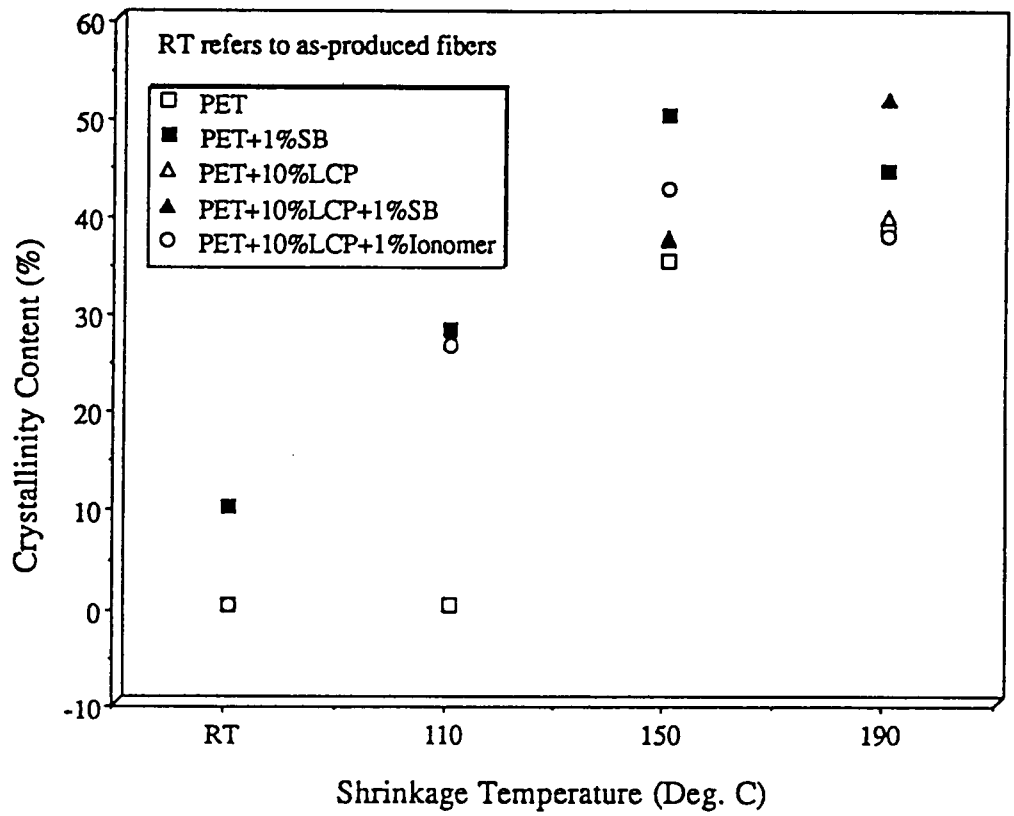

Figure 16. The Effect of Temperature on the Crystallinity of PET Melt Blown Webs with Additives.

crystallization behavior the fibers. Thus having a crystalline material to begin with is crucial in further heat treatments like annealing to prevent thermal shrinkage.

The results discussed above were also confirmed with FTIR experiments. Two peaks were identified from the previous literature on FTIR spectra of PET [23, 55, 56, 62 and 81]. These are 973 cm^{-1} for crystallization and trans content of crystalline and amorphous regions, and 898 cm^{-1} for purely gauche isomer of PET molecules. Crystallites essentially have trans isomer, whereas the amorphous materials either have trans or gauche, or both. In the case of PET fibers, any increase in the trans isomer could be attributed to the increase in crystallinity or oriented rigid amorphous molecules. The crystallinity peak 973 cm^{-1} was normalized with 794 cm^{-1} peak that was not influenced by any physical mechanism. The ratio of their absorbances was plotted against shrinkage temperature for comparative evaluation. The trend as shown in Figure 17 is similar to that observed from the DSC experiments. The reduction in the ratio of the 973 and 794 cm^{-1} peaks for PET on annealing at 110°C could be attributed to the disorientation, or reduction in the trans isomer. The influence of crystallites in the as-produced fibers on the ratio of the absorbances is clearly seen in the case fibers that contained PET with Sodium benzoate.

The ratio of absorbances 973 and 898 cm^{-1} also gives an indication about the orientation and crystallinity of the melt blown fibers. The above ratios were also calculated for ice-cooled amorphous clear film of PET that had a value of 0.61 and 0.46 for 973/794 and 973/898 respectively. This indicates that the higher values of 0.9 and above obtained for essentially amorphous PET fibers could be due to the presence of rigid amorphous segments or due to crystallites that were not detected by

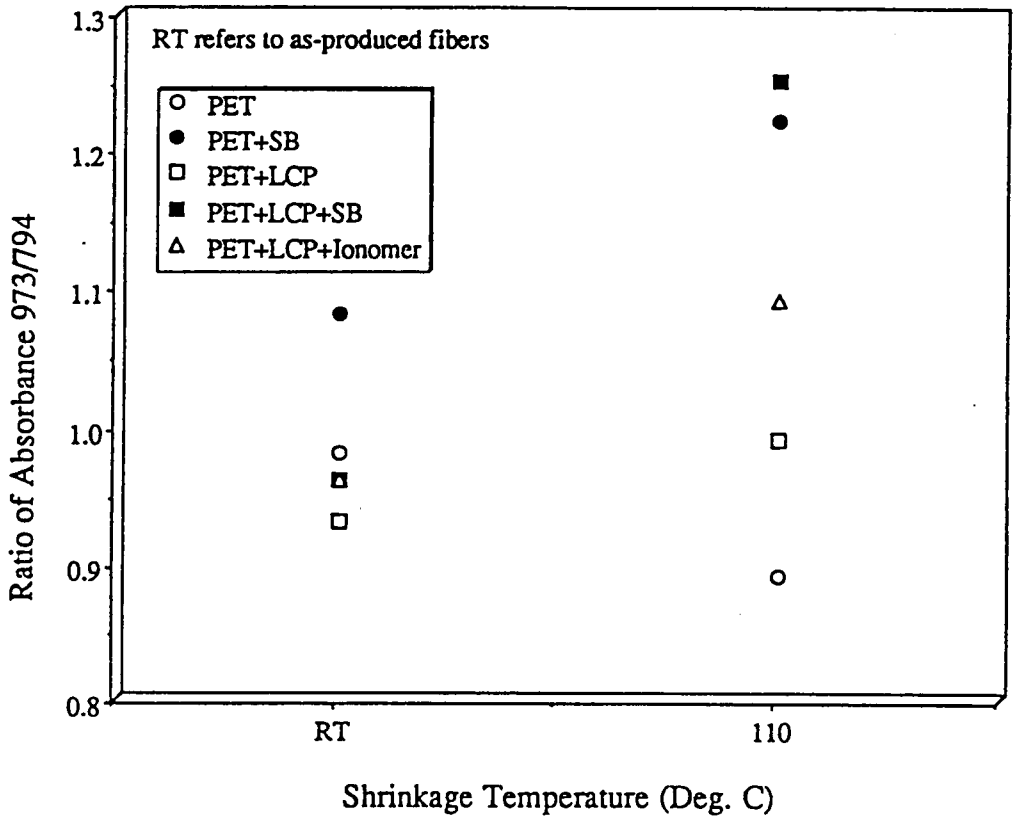

Figure 17. Absorbance Ratio 973/794 for PET Melt Blown Fibers with Additives.

DSC. It is the disorientation that is predominant in the case of PET fibers with no additives, and crystallization that is prevalent in the case of fibers that contained additives on annealing at 110°C as shown in Figure 18. PET with sodium benzoate had higher orientation and crystallinity compared to other samples.

The birefringence is a measure of orientation and as can be seen from Figure 19, PET and PET with sodium benzoate had considerably higher orientation compared to PET blended with other additives. This could be another reason for the low shrinkage values of PET/LCP fibers. The reason for higher birefringence values could be due to the smaller diameter fibers in the case of webs made of PET/sodium benzoate. Fiber diameter was measured from the SEM pictures and the results are shown in Figure 20. The mean values are shown by the dark lines and the outliers by circles and stars. The box contained about 50 percentile values. Fiber distribution is also indicated by the lengths of the box and tail. The fibers made of PET and PET/sodium benzoate had narrower distribution compared to other samples in the figure. A mean value of less than 2 microns was obtained with PET and sodium benzoate. Other samples had considerably higher fiber diameters, especially the ones that contained LCP as an additive. The reason could be that the LCP being a rigid polymer, drawing is much more difficult when compared to the PET matrix. Also as will be shown later, the reduction in viscosity on adding Sodium benzoate to PET is another reason for drawing and smaller fiber diameters that increase the orientation of the molecules. The values for mean and coefficient of variation are shown in Table 11.

Mechanical properties of the fibers/webs are seriously affected by the addition of nucleating agents. As shown in Table 12, there was a significant reduction in the

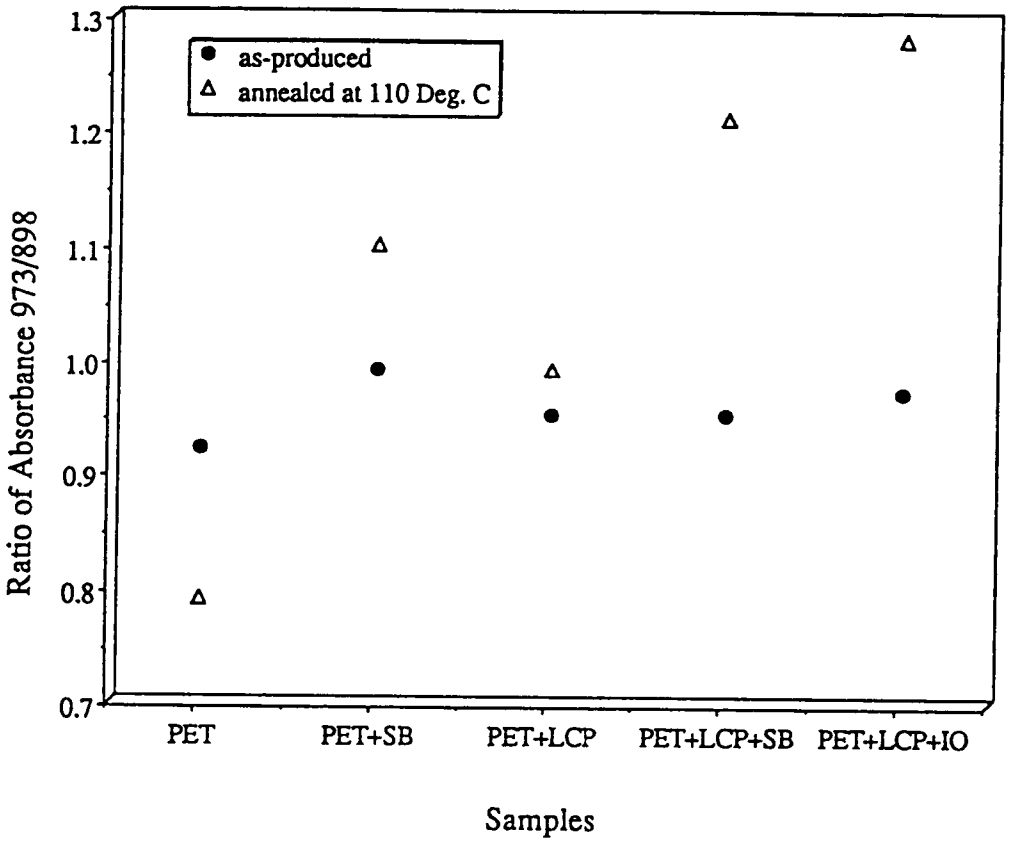

Figure 18. Absorbance Ratio 973/898 for PET Melt Blown Fibers with Additives.

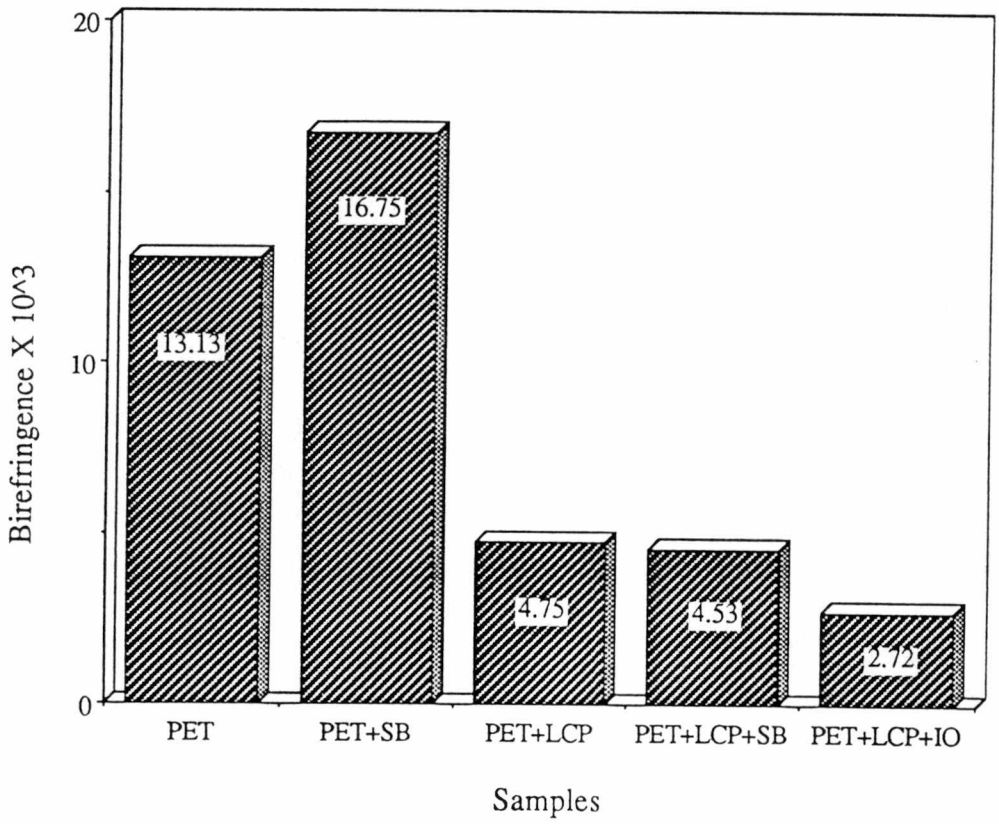

Figure 19. Birefringence Values for PET Melt Blown Fibers with Additives.

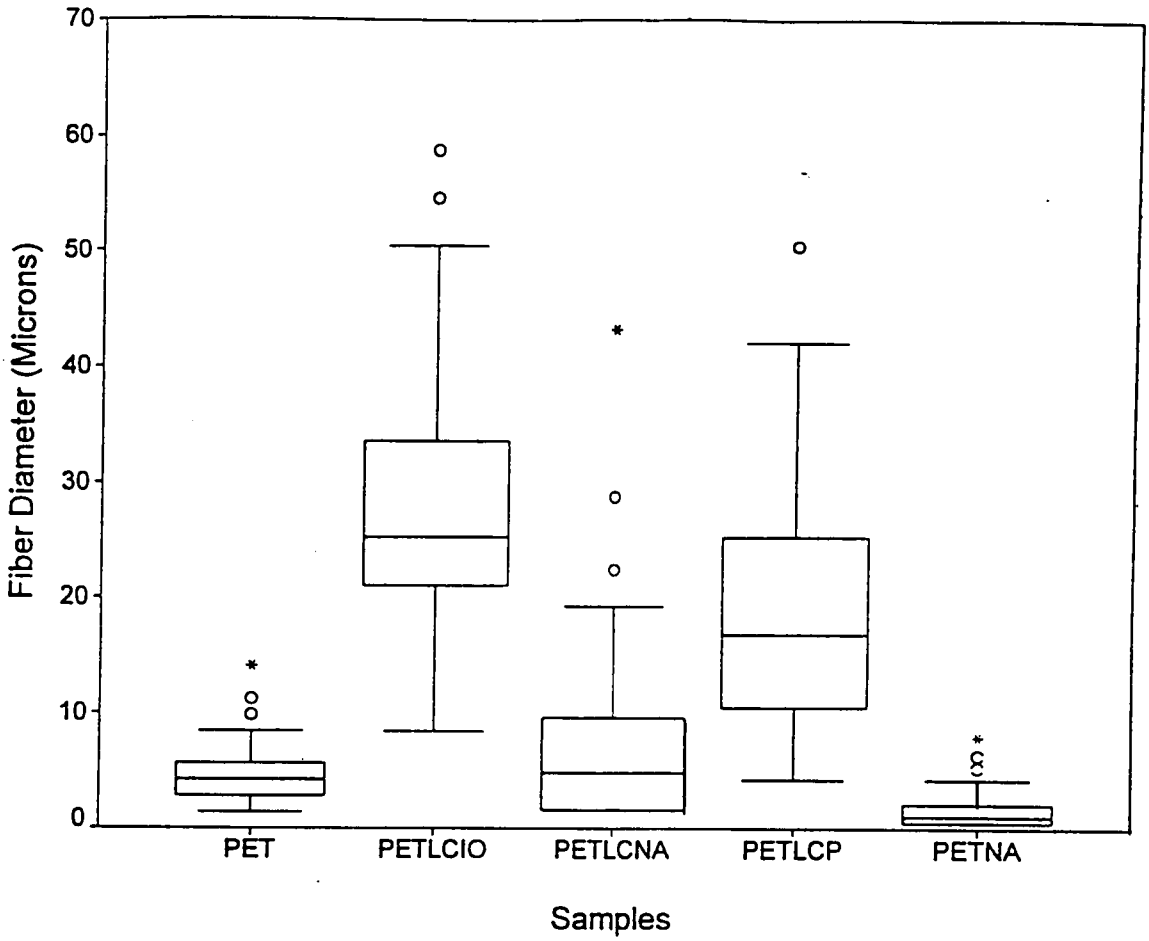

PET	-	PET fibers with no additives
PETNA	-	PET fibers with Sodium Benzoate
PETLCP	-	PET fibers with LCP
PETLCNA	-	PET fibers with LCP and Sodium Benzoate
PETLCIO	-	PET fibers with LCP and Ionomer

Figure 20. Box and Whisker Plot for Fiber Diameters of PET Melt Blown Webs with Additives.

Table 11. Mean, Standard Deviation and CV% of Fiber Diameters for PET Melt Blown Fibers Produced with Additives.

Sample ID	Mean (μ)	Standard Deviation (μ)	Coefficient of Variation (%)
PET	4.3	2.4	56
PET + 1% SB	1.6	1.4	88
PET + 10% LCP	17.7	10.3	58
PET + 10% LCP + 1% SB	6.7	6.5	97
PET + 10% LCP + 1% Ionomer	28.0	9.8	35

Table 12. Mechanical Properties of PET Melt Blown Webs Produced with Additives.

Sample ID	Tenacity (mN/tex)	Breaking Elongation (%)	Initial Modulus (N/tex)	Breaking Energy (Kg-m)
PET	16.2	42.0	0.68	0.097
PET + 1% SB	16.2	3.4	0.73	0.003
PET + 10% LCP	2.0	4.8	0.18	0.001
PET + 10% LCP + 1% SB	2.1	5.1	0.10	0.003
PET + 10% LCP + 1% Ionomer	0.5	14.9	0.05	0.001

tensile strength of fibers made of PET/LCP. PET fibers that contained sodium benzoate alone had similar tenacity values as that of fibers that contained no additives. Although, LCP is a high strength and high modulus polymer, the poor adhesion between LCP and PET matrix could be the main reason for the lower tenacity values. The fibrils of LCP could be dispersed in PET matrix with no connectivity thus not contributing to the total strength of the fiber. Thus although, LCP acts as a reinforcing element as far as thermal properties are concerned, the resulting composite fiber had poor mechanical properties. The poor strength of individual fibers could also be due to the larger diameter of fibers with more defects. The strength of PET melt blown webs is due to interfiber sticking or bonding and entanglements. It appears that by the time the fibers reach the collector drum, LCP helps cool the fiber sufficiently to transform it to a glassy solid. This reduces the contact area between fibers in the web, which also contributes to poor mechanical properties. As could be seen from the breaking elongation values, PET fibers appear to be more ductile and thus tougher than PET fibers that contained any type of additive. In the case of PET fibers that contained sodium benzoate, the brittle nature of the webs is due to the large number of entanglements or bonding points apart from the brittle nature of individual fibers. The poor elongation of other types of fibers is due to the inherent defective nature of fibers themselves. The modulus was found to be higher in the case of PET /sodium benzoate and the breaking energy lower. Other fibers had considerably lower modulus and breaking energy values.

The physical properties of melt blown webs with additives are shown in Table 13. It was not possible to keep a constant basis weight and thickness of the samples because of the poor drawing action when LCP was blended with PET. However, loftier webs were produced in the case of blends. Webs that contained LCP had

Table 13. Physical Properties of PET Melt Blown Webs and PET Polymer with Additives.

Sample	Basis Weight (GSM)	Thickness (μ)	Air Permeability ($m^3/m^2/sec$)	Bursting Strength (kPa)	Viscosity (Pa.s)
PET	45.27	211	0.38	35.94	198
PET+1%SB	23.16	248	0.29	11.06	86
PET+10%LCP	43.14	863	5.84	8.99	442
PET+10%LCP +1%SB	137.62	1195	1.29	6.91	98
PET+10%LCP +1%Ionomer	105.95	1479	4.19	13.13	406

higher air permeability values because of larger fiber diameters. It is very evident that the smaller fiber diameter is the reason for lower air permeability values and thus higher filtration efficiency of the PET melt blown webs that contained sodium benzoate. Bursting strength was observed to be lower in the case of webs that contained the additives.

The newtonian viscosity of neat and compounded PET polymers are also shown in Table 13. The shear rate during melt blowing PET could be ranging from 300-600 per second depending on the throughput rate. Lower throughput rates result in higher shear rate, lower polymer melt viscosity and thus smaller diameter fibers. The range of measurement of viscosity was so chosen to fall between the above mentioned shear rates. It can be seen from Table 13 that sodium benzoate not only acted like a nucleating agent but as a plasticizer also, thus reducing the viscosity of PET. However, addition of LCP increased the viscosity of PET and this explains the larger fiber diameter in the case fibers from of PET/LCP blends. Addition of sodium benzoate to PET/LCP blends resulted in a polymer system with intermediate viscosity values.

4.3. PET Melt Blown Webs Produced under Different Processing Conditions without Additives

In order to investigate the mechanism of shrinkage, PET samples were melt blown, under varying process conditions such as the throughput, die-to-collector distance, air pressure at the die, air temperature and die temperature. The results from the as-produced fibers are shown in Tables 14 and 15 and in Figures 21-25. An ice cooled amorphous PET film was taken as the reference material. The effect of

Table 14. Transition Temperatures and Percent Crystallinity Values of PET Melt Blown Webs Produced under Different Processing Conditions.

Material	DSC Parameters		
	T_{ch}	T_m	% Crystallinity on heating ($\Delta H_m - \Delta H_{ch}$)
PET (ice cooled amorphous film)	133.5	258.1	N. D.
PET # 1	130.5	254.2	N. D.
PET # 2	129.4	254.1	1.95
PET # 3	129.3	254.1	4.43
PET # 4	130.3	255.1	1.00
PET # 5	132.5	254.1	N. D.
PET # 6	132.5	255.3	4.35
PET # 7	135.3	254.2	4.42
PET # 8	131.1	255.4	8.13

NOTE : The samples were heated to 300°C from 50°C at a rate of 20°C/min.
N. D. means Not Detected

Table 15. Glass Transition Temperatures and the Amount of Different Structural Entities Present in As-produced PET Melt Blown Webs without any Additive.

Sample ID	T_g (°C)	Percent Crystalline Fraction	Percent Amorphous Fraction	Percent Rigid Amorphous Fraction	Shrinkage (%)
PET FILM	81.4	N. D.	70.79	29.21	-----
PET #1	83.5	N. D.	19.47	80.53	20.94
PET #2	83.4	1.95	14.61	83.44	19.37
PET #3	84.1	4.43	21.86	73.71	3.94
PET #4	83.8	1.00	12.16	86.84	37.95
PET #5	83.3	N. D.	24.35	75.65	36.69
PET #6	82.5	4.35	14.64	81.01	33.39
PET #7	83.8	4.42	14.59	80.99	36.85
PET #8	85.3	8.13	19.37	72.50	8.98

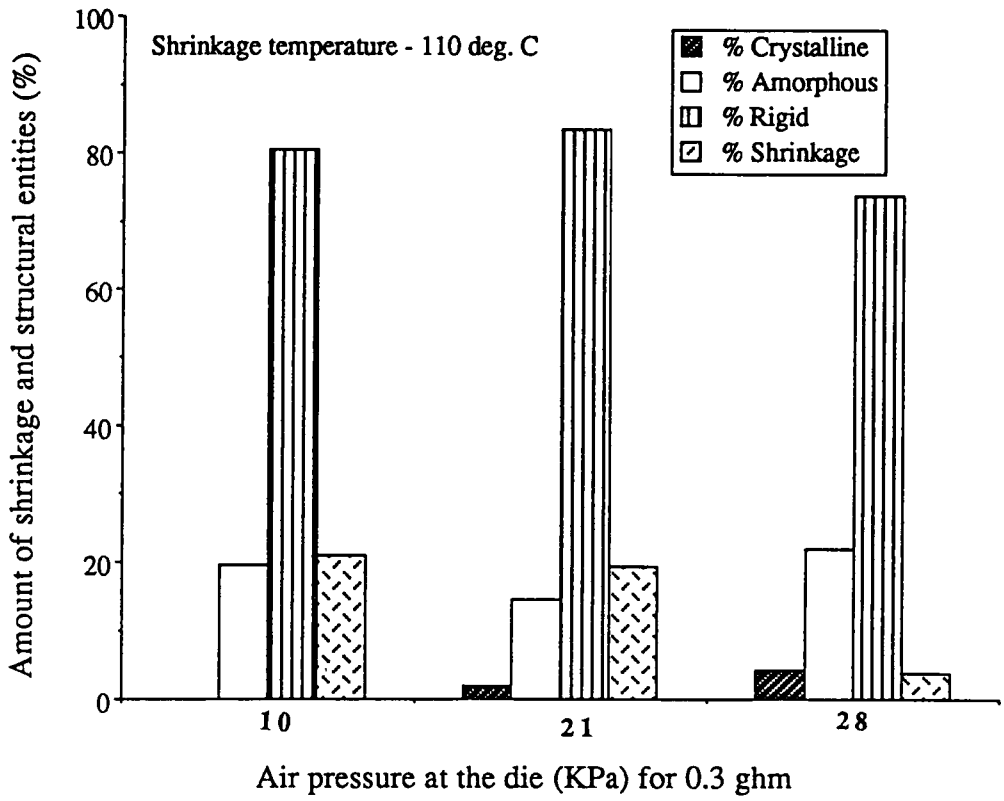

Figure 21. The Effect of Air Pressure at the Die on the Level of Shrinkage and Different Structural Entities Present in PET Melt Blown Webs without Additives.

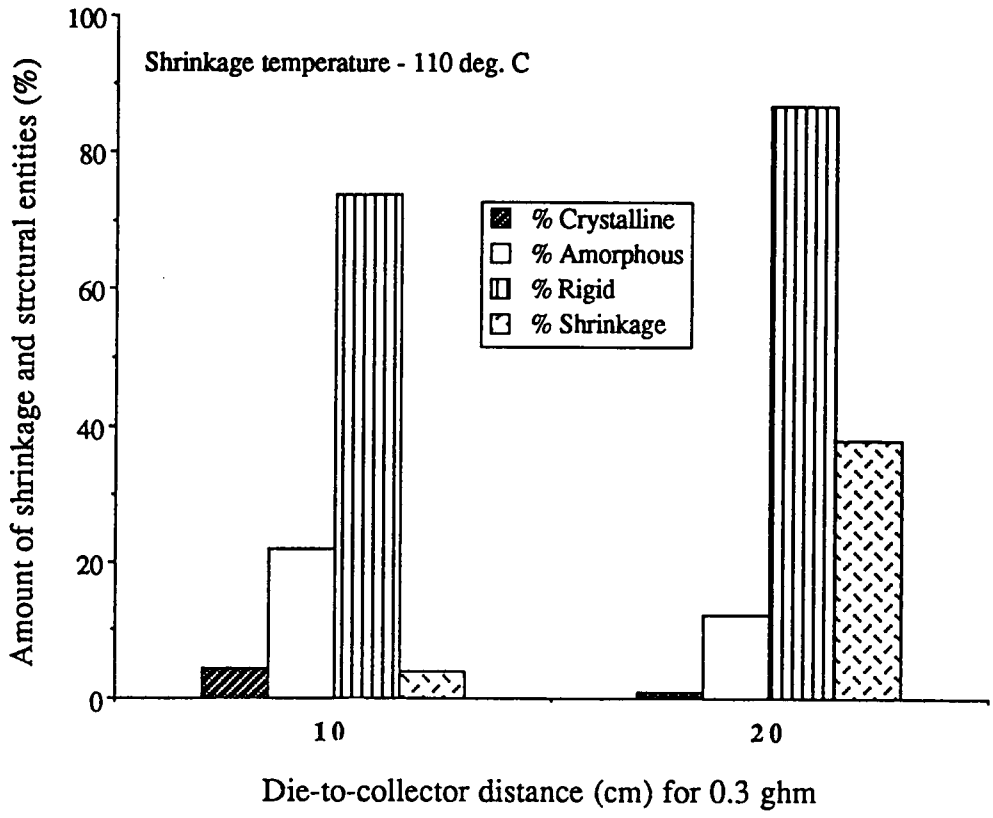

Figure 22. The Effect of Cooling Length on the Level of Shrinkage and Different Structural Entities Present in PET Melt Blown Webs without Additives.

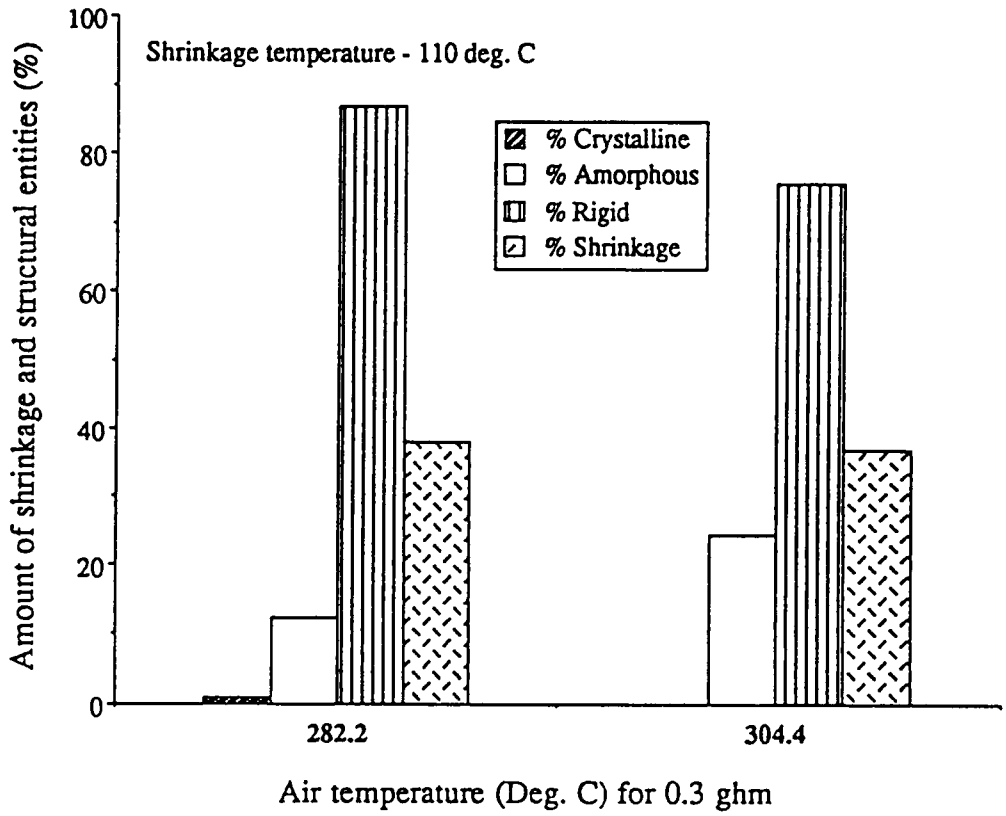

Figure 23. The Effect of Air Temperature on the Level of Shrinkage and Different Structural Entities Present in PET Melt Blown Webs without Additives.

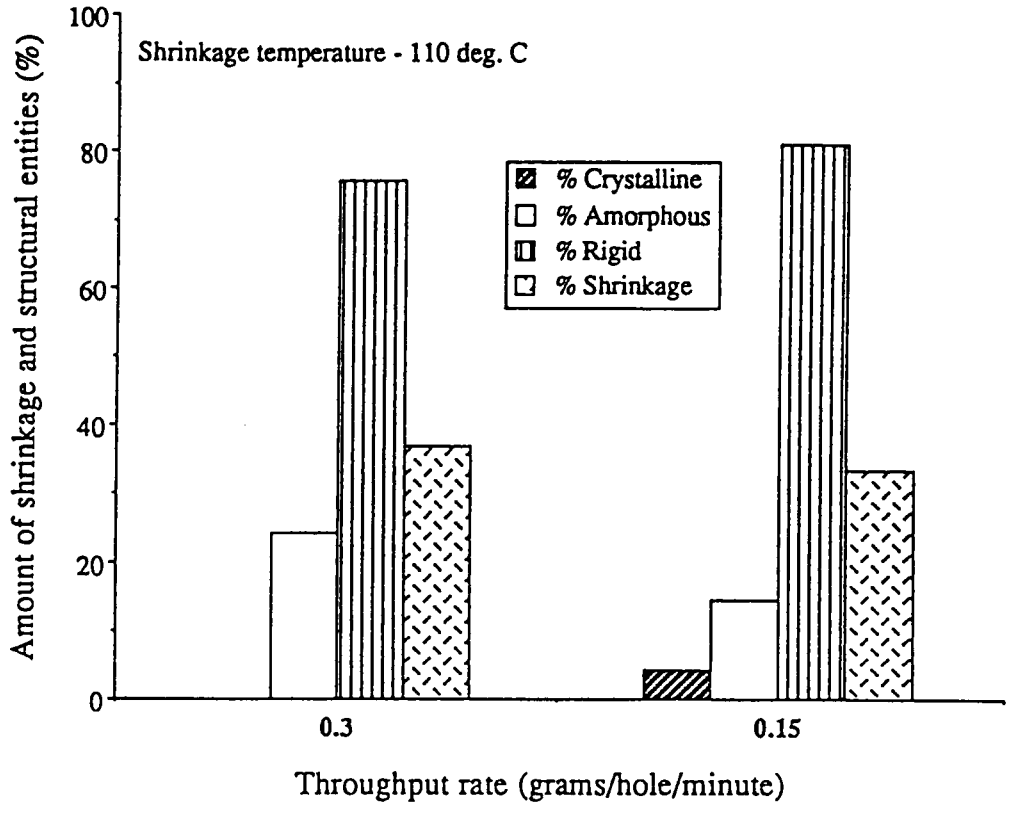

Figure 24. The Effect of Throughput Rate on the Level of Shrinkage and Different Structural Entities Present in PET Melt Blown Webs without Additives.

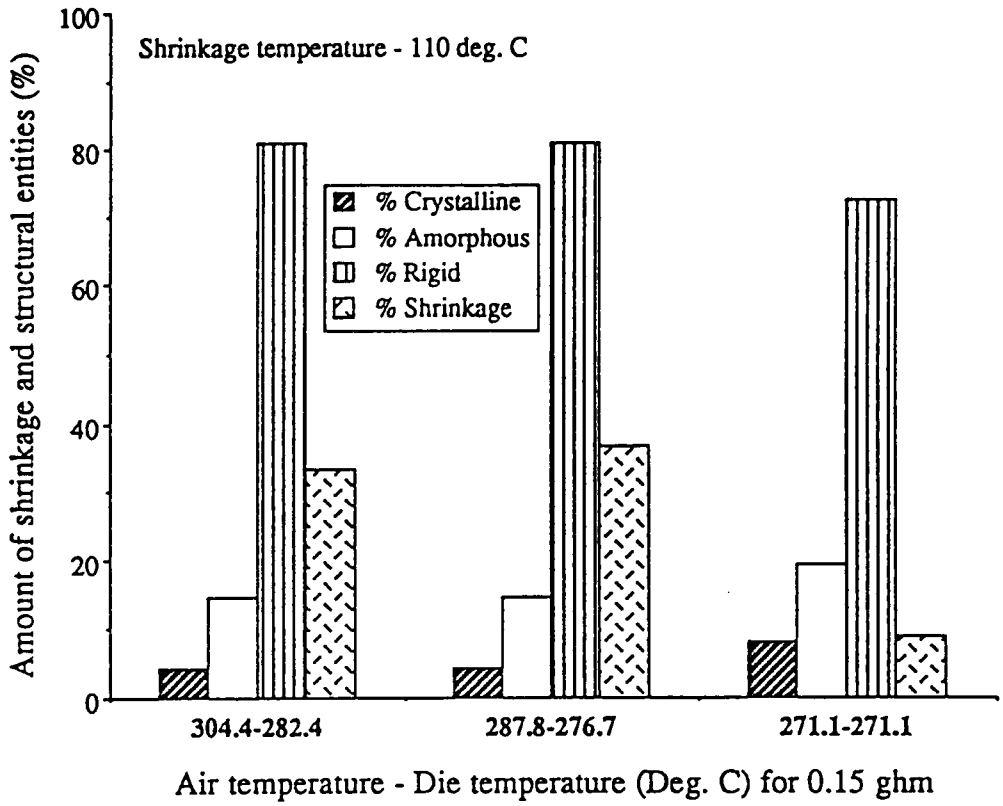

Figure 25. The Effect of Air-Die Temperature Difference on the Level of Shrinkage and Different Structural Entities Present in PET Melt Blown Webs without Additives.

orientation during melt blowing could be seen from the increase in the T_g and the rigid amorphous content of the processed fibers. There was no appreciable difference in the T_{ch} and T_m values of the webs produced under the different conditions. The crystalline fraction was found to slightly increase on increasing the air pressure at the die. This also resulted in a slight decrease in the rigid amorphous content. Interestingly, the shrinkage values were found to be much lower in the case of melt blown webs produced at 4 psi air pressure at a throughput of 0.3 ghm. Thus it can be seen that the dimensional stability of webs could also be improved by processing PET at suitable conditions without any nucleating additive. Increasing the cooling distance, i.e. the die-to-collector distance resulted in a decrease in crystallinity and an increase in the rigid amorphous content. The shrinkage value was found to be close to 40%. An increase of about 20°C in air temperature was not influential in reducing the shrinkage values. Although there was a reduction in rigid amorphous content, no on-line thermal crystallization or annealing was found to occur. The web crystallinity was found to increase slightly on reducing the throughput to 0.15 ghm from 0.3 ghm. However, only a slight reduction in shrinkage was observed. The slight increase in crystalline and rigid amorphous fractions at low throughput rate could be due to the increase in elongation rate due to reduction in velocity of polymer at the die tip for the same air pressure. It is not clear whether this would result in any on-line stress induced crystallization. The ideal condition for processing PET of 0.9 I. V. could be the last sample as shown in Figure 25, equal die and air temperatures, 271°C in this case, the crystallinity was found to increase with reduction in rigid amorphous fraction and a simultaneous decrease in shrinkage.

A statistical correlation between percent shrinkage at 110°C versus crystalline, amorphous and rigid amorphous contents of the fiber was obtained as shown in Table

16. Although the data points were limited, a clear trend was observed between percent shrinkage values and different entities present in the fiber structure. Shrinkage was found to be negatively correlated with the amount of crystalline and amorphous fractions present in the fiber. The rigid amorphous fraction was positively correlated with shrinkage indicating that an increase in rigid amorphous content would result in an increase of thermal shrinkage of the melt blown PET webs. This result was found to be significant at the 90% confidence level. Rigid amorphous content also had higher correlation values with shrinkage compared to crystalline and amorphous fractions. Several statistical models were analyzed for the observed data points and the one with significant F-value, in this case an exponential model was chosen as shown in Table 17. The observed trends were also plotted along with the predicted model in Figures 26-28.

Shrinkage studies were also performed at 150 and 190°C. The results are shown in Figure 29. Three sets of samples are shown to have similar percent shrinkage values. The presence of crystallites in the as-produced fibers has considerable influence on the shrinkage values of fibers. The shrinkage was found to increase with shrinkage temperature in the case of fibers that had no detectable crystallinity. The shrinkage values remained the same in the case of fibers that had crystallites in the as-produced material. The rigid amorphous content was found to decrease on annealing as shown in Figure 30. The reason being the participation of oriented amorphous molecules in shrinkage and disorientation at 110°C and 190°C. At 150°C, the lowest values for the rigid amorphous content were observed. Participation of rigid amorphous material in the crystallization process is the reason for this reduction in the rigid amorphous content. At 150°C, the fibers undergo competing mechanisms of shrinkage and crystallization. The change in the rigid

Table 16. Correlation Between the Shrinkage and Different Structural Entities Present in PET Melt Blown Webs Produced without Additives (Annealing Temperature - 110°C).

	Shrinkage	Cryst.	Amor.	Rigid Amor.
Shrinkage	1.0	-0.48	-0.40	0.62
Cryst.	-0.48	1.0	-0.06	-0.52
Amor.	-0.40	-0.06	1.0	-0.82
Rigid Amor.	0.62	-0.52	-0.82	1.0

Table 17. Different Statistical Models and their Significance.

Independent: Rigid Amor.							
Dependent	Mth	Rsq	d.f.	F	Sigf.	b0	b1
Shrinkage	LIN	.381	6	3.69	.103	-107.90	1.6723
Shrinkage	LOG	.389	6	3.81	.099	-558.68	133.452
Shrinkage	INV	.396	6	3.94	.095	159.038	-10616
Shrinkage	QUA	.434	5	1.91	.241	-1020.2	24.7888
Shrinkage	CUB	.434	5	1.91	.241	-1020.2	24.7888
Shrinkage	COM	.445	6	4.82	.071	.0032	1.1166
Shrinkage	POW	.456	6	5.03	.066	3.6E-16	8.8149
Shrinkage	S	.466	6	5.23	.062	11.8722	-702.18
Shrinkage	GRO	.445	6	4.82	.071	-5.7574	.1103
Shrinkage	EXP	.445	6	4.82	.071	.0032	.1103
Shrinkage	LGS	.445	6	4.82	.071	316.514	.8956

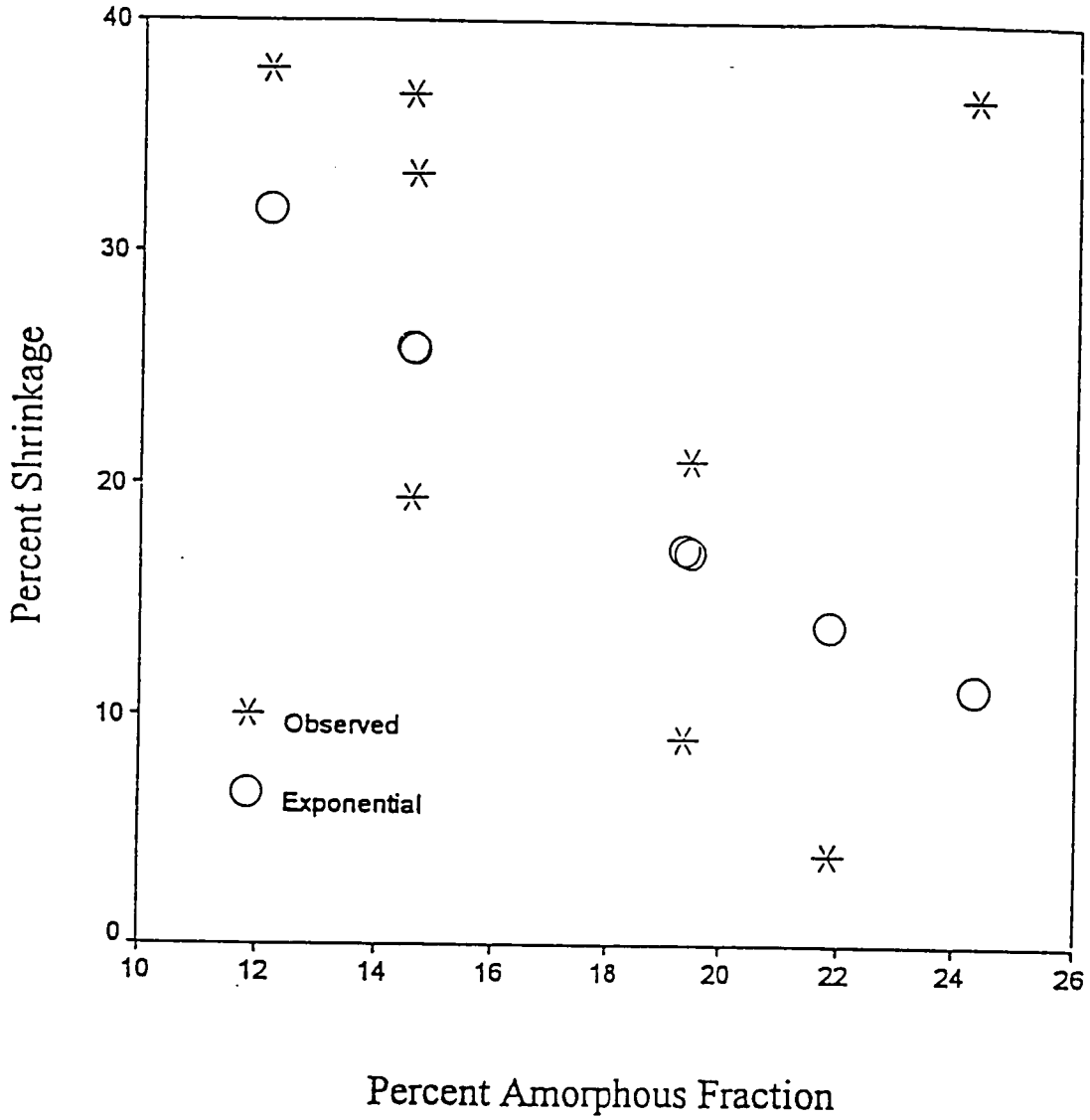

Figure 26. Relationship Between Subsequent Shrinkage and Rigid Amorphous Content for PET Melt Blown Webs without Additives.

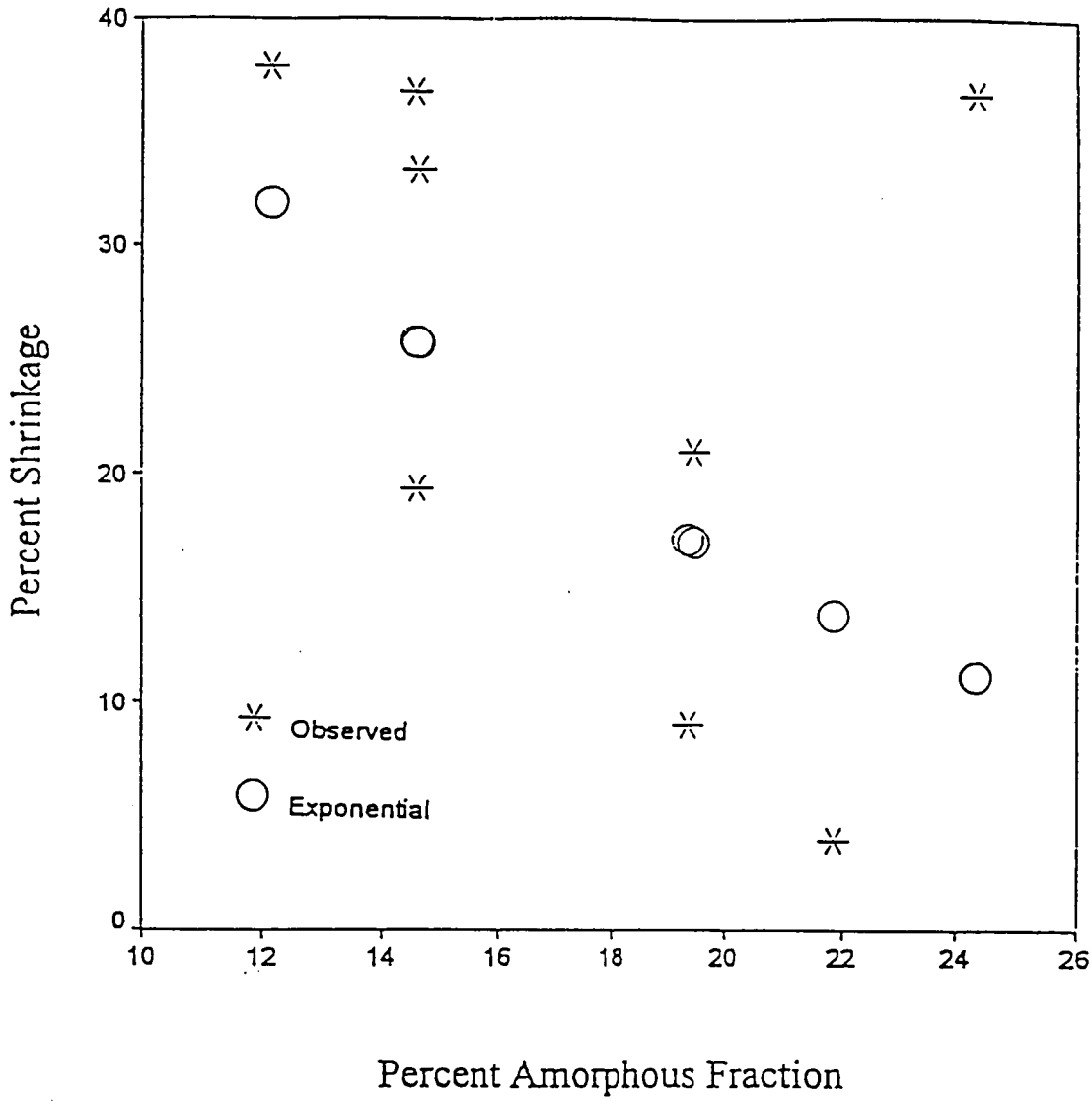

Figure 27. Relationship Between Subsequent Shrinkage and Amorphous Content for PET Melt Blown Webs without Additives.

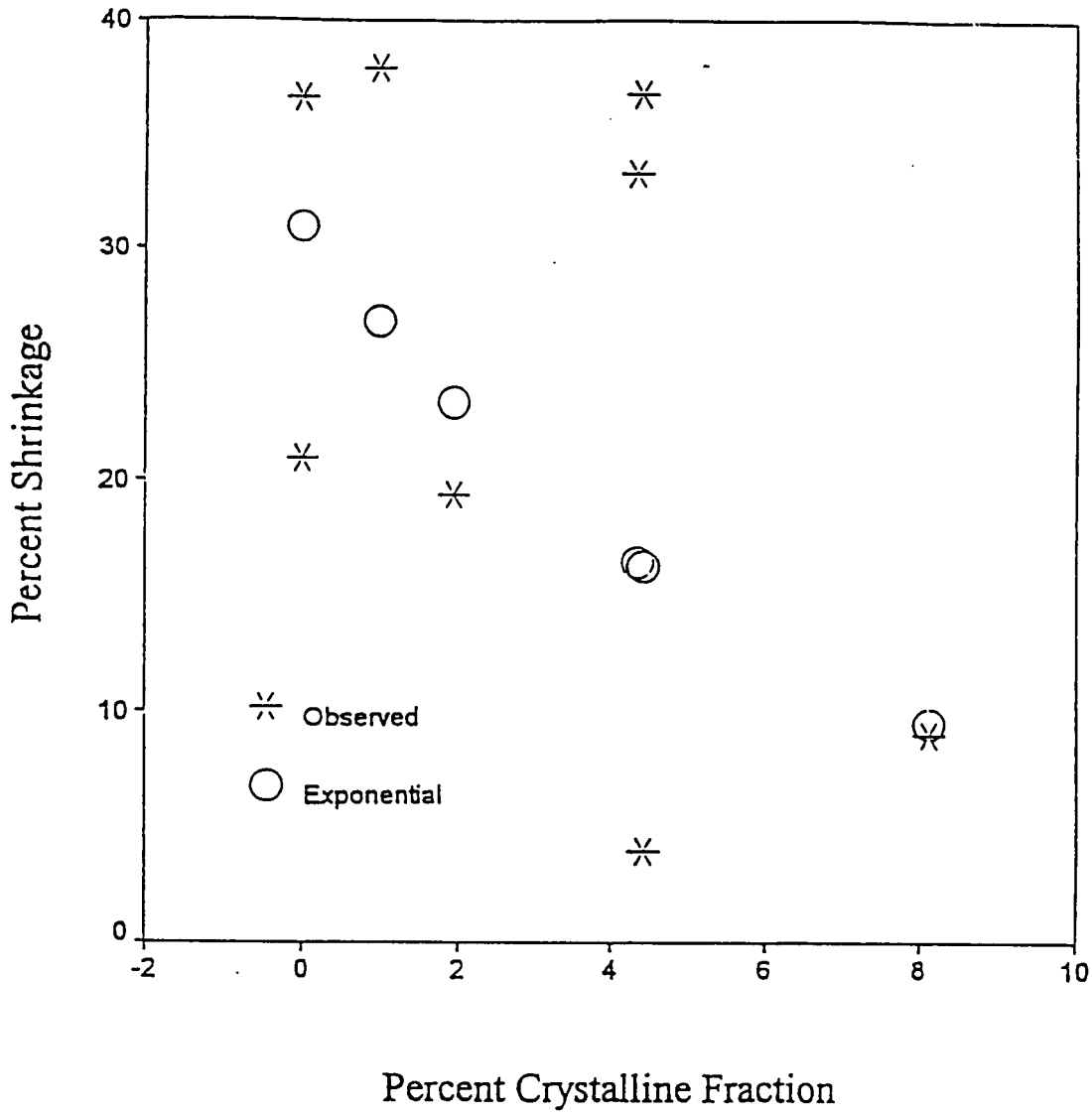

Figure 28. Relationship Between Subsequent Shrinkage and Crystallinity Content for PET Melt Blown Webs without Additives.

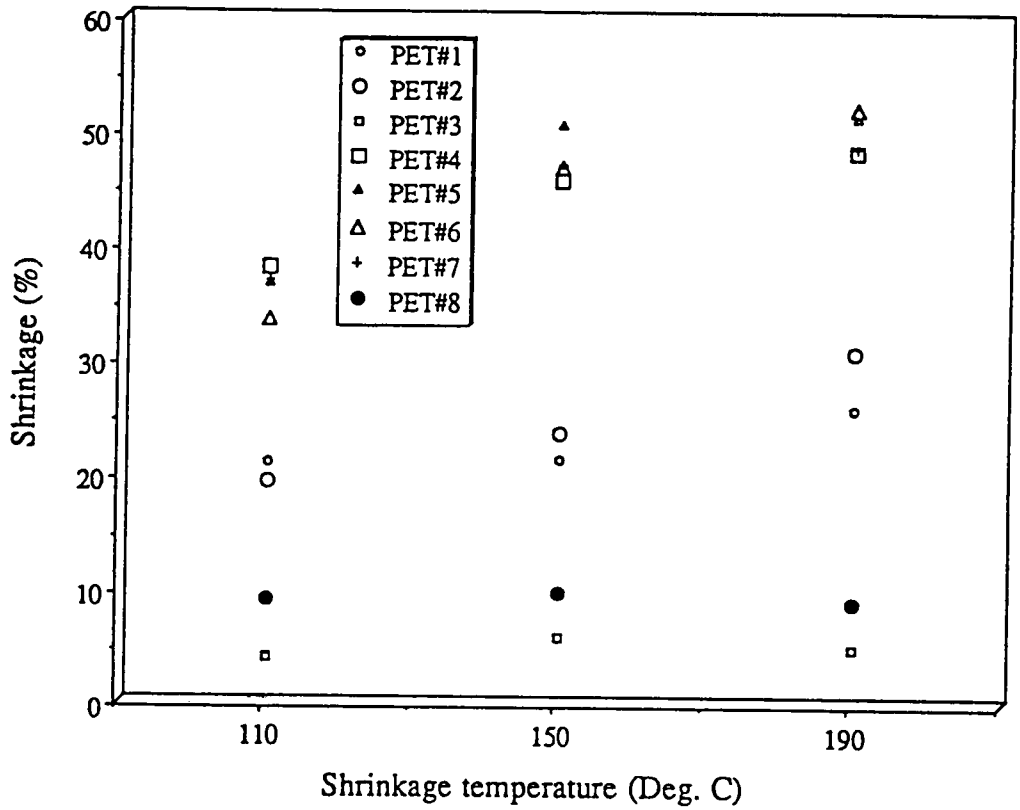

Figure 29. Shrinkage Behavior of PET Melt Blown Fibers Produced under Different Process Conditions without Additives.

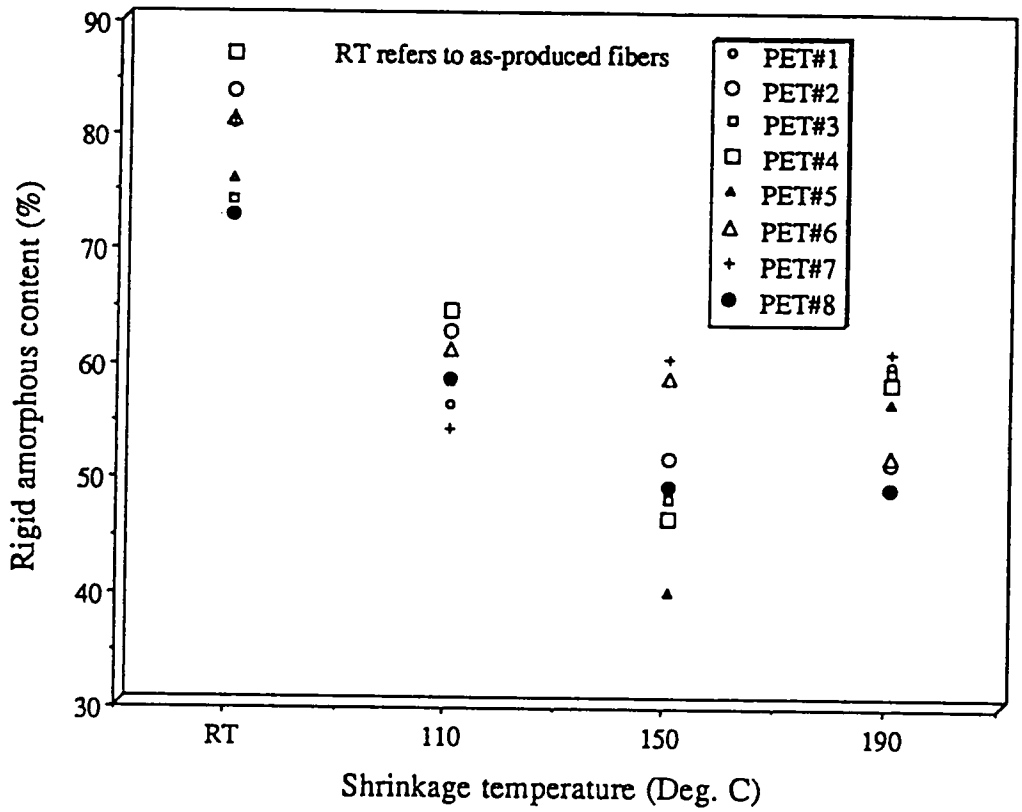

Figure 30. The Effect of Temperature on the Rigid Amorphous Content of PET Melt Blown Fibers without Additives.

amorphous content is also determined by the initial status of the material such as the relative portions of the crystalline and rigid amorphous segments. Thus the trend observed is similar to the one observed in the case of PET fibers with nucleating additives. No appreciable crystallinity was detected in the case of essentially amorphous fibers annealed at 110°C for 3 minutes. However, the T_{ch} being 129°C, the crystallinity was found to rapidly increase at 150°C and at 190°C as shown in Figure 31. Here again, the value of final percent crystallinity was dependent on the initial status of the material such as the presence of detectable crystallites/nuclei present in the fiber.

The results obtained from the DSC were compared with the results from FTIR experiments and the observed trend were similar. Figure 32 illustrates the orientation and crystallization of the different PET melt blown fibers produced under different processing conditions without additives. The trans content was found to increase on increasing the air flow rate. An increase in the cooling distance results in a decrease in the trans content although there was an increase in orientation. An increase in the air temperature resulted in a slight increase in the trans content. The 973 cm^{-1} peak contains the trans isomer for both the crystalline and oriented rigid amorphous segments. An increase in throughput resulted in a considerable increase in the absorbance ratio. The decrease in the absorbance ratio for sample #8 could be attributed to the reduction in the rigid amorphous content of the fiber samples produced at the same throughput rate. This also explains the reason for the lower percent shrinkage values for PET #8. Two samples that had totally different shrinkage values at different shrinkage temperatures were analyzed for their absorbance ratio as shown in Figure 33. PET#4 as-produced fibers were essentially amorphous with no detectable crystallinity when compared to PET#8 that had

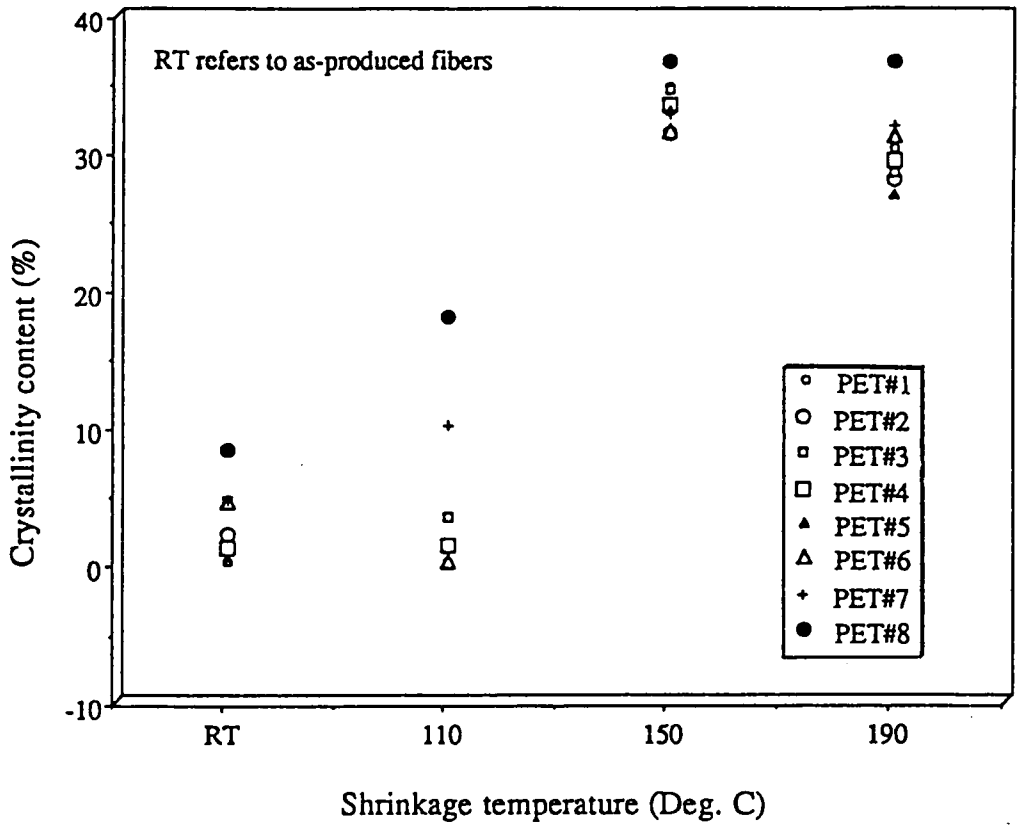

Figure 31. The Effect of Temperature on the Crystallinity of PET Melt Blown Webs without Additives.

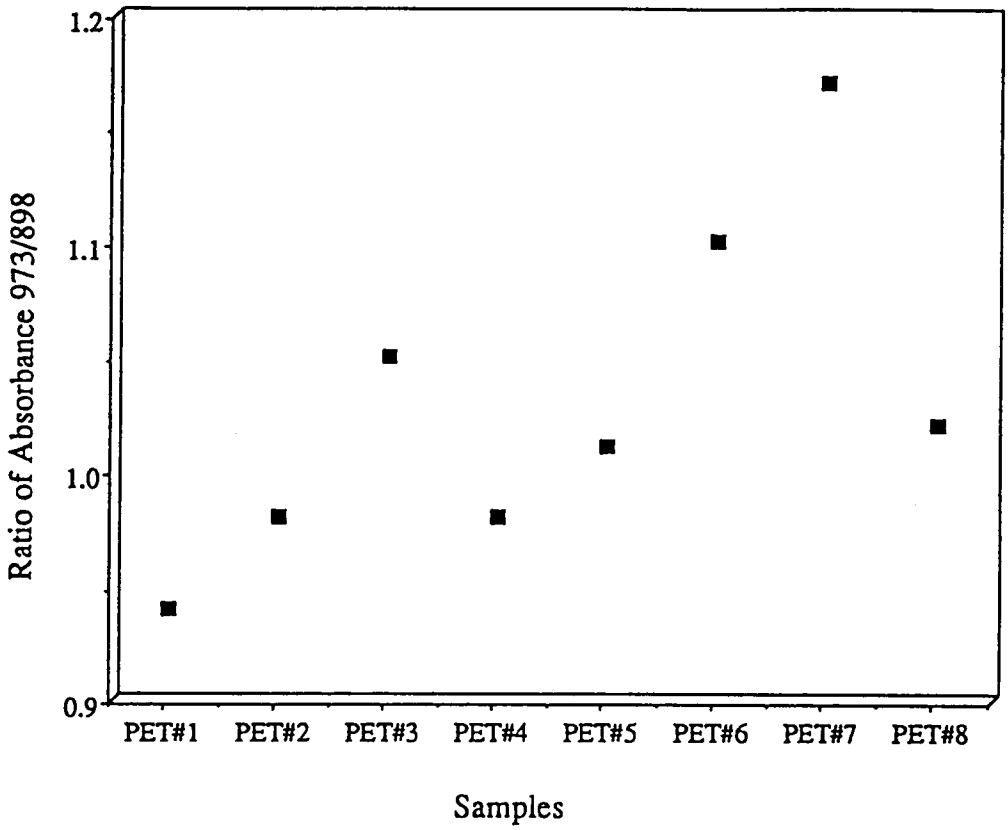

Figure 32. The Ratio of Absorbance 973/898 for PET Melt Blown Fibers without Additives.

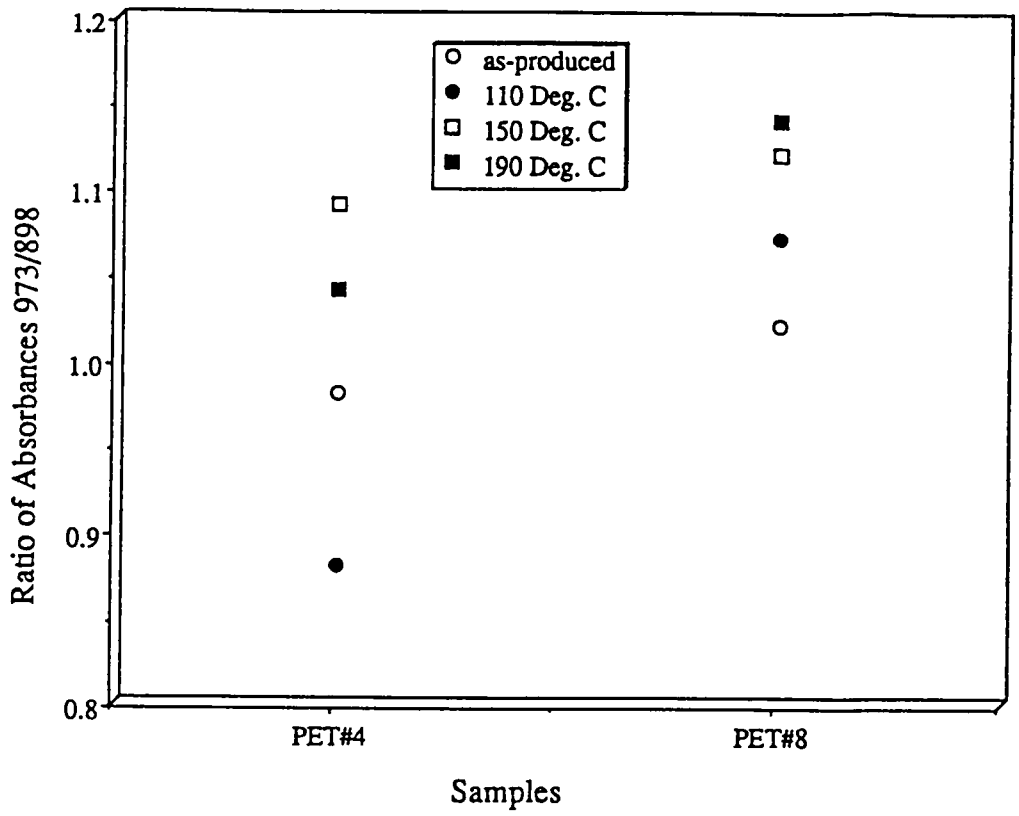

Figure 33. The Ratio of Absorbance 973/898 for Annealed PET Melt Blown Fibers without Additives.

significant amount of crystallinity values. The reduction in the absorbance ratio 973/898 at 110°C for PET#4 is due to the participation of oriented trans segments in the shrinkage or disorientation process producing more gauche isomers. The trend was reversed at the same temperature for PET#8 because of the crystallites acting as nucleating sites on annealing. At any shrinkage temperature, the ratios (973/898) were always higher for PET#8 for the same reason. The same trend is also illustrated in Figure 34 for absorbance ratios of 973 and 794 cm^{-1}.

The effect of increase in air flow rate on the birefringence of fibers is shown in Figure 35. The increase in birefringence was observed to be 10 times higher when changing the die air pressure from 1.5 to 4 psi as can be seen in the case of PET#s 1, 2 and 3. All other samples had similar birefringence values. The observed higher birefringence values are also due to the smaller fiber diameters as shown in Figure 36. The mean fiber diameter was much higher in the case of PET#1 compared to other samples shown in the figure. All other samples except PET#1 had much narrower range and distribution of fiber diameters. The mean values and the coefficient of variation are shown in Table 18. An increase in the cooling length/collection distance, or the air temperature, resulted in a slight increase in mean fiber diameter in the case of fibers produced at higher throughput rates. Finer fibers were obtained at lower throughput rates. The fiber diameter has a direct influence on the filtration efficiency of the melt blown webs by providing a larger surface area for filtration of dust particles. Much lower variation in the fiber diameter was observed in the case of melt blown PET fibers produced at low throughput rate and high air pressure because of the improvement obtainable in the drawing action on spinline.

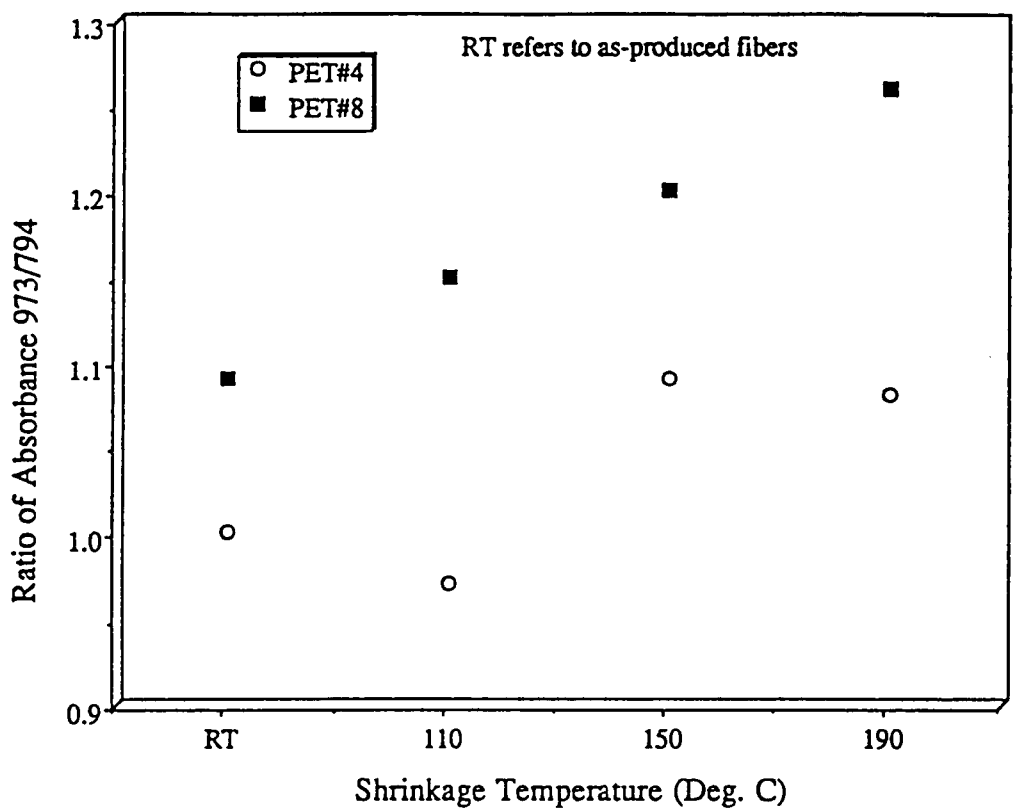

Figure 34. The Ratio of Absorbance 973/794 for PET Melt Blown Fibers at Different Shrinkage Temperatures.

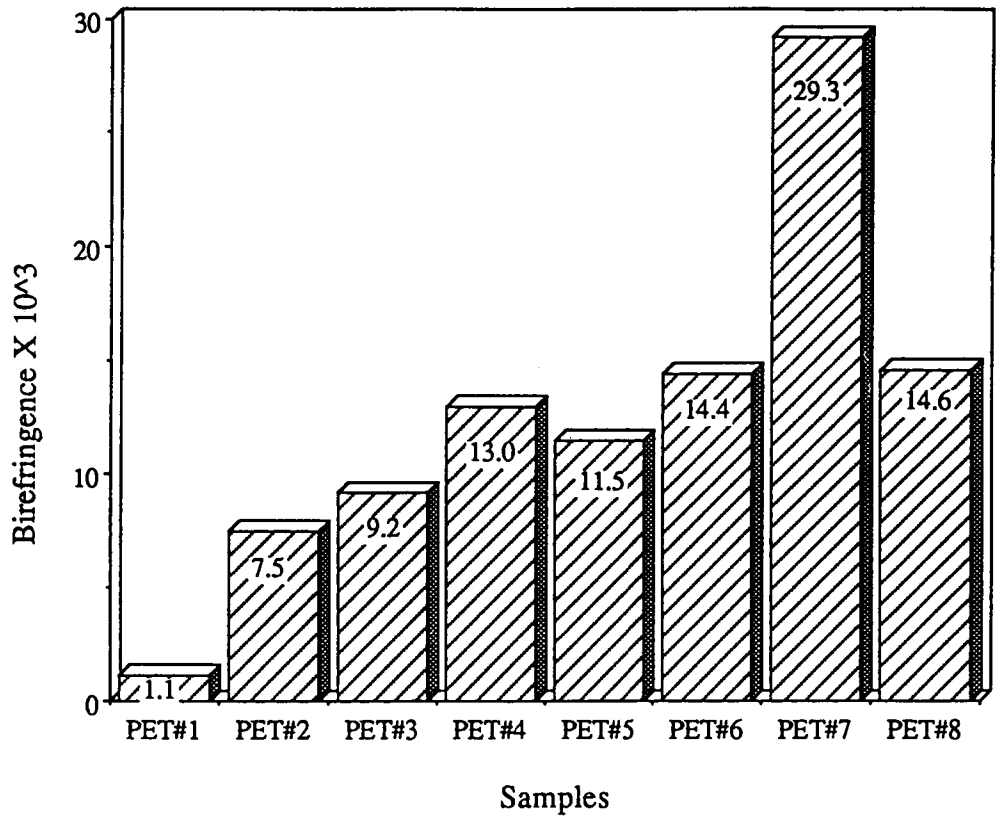

Figure 35. Birefringence Values for PET Melt Blown Fibers without Additives.

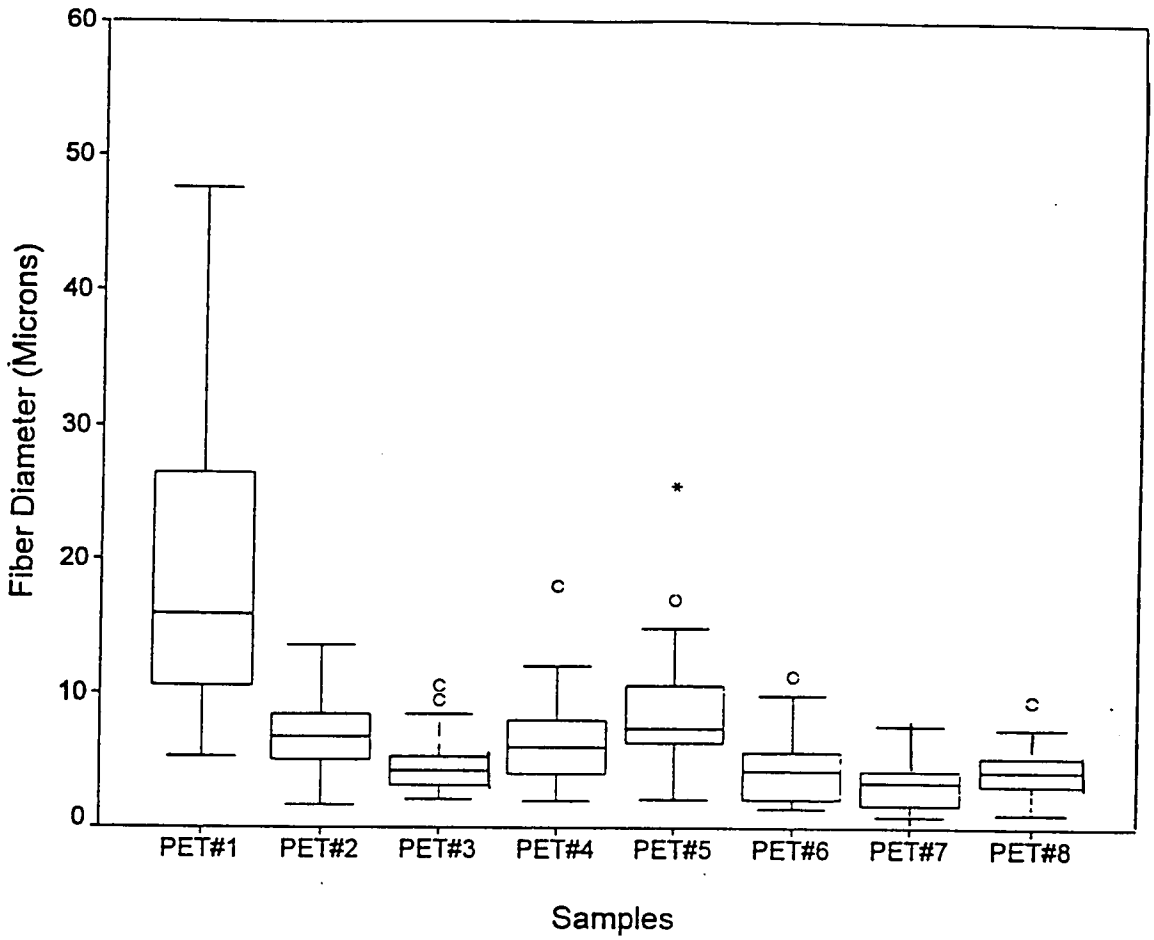

Figure 36. Box and Whisker Plot for Fiber Diameters of PET Melt Blown Webs without Additives.

Table 18. Mean, Standard Deviation and CV% of Fiber Diameters for PET Melt Blown Fibers Produced Without Additives.

Sample ID	Mean (μ)	Standard Deviation (μ)	Coefficient of Variation (%)
PET#1	19.4	9.8	50
PET#2	6.6	2.4	36
PET#3	4.7	1.8	38
PET#4	6.7	3.0	45
PET#5	7.7	3.6	57
PET#6	4.4	2.4	54
PET#7	3.2	1.5	36
PET#8	4.4	1.7	38

The effect of changing different processing variables on the mechanical properties of the melt blown PET webs is shown in Table 19. It is evident that an increase in strength was obtained by increasing the air pressure at the die for the same throughput [PET#1 to PET#3]. This is due to the orientation of the molecular chains and finer fibers. The finer the fibers, the greater the number of fibers in a given cross section of the webs. This results in improved tenacity values. A slight increase in elongation and breaking energy indicates that the webs become tougher on increasing the air flow rate for the same throughput rate. A slight decrease in modulus was observed in the case of PET#3. An increase in cooling length or collection distance would reduce the thermal sticking or bonding between the fibers in the melt blown web. Similar results were obtained on increasing the air temperature. Although, the values of initial modulus were comparable, the webs became tougher as indicated by the higher breaking elongation and breaking energy values. The breaking tenacity showed a maximum for lower throughput rate samples. Almost all the samples produced had ductile failure except PET#8. The failure behavior of PET#8 webs was observed to be laminar type. There was very minimal thermal sticking between fibers that resulted in poor elongation and breaking energy values. Although, PET#8 is the ideal fabric for its improved thermal properties, it had poor mechanical properties. These samples also had much higher coefficient of variation when compared to the rest of the webs produced.

The physical properties of PET melt blown webs produced under different processing conditions without any type of additive are shown in Table 20. An increase in the air pressure at the die was found to decrease the basis weight and thickness of webs. A decrease in fiber diameter also caused a reduction in the air permeability and an increase in filtration efficiency. Bursting strength increased with

Table 19. Mechanical Properties of PET Melt Blown Webs Produced without Additives.

Sample ID	Tenacity (mN/tex)	Breaking Elongation (%)	Initial Modulus (N/tex)	Breaking Energy (Kg-m)
PET#1	11.0	27.3	0.55	0.028
PET#2	14.7	27.2	0.64	0.032
PET#3	19.7	30.9	0.44	0.050
PET#4	14.0	78.3	0.52	0.102
PET#5	13.9	112.0	0.46	0.133
PET#6	20.0	57.4	0.57	0.062
PET#7	20.8	36.5	0.64	0.032
PET#8	11.0	9.0	0.67	0.002

Table 20. Physical Properties of PET Melt Blown Webs without Additives.

Sample	Basis Weight (GSM)	Thickness (μ)	Air Permeability ($m^3/m^2/sec$)	Bursting Strength (kPa)
PET#1	32.50	383	3.85	20.73
PET#2	26.38	199	1.36	21.43
PET#3	29.08	156	0.59	31.80
PET#4	32.47	263	0.97	21.43
PET#5	29.31	238	1.18	20.73
PET#6	19.19	191	0.85	15.89
PET#7	15.93	199	0.77	17.28
PET#8	19.39	227	2.05	35.94

an increase in air pressure at the die. The basis weight and thickness were found to increase on increasing the cooling length or collection distance. The air permeability increased and the bursting strength decreased. Similar results were obtained on increasing the air temperature for the same throughput rate, die to collector distance and air pressure at the die. A decrease in fiber diameter at lower throughput rate is manifested as a decrease in basis weight, thickness and air permeability when compared to webs produced at a higher throughput rate except in the case of PET#8. The web construction of PET#8 was quite different from webs produced at the same throughput rate. The webs were loftier and permeable with very soft hand and high bursting strength.

5. Conclusions

It is now clearly evident that the nucleating ability of some of the commercially available additives can be exploited in situations where the level of spinline stress is as low, as in melt blowing. Kinetic studies confirm the fact that the overall crystallization rate of the system with certain nucleating additives is much higher than that of pure PET. The shrinkage mechanisms of PET melt blown fibers have direct relationship with the relative amount of crystalline, amorphous and rigid amorphous contents. The shrinkage behavior of melt blown fibers with additives/other reinforcing polymers is quite different and is determined by the disposition of the filler or reinforcing material in the matrix of the polymer.

These observations were confirmed by detailed analyses of the as-produced melt blown fibers and heat shrunk web samples by using thermal analysis, FTIR and birefringence techniques. The fractions of crystalline and rigid amorphous material present in the fibers determine the shrinkage values at temperatures above glass transition. The crystallites serve as tie links or reinforcing elements to prevent shrinkage of the fibers when present in sufficient quantities. The poor orientation of the polymer molecules along the fiber axis and the rigidity of LCP are the main reasons for the better dimensional stability of PET/LCP fibers at elevated temperatures. Although, the PET/LCP fibers have adequate dimensional stability, they have very poor mechanical properties because of the lack of interfacial adhesion between LCP fibrils and the PET matrix and thus LCP fibrils forming the weak points. The fibers had lower strength and brittle fracture. Fracture studies revealed the presence of LCP fibrils in the PET matrix. The structural similarities between

LCP and PET were exploited for easier processing of the blends into melt blown fibers although with poor mechanical and physical properties. However, it was possible to maintain the soft hand of the melt blown webs. Sodium benzoate, a commercial nucleating agent helped produce fine fibers with very good mechanical and physical properties.

Process variables such as the throughput, air pressure at the die, cooling length and air temperature were found to affect the structure and properties of the melt blown fibers. It was shown that by ingenuously selecting the process conditions one would be able to produce fine melt blown fibers that maintained their dimensional stability even at elevated temperatures.

6. Recommendations for Future Work

The ways to produce dimensionally stable melt blown webs from a high performance polymer, poly(ethylene terephthalate) are illustrated in this dissertation work. However, the thermal stability was obtained only with some compromise in the physical and mechanical properties. Future work on the same lines could be aimed at the following:

1. Production of fine PET/LCP melt blown webs with smaller fiber diameters through process modifications such as improved drawing techniques or use of a different type of liquid crystalline polymer.

2. Modification of interfacial properties between PET and LCP components. This could be accomplished by using an additive that is compatible with both the polymers or through transesterification. The later could be carried out by increasing the residence time during processing by keeping a nitrogen blanket.

3. Varying the composition of the additives. The percentage of sodium benzoate could be reduced to see if the ductile nature of PET fibers could be preserved.

4. Analysis of the fiber structure by other experimental techniques. The determination of crystal sizes and the distribution of crystallites of the as-produced and shrunk fibers through X-ray diffraction could throw light on the way the tie elements are incorporated into the fibers.

Bibliography

Bibliography

1. Malkan, S. R. and Wadsworth, L. C., *International Textiles Bulletin: Nonwovens*, 37, 2, 46-52 (1991)
2. Malkan, S. R. and Wadsworth, L. C., *International Textiles Bulletin: Nonwovens*, 37, 3, 22-28 (1991)
3. Buntin, R. R. and Lohkamp, D. T., *TAPPI*, 56, 4, 74-77 (1973)
4. Davey, C. R., *Book of papers, INDATEC 1987*, Hilton Head, SC, 232-237, May 18-21 (1987)
5. Davey, C. R., *Nonwovens: An Advanced Tutorial,* Ed., A. F. Turbak and T. L. Vigo, TAPPI press, Atlanta, GA, 159-172 (1989)
6. Malkan, S. R., and Wadsworth, L. C., *INDA JNR.*, vol.3, no. 2, 21-34 (1991)
7. Malkan, S. R., and Wadsworth, L. C., *INDA JNR.*, vol.3, no. 3, 21-29 (1991)
8. Haynes, B. and Milligan, M., *INDA JNR.*, vol. 3, no. 4, 20-25 (1991)
9. Wadsworth, L. C. et al., *Book of papers, TAPPI Nonwovens Conference*, Macro Island, FL, 1-7, May 4-11, 1990
10. Dever, M., Wadsworth, L. C. and Lee, Y., *INDA JNR.*, vol. 3, no. 1, 19-24 (1991)
11. Zhang, Y., M. S. Thesis, The University of Tennessee, Knoxville (1991)
12. Bhat, G. S., Zhang, Y., and Wadsworth, L. C., *Proceedings of the TAPPI Nonwovens Conference*, Macro Island, FL, 61-68, May 1992
13. Vasanthakumar, N., Bhat, G. S., Wadsworth, L. C., and Joy, D., *International Nonwovens Journal*, vol. 6, no. 1, 42-46 (1994)
14. Bhat, G. S., Vasanthakumar, N., Nityananda, R. and Wadsworth, L. C., *Proceedings of 22nd NATAS Conference*, 96-101 (1993)
15. Concise Encyclopedia of Polymer Science and Engineering edited by Kroschwitz, J. I., 229-235 (1990)

16. Armistead, K. and Goldberg-Wood, G., *Advances in polym. sci.*, vol. 100, 219-311 (1992)

17. Winter school notes IIT Delhi, 1990 (private communication)

18. Frank, F. C., *Disc Faraday Soc.*, 25:205 (1958)

19. Hoffman, J. D., *polymer* 24:3 (1983)

20. Sadler, D. M., Harris, R., *J. polym. sci., polym. phys. edn.*, 20;561 (1982)

21. Spells, S. J., Keller, A. and Sadler, D. M., *polymer* 25:749 (1984)

22. Cheng, S. D. "Macromolecules" in *Polymer Analysis and Characterization* by Barth, H. G. (1988)

23. Cobbs, W. H. and Burton, R. L., *J. Polym. Sci.*, vol. 10, no. 3, 275-290 (1953)

24. Volmer, M., *Kintik der phasenbildung*, Steinkopff, Dresden (1939)

25. Becker, R. and Doring, W., Ann. physik, 24, 719 (1935)

26. Fischer, J. C., Hollomon, J. H. and Turnbull, D., J. Applied phys., 19, 775-84 (1948)

27. Van Antwerpen, F. and Van Krevelen, D. W., *J. Polym. Sci.*, vol. 10, 2423-2435 (1972)

28. Jabarin, S. A., *Polym. Engg. & Sci.*, vol. 29, no. 18, 1259-1264 (1989)

29. Jabarin, S. A., *J. Appl. Polym. Sci.*, vol. 34, 85-96 (1987)

30. Jabarin, S. A., *J. Appl. Polym. Sci.*, vol. 34, 97-102 (1987)

31. Jabarin, S. A., *J. Appl. Polym. Sci.*, vol. 34, 103-108 (1987)

32. Lin, C. C., *Polym. Engg. & Sci.*, vol. 23, no. 3 (1983)

33. Douillard, A., et al. *Polymer*, vol. 34, no. 8 (1993)

34. Kim, S. P., et al., *Polym. Engg. & Sci.*, vol. 31, no. 2, 110-115 (1991)

35. Aharoni, S. M., *J. Appl. polym. sci.*, vol. 29, 853-865 (1984)

36. Turturro, G., Brown, G. R., and St. Pierre, L. E., *polymer*, 25, 659 (1984)

37. Gumther, B., and Zachmann, H. G., *polymer*, vol. 24, 1008-1014 (1983)

38. Legras, R., Bailly, C., Daumerie, M., DeKominck, J. M., Mercier, J. P., Zichy, V., and Nield, E., *polymer*, vol. 25, 835-844 (1984)

39. Lawton, E. L., *polym. engg. & sci.*, vol. 25, no. 6, 348-354 (1985)

40. Joseph, E. G., Wilkes, G. L., and Baird, D. G., *polym. prep. Am. chem. soc. div. polym. chem.*, 24, 304 (1983)

41. Bhattacharya, S. K., Tendolkar, A., and Misra, A., *mol. cryst. liq. cryst.*, vol. 153, 501-513 (1987)

42. Sharma, S. K., Tendolkar, A., and Misra, A., *mol. cryst. liq. cryst.*, vol. 157, 597 - 614 (1988)

43. Bourland, L., *plastics engg.*, 39-41, July 1987

44. Barrett, L. W., Sperling, L. H., Gilmer, J., and Mylonakis, G., *J. Appl. polym. sci.*, vol. 48, 1035-1050 (1993)

45. Barrett, L. W., and Sperling, L. H., *polym.engg. & sci.*, vol. 33, no. 14, 913-922 (1993)

46. Peterlin, A., *polym. engg. & sci.*, vol. 16, no. 3, 126-137 (1976)

47. Yeh, G. S. Y., *polym. engg. & sci.*, vol. 16, no. 3, 138-144 (1976)

48. Yeh, G. S. Y., *polym. engg. & sci.*, vol. 16, no. 3, 145-151 (1976)

49. Keller, A., and Machin, M. J., *J. macromol. sci. (phys.)*, B1, 41 (1967)

50. Spruiell, J. E., McCord, D. E., and Beuerlein, R. A., *Trans. of the soc. of rheology*, 16:3, 535-555 (1972)

51. Heffelfinger, C. J., and Schmidt, P. G., *J. appl. polym. sci.*, vol. 9, 2661-2680 (1965)

52. Misra, A., and Stein, R. S., *J. polym. sci., polym. phys. edn.*, vol. 17, 235-257 (1979)

53. Matsuo, M., Tamada, M., Terada, T., Sawatari, C., and Niwa, M., *Macromolecules*, 15, 988-998 (1982)

54. Terada, T., Sawatari, C., Chigono, T., and Matsuo, M., *Macromolecules*, 15, 988-1004 (1982)

55. Gupta, V. B., Ramesh, C., and Seisler, H. W., *J. polym. sci., polym. phys. edn.*, vol. 23, 405-411 (1985)

56. Van Den Heuvel, C. J. M., Heuvel, H. M., Fassen, W. A., Veurink, J. and Lucas, L. J., *J. appl. polym. sci.*, vol. 49, 925-934 (1993)

57. Heuvel, H. M., and Huisman, R., *J. appl. polym. sci.*, vol. 22, 2229-2243 (1978)

58. Gupta, R. K., and Auyeung, K. F., *J. appl. polym. sci.*, vol. 34, 2469-2484 (1987)

59. Garg, S. K., *J. appl. polym. sci.*, vol. 29, 2111-2116 (1984)

60. Gupta, R. K., and Auyeung, K. F., *polym. engg. & sci.*, vol. 29, no. 16, 1147-1156 (1989)

61. Smith, F. S., and Steward, R. D., *polymer*, vol. 15, 283-286 (1974)

62. Wilson, M. P. W., *polymer*, vol. 15, 277-282 (1974)

63. Mascia, L. and Fekkai, Z., *polymer*, vol. 34, no. 7 (1993)

64. Williams, D. J., *Advances in Polymer Technology*, vol. 10, no. 3, 173-184 (1990)

65. Dutta, D., Fruitwala, H., Kohli, A., and Weiss, R. A., *polym. engg. & sci.*, vol. 30, no. 17, 1005-1018 (1990)

66. Kamal, M. R., Khennache, O., and Goyal, S. K., *polym. engg. & sci.*, vol. 29, no. 16, 1089-1096 (1989)

67. Lenz, R. W., Rao, A. K., Reddy, C. R., Bafna, S., and Bhattacharya, S., *J. polym. sci., part B, polym. phys.* vol. 27, 2117-2130 (1989)

68. Perkins, W. G., Marcelli, A. M., and Frerking, Jr., H. W., *J. appl. polym. sci.*, vol. 43, 329-349 (1991)

69. Sukhadia, A. M., Done, D., and Baird, D. G., *polym. engg. & sci*, vol. 30, no. 9, 519-526 (1990)

70. Kyotani, M., Kaito, A., and Nakayama, K., *Sen - I Gakkaishi*, vol. 47, no. 8, 403-406 (1991)

71. Mithal, A. K., and Tayebi, A., *polym. engg. & sci.*, vol. 31, no. 21, 1533-1538 (1991)

72. Mehta, S., and Deopura, B. L., *polym. engg. & sci.*, vol. 33, no. 14, 931-936 (1993)

73. Lee, W. C., Dibenedetto, A. T., Gromek, J. M., Nobile, M. R., and Acierno, D., *polym. engg. & sci.*, vol. 33, no. 3, 156-165 (1993)

74. Daubney, R. P., Bunn, C. W. and Brown, C. J., Proc. Royal Soc. London, 226A, 531 (1954)

75. Ward, I. M., *Textile Research Journal*, 650-664, July 1961

76. Fischer, E. W. and Fakirov, S., *J. Mater. Sci.*, 11, 1041-1065 (1976)

77. Fu, Y., Busing, W. R., Jin, Y., Affholter, K. A., and Wunderlich, B., *Macromolecules*, 26, 2187-2193 (1993)

78. Fu, Y., Busing, W. R., Jin, Y., Affholter, K. A. and Wunderlich, B., *Macromol. chem. phys.*, 195, 803-822 (1994)

79. Fu, Y., Annis, B., Boller, A., Jin, Y. and Wunderlich, B., *J. Polym. Sci.: Part B: Polymer Physics*, vol. 32, 2289-2306 (1994)

80. *ATHAS data bank*, 1993

81. Fina, L. J. and Koenig, J. L., Macromolecules, 17, 2572-2579 (1984)

VITA

Vasanthakumar Narayanan was born in Dharmapuri, India on June 16, 1967. He received his Bachelor of Science degree in Textile Engineering from A. C. Technology, Anna University, Madras in May 1988. He went to the capital city of New Delhi and received his Masters degree in Textile Engineering at the Indian Institute of Technology in December 1990. Before coming to the united States, he was working as a R&D engineer at Vardhman Mills, Punjab, India. He entered the Textile Science program at the College of Human Ecology at the University of Tennessee, Knoxville in August 1991 and received his doctoral degree in May 1995.

He is currently employed as a Research Scientist at Techmer PM Polymer Modifiers, Clinton, TN 37716.